

Ministry of Education and Science of the Russian Federation
Federal Independent Educational Institution
«NATIONAL RESEARCH TOMSK POLYTECHNIC UNIVERSITY»

Research School of Chemistry & Applied Biomedical Sciences
 Program/specialty 12.04.04 «Biotechnical systems and technologies»

MASTER'S THESIS

Topic of the work
Исследование плазмон-индуцированной фотокаталитической реакции на уровне одиночных наночастиц Investigation of plasmon-induced photocatalytic reaction at the single nanoparticle level

UDC: 533.95:538.9-022.532:615.831.4

Student

Group	Full name	Signature	Date
9DM8I	Averkiev Andrey Alekseevich		

Scientific Supervisor and Technical Advisor

Position	Full name	Academic degree, rank	Signature	Date
Professor	Raul David Rodriguez	PhD		

ADVISORS:

Section «Financial Management, Resource Efficiency and Resource Saving»

Position	Full name	Academic degree, rank	Signature	Date
Associate Professor	Menshikova Ekaterina Valerievna	Candidate of Philosophy Sciences		

Section «Social Responsibility»

Position	Full name	Academic degree, rank	Signature	Date
Associate Professor	Mikhail Vladimirovich Gorbenko	Candidate of Technical Sciences		

Advisor-linguist of the Department of Foreign Languages

Position	Full name	Academic degree, rank	Signature	Date
Associate Professor	Kuimova Marina Valerievna	Candidate of Pedagogical Sciences		

ADMIT OT DEFENSE:

Head of the program	Full name	Academic degree, rank	Signature	Date
Associate Professor	Gubarev Fedor Aleksandrovich	Candidate of Physical and Mathematical Sciences		

Planned program learning outcomes

Код результата	Результат обучения (выпускник должен быть готов)	Требования ФГОС, критериев и/или заинтересованных сторон
Профессиональные компетенции		
P1	Применять глубокие специальные естественнонаучные, математические, социально-экономические и профессиональные знания в инновационной инженерной деятельности при разработке, производстве, исследовании, эксплуатации, обслуживании и ремонте современной биомедицинской и экологической техники	Требования ФГОС (ОК-2, ОПК-2), Критерий 5 АИОР (п. 5.2.1), согласованный с требованиями международных стандартов <i>EUR-ACE</i> и <i>FEANI</i>
P2	Ставить и решать инновационные задачи инженерного анализа и синтеза с использованием специальных знаний, современных аналитических методов и моделей	Требования ФГОС (ОПК-1, 3; ПК- 1 – 4), Критерий 5 АИОР (п. 5.2.2), согласованный с требованиями международных стандартов <i>EUR-ACE</i> и <i>FEANI</i>
P3	Выбирать и использовать необходимое оборудование, инструменты и технологии для ведения инновационной практической инженерной деятельности с учетом экономических, экологических, социальных и иных ограничений	Требования ФГОС (ОК-9, ПК-10, 14, 18). Критерий 5 АИОР (пп. 5.2.3, 5.2.5), согласованный с требованиями международных стандартов <i>EUR-ACE</i> и <i>FEANI</i>
P4	Выполнять комплексные инженерные проекты по разработке высокоэффективной биомедицинской и экологической техники конкурентоспособной на мировом рынке	Требования ФГОС (ОК-2, 3; ПК-5 – 11, 14), Критерий 5 АИОР (пп. 5.2.3, 5.2.5), согласованный с требованиями международных стандартов <i>EUR-ACE</i> и <i>FEANI</i>
P5	Проводить комплексные инженерные исследования, включая поиск необходимой информации, эксперимент, анализ и интерпретацию данных с применением глубоких специальных знаний и современных методов для достижения требуемых результатов в сложных и неопределенных условиях	Требования ФГОС (ОК-2, 3; ОПК-5, ПК-1 – 4). Критерий 5 АИОР (пп. 5.2.2, 5.2.4), согласованный с требованиями международных стандартов <i>EUR-ACE</i> и <i>FEANI</i>
P6	Внедрять, эксплуатировать и обслуживать современное высокотехнологичное оборудование в предметной сфере биотехнических систем и технологий, обеспечивать его высокую эффективность, соблюдать правила охраны здоровья и безопасности труда, выполнять требования по защите окружающей среды	Требования ФГОС (ОПК-1, 2), Критерий 5 АИОР (пп. 5.2.5, 5.2.6), согласованный с требованиями международных стандартов <i>EUR-ACE</i> и <i>FEANI</i>
Универсальные компетенции		
P7	Использовать глубокие знания в области проектного менеджмента для ведения инновационной инженерной деятельности с учетом юридических аспектов защиты интеллектуальной собственности	Требования ФГОС (ОПК-2; ПК-14, 15). Критерий 5 АИОР (п. 5.3.1), согласованный с требованиями международных стандартов <i>EUR-ACE</i> и <i>FEANI</i>
P8	Владеть иностранным языком на уровне, позволяющем активно осуществлять коммуникации в профессиональной среде и в обществе, разрабатывать документацию, презентовать и защищать результаты инновационной инженерной деятельности	Требования ФГОС (ОК-1), Критерий 5 АИОР (п. 5.3.2), согласованный с требованиями международных стандартов <i>EUR-ACE</i> и <i>FEANI</i>
P9	Эффективно работать индивидуально и в качестве члена и руководителя команды, состоящей из специалистов различных направлений и квалификаций, с делегированием ответственности и полномочий при решении инновационных инженерных задач	Требования ФГОС (ОК-3, ОПК-3; ПК-3, 12, 13), Критерий 5 АИОР (п. 5.3.3), согласованный с требованиями международных стандартов <i>EUR-ACE</i> и <i>FEANI</i>
P10	Демонстрировать личную ответственность, приверженность и готовность следовать профессиональной этике и нормам ведения инновационной инженерной деятельности	Критерий 5 АИОР (п. 5.3.4), согласованный с требованиями международных стандартов <i>EUR-ACE</i> и <i>FEANI</i>
P11	Демонстрировать глубокие знание правовых, социальных, экологических и культурных аспектов инновационной инженерной деятельности, компетентность в вопросах охраны здоровья и безопасности жизнедеятельности	Критерий 5 АИОР (п. 5.3.5), согласованный с требованиями международных стандартов <i>EUR-ACE</i> и <i>FEANI</i>
P12	Самостоятельно учиться и непрерывно повышать квалификацию в течение всего периода профессиональной деятельности	Требования ФГОС (ОК-2, 4; ОПК-4), Критерий 5 АИОР (п. 5.3.6), согласованный с требованиями международных стандартов <i>EUR-ACE</i> и <i>FEANI</i>

Ministry of Education and Science of the Russian Federation
Federal Independent Educational Institution
«NATIONAL RESEARCH TOMSK POLYTECHNIC UNIVERSITY»

Research School of Chemistry & Applied Biomedical Sciences
 Program/specialty 12.04.04 «Biotechnical systems and technologies»

APPROVED BY
 Head of the Program

F.A.Gubarev

 (Signature) (Date)

ASSIGNMENT
for the Master's Thesis completion

In the form:

Master's Thesis

For a student:

Group	Full Name
9DM8I	Averkiev Andrey Alekseevich

Topic of the work:

Исследование плазмон-индуцированной фотокаталитической реакции на уровне одиночных наночастиц
Investigation of plasmon-induced photocatalytic reaction at the single nanoparticle level
Approved by the order of the Head (date, number)

Deadline for completion of the Master's Thesis:	
---	--

TERMS OF REFERENCE:

<p>Initial data for work: <i>(the name of the object of research or design; performance or load; mode of operation (continuous, periodic, cyclic, etc.); type of raw material or material of the product; requirements for the product, product or process; special requirements to the features of the operation of the object or product in terms of operational safety, environmental impact, energy costs; economic analysis, etc.).</i></p>	<p>The object of the research: plasmon-induced photocatalytic reaction. Subject matter of the research: competition of electromagnetic field enhancement and photochemical conversion in photocatalytic plasmon-induced reaction for the application of plasmonics in photochemistry and medicine, in particular for theranostics of cancer tumors. Results of this research can be used for developing of optimized plasmonic nanoparticles covered with 4-nitrobenzenethiol (4-NBT) or another photocatalytic active molecule for <i>in-vitro</i> and <i>in-vivo</i> testing in biomedical applications. Also, this result may be helpful for nanobiosensors creation and photochemistry industries due to high electromagnetic field enhancement and photothermal properties.</p>
<p>List of the issues to be investigated, designed and developed <i>(analytical review of literary sources in order to elucidate the achievements of world science and technology in the field under</i></p>	<p>To accomplish the task, it is necessary to investigate a number of questions: •Writing a literature review and analysis on the topic; •Research of existing solutions in this area;</p>

<i>consideration, the formulation of the problem of research, design, construction, the content of the procedure of the research, design, construction, discussion of the performed work results, the name of additional sections to be developed; work conclusion).</i>	<ul style="list-style-type: none"> • Planning of the experiment; • Completing simulation experiment of this research; • Completing experiment of this research; • Investigation of the results and their interpretation; • Evaluation of the feasibility of further <i>in-vitro</i> and <i>in-vivo</i> research; • Feasibility study; • Industrial and environmental safety.
List of graphic material (with an exact indication of mandatory drawings)	
Advisors on the sections of the Master's Thesis	
Chapter	Advisor
Section «Financial Management, Resource Efficiency and Resource Saving»	Associate professor, Menshikova Ekaterina Valerievna
Section «Social Responsibility»	Associate Professor, Mikhail Vladimirovich Gorbenko

Date of issuance of the assignment for Master's Thesis completion according to a line schedule	
---	--

The task was issued by the Scientific Supervisor and Technical Advisor:

Position	Full Name	Academic degree, rank	Signature	Date
Professor	Raul David Rodriguez	PhD		

The assignment was accepted for execution by the student:

Group	Full Name	Signature	Date
9DM8I	Averkiev Andrey Alekseevich		

**ASSIGNMENT FOR SECTION
«FINANCIAL MANAGEMENT, RESOURCE EFFICIENCY AND RESOURCE
SAVING»**

To the student:

Group	Full name
9DM8I	Averkiev Andrey Alekseevich

School	RSCABS	Division	
Degree	Master	Educational Program	12.04.04 Biotechnical systems and technologies

Input data to the section «Financial management, resource efficiency and resource saving»:

1. Resource cost of scientific and technical research (STR): <i>material and technical, energetic, financial and human</i>	– Salary costs – 264193 rubles – STR budget – 938098 rubles.
2. Expenditure rates and expenditure standards for resources	– Electricity costs – 5,8 rub per 1 kW
3. Current tax system, tax rates, charges rates, discounting rates and interest rates	– Labor tax – 27,1 %; – Overhead costs – 30%;

The list of subjects to study, design and develop:

1. Assessment of commercial and innovative potential of STR	– comparative analysis with other researches in this field;
2. Development of charter for scientific-research project	– SWOT-analysis;
3. Scheduling of STR management process: structure and timeline, budget, risk management	– calculation of working hours for project; – creation of the time schedule of the project; – calculation of scientific and technical research budget;
4. Resource efficiency	– integral indicator of resource efficiency for the developed project.

A list of graphic material (with list of mandatory blueprints):

1. Competitiveness analysis
2. SWOT- analysis
3. Gantt chart and budget of scientific research
4. Assessment of resource, financial and economic efficiency of STR
5. Potential risks

Date of issue of the task for the section according to the schedule	3.02.2020
--	-----------

Task issued by adviser:

Position	Full name	Scientific degree, rank	Signature	Date
Associate professor	E.V. Menshikova	Candidate of Philosophy Sciences		

The task was accepted by the student:

Group	Full name	Signature	Date
9DM8I	Averkiev Andrey Alekseevich		

ASSIGNMENT FOR THE SECTION «SOCIAL RESPONSIBILITY»

For the student:

Group	Full name
9DM8I	Averkiev Andrey Alekseevich

School	RSCABS	Department	
Level of education	Master's degree	Program/Specialty	12.04.04 Biotechnical systems and technologies

Initial data to the section «Social responsibility»:	
1. <i>Characteristics of the object of study (substance, material, device, algorithm, method, working area) and its areas of application</i>	<i>Investigation of Plasmon-induced photocatalysis at the nanoparticles in the micro- and nano- scale using TERS coupled with AFM methodology to see the LSPR, temperature, laser power density and time of exposure influences.</i>
The list of issues to be investigated, designed and developed:	
1. Legal and organizational safety issues: 1.1. <i>Special legal norms of labor legislation.</i> 1.2. <i>Organizational arrangements for the layout of the working area.</i>	<i>Special legal norms of labor legislation (medical examination of employees, safety instructions, provision of personal protective equipment). Requirements for the organization of the workplace.</i>
2. Industrial safety: 2.1. <i>Analysis of harmful and dangerous factors that can be created by object of study.</i> 2.2. <i>Analysis of harmful and dangerous factors that may arise in the laboratory during research.</i> 2.3. <i>Justification of measures to protect the researcher from the effects of hazardous and harmful factors.</i>	<i>Harmful industrial factors:</i> 1) <i>Eyes and respiratory tract contact with chemicals;</i> 2) <i>decrease in illumination of the room;</i> 3) <i>adverse electromagnetic environment;</i> 4) <i>microclimate deviations.</i> <i>Hazardous industrial factors:</i> 1) <i>chemical hazard;</i> 2) <i>laser equipment irradiation;</i> 3) <i>an increased value of voltage in using equipment;</i> 4) <i>fire hazard;</i>
3. Environmental safety: 3.1. <i>Analysis of the impact of the object of research on the environment.</i> 3.2. <i>Analysis of the "life cycle" of the object of study.</i> 3.3. <i>Justification of measures to protect the environment.</i>	<i>When using devices necessary for the implementation of graduation thesis, the atmosphere, hydrosphere or lithosphere is not harmed, since no harmful substances are released into the air and water. In the event of a device malfunction, this technology is also recycled.</i>
4. Safety in emergency situations: 4.1. <i>Analysis of probable emergencies that may occur in the laboratory during research.</i> 4.2. <i>Justification of measures to prevent emergencies and the development of procedures in case of an emergency.</i>	<i>When performing this graduation thesis, the most likely type of emergency is fire. The list of measures to reduce the threat of possible emergencies is given.</i>

Date of assignment for the section on a linear schedule	3.02.2020
--	-----------

Assignment was issued by an advisor:

Position	Full name	Degree	Signature	Date
Associate professor	Mikhail Vladimirovich Gorbenko	Candidate of Technical Sciences		

Assignment was accepted for execution by the student:

Group	Full name	Signature	Date
9DM8I	Averkiev Andrey Alekseevich		

Abstract

This Master's thesis contains 117 pages, 37 figures, 23 tables, 75 references, 4 appendices.

Key words: plasmonics, photocatalysis, theranostics, nanoparticles, SERS, TERS, Raman spectroscopy, electromagnetic field, temperature, photochemistry.

The object of the research: plasmon-induced photocatalytic reaction.

Subject matter of the research: competition of electromagnetic field enhancement and photo-chemical conversion in photocatalytic plasmon-induced reaction for the application of plasmonics in photochemistry and medicine, in particular for theranostics of cancer tumors.

The purpose of this work is to investigate the correlation of electromagnetic enhancement and photo-chemical conversion effects in plasmon-induced photocatalytic reactions at the single nanoparticle level.

Exact physical mechanism of plasmon photocatalysis is still under debate nowadays. In particular, the role of localized temperature remains a controversial issue. In this work we use self-assembled monolayers as a reference for photocatalytic activity investigated using Raman spectroscopy with surface and conical amplification with a resolution of less than 5 nm at the level of one nanoparticle. Our results show that thermal energy promotes plasmon-mediated photocatalytic conversion, which does not correlate with the Raman gain. We found that the photocatalytic reaction does not represent the largest contribution of the signal to micro- and nano-Raman spectroscopy, and thus, these methods underestimate the efficiency of the plasmon system. In addition to the fundamental understanding of plasmon photocatalysis, our findings are of great importance for the application of plasmonics in photochemistry and medicine. For example, in tumor theranostics, the trade-off between the energy spent on photothermal heating (therapy) and signal amplification (diagnostics) implies that these two functions cannot be simultaneously enhanced in systems with one nanoparticle.

Results of this research can be used for developing of optimized plasmonic nanoparticles covered with 4-NBT or another photocatalytic active molecule for *in vitro* and *in vivo* testing in biomedical applications. Also, this result may be helpful for nanobiosensors creation and photochemistry industries due to high electromagnetic field enhancement and photothermal properties.

The main design, technological and technical and operational characteristics: laboratory conditions of operation.

Degree of implementation: data obtained in the thesis work are ready for *in vitro* and *in vivo* testing.

Scope: Research laboratories, *In vitro* and *in vivo* testing centers, Medicine centers, Private clinics, University laboratories.

Definitions, designations, abbreviations, normative references

References to the following standards are used in this work:

1. SP 52.13330.2011. Natural and artificial lighting;
2. GOST 12.2.032-78 Occupational Safety Standards System (OSS). Workplace when working sitting. General ergonomic requirements;
3. GOST 12.2.033-78 OSS. The workplace when performing work while standing. General ergonomic requirements;
4. PND F 12.13.1-03. Guidelines. Safety during the work in analytical laboratories (general provisions);
5. SanPiN 2.2.2/2.4.1340-03. Hygienic requirements for personal electronic computers and work organization;
6. GOST 12.0.003-2015 OSS. Dangerous and harmful production factors. Classification;
7. GOST 12.1.007-76 OSS. Harmful substances. Classification and general safety requirements;
8. GOST 12.1.005-88. General sanitary and hygienic requirements for working area air;
9. SanPiN 2.2.4.3359-16. Sanitary and epidemiological requirements for physical factors in the workplace;
10. SP 60.13330.2016 Heating, ventilation and air conditioning. Updated edition of SNiP 41-01-2003;
11. SP 52.13330.2016 Natural and artificial lighting. Updated edition of SNiP 23-05-95;
12. SN 2.2.4/2.1.8.566–96. Industrial vibration, vibration in the premises of residential and public buildings;
13. GOST 12.1.030-81 OSS. Electrical safety. Protective grounding, grounding;
14. GOST 12.1.038-82 OSS. Electrical safety. Maximum permissible levels of touch voltages and currents;

15. GOST 12.1.045-84 OSS. Electrostatic fields. Permissible levels at the workplace and control requirements;
16. GOST 12.1.006-84 OSS. Electromagnetic fields of radio frequencies. General safety requirements;
17. R 2.2.2006-05. Guidelines for the hygienic assessment of working environment and labor factors. Criteria and classification of working conditions;
18. SanPiN 2.2.2/2.4.1340–03. Sanitary and epidemiological rules and regulations "Hygienic requirements for personal electronic computers and the organization of work.";
19. SanPiN 2.2.4.548–96. Hygienic requirements for the microclimate of industrial premises.

The following abbreviations are used in this thesis:

SERS – Surface enhanced Raman spectroscopy;

TERS – Tip enhanced Raman spectroscopy;

AFM – atomic force microscopy;

4-NBT – 4-nitrobenzenthionine;

4-ABT – 4-aminobenzenethionine;

DMAB – dimercaptoazobenzene;

NP – nanoparticles;

PNP – plasmonic nanoparticles;

EM – electromagnetic;

SPR – surface plasmon resonance;

LSPR – localized surface plasmon resonance;

HR – high resolution;

TEM – transmission electron microscopy;

SPM – scanning sample microscopy;

CCD - charge coupled device;

UV – ultraviolet;

IR – infrared;

PC – personal computer;

Content

Introduction	14
1 Literature review	16
1.1 Physical and chemical fundamentals of plasmonics	16
1.1.1 Determination of plasmons	16
1.1.2 Surface plasmon resonance	17
1.1.3 Localized surface plasmon resonance	20
1.2 Spectroscopy techniques	22
1.2.1 Raman spectroscopy	22
1.2.2 Surface Enhanced Raman Spectroscopy	26
1.2.3 Tip Enhanced Raman Spectroscopy	32
1.3 Plasmon-induced photocatalytic reaction	35
1.3.1 Photocatalysis	35
1.3.2 Plasmon-induced hot electrons	38
2 Materials and methods	39
2.1 The name of the research	39
2.2 Objectives of the research	39
2.3 Places of research	40
2.4 Test substances	41
2.4.1 Information about the objects of the research	41
2.4.1.1 Preparing the substance for use	46
2.4.1.2 Actions with residues	46
2.5 Research methods	46
2.5.1 Fabrication of Ag Nanocubes and Au Nanocages.	46
2.5.2 Au/Ag Nanocuboids synthesis	47
2.5.3 Characterization of plasmonic nanoparticles	47
2.5.4 Experimental setup and measurement technique	47
2.5.5. Finite element method in COMSOL Multiphysics for creation of 3D simulation model	49
3 Results and discussion	50
3.1 Raman spectroscopy insights on plasmon-induced photocatalysis	50
3.2 SERS spectra comparison of 4-NBT on Au/Ag nanocages and Au/Ag nanorods. Influence from LSPR	52
3.3 Temperature influence on photocatalytic activity	54

3.4 TERS maps with HR insights of individual plasmonic nanoparticles.....	55
3.5 Photons influence on the photocatalytic reaction	59
3.6 Simulation model of Au nanosphere in COMSOL Multiphysics.....	60
3.7 Simulation model of TERS experiment in COMSOL Multiphysics	62
3.8 Simulation model of temperature evaluation in COMSOL Multiphysics.	63
4 Financial management, resource efficiency and resource saving.....	65
4.1 Competitiveness analysis of technical solutions.....	65
4.2 SWOT analysis.....	67
4.3 Project Initiation.....	69
4.4 Scientific and technical research budget.....	73
4.5 Evaluation of the comparative effectiveness of the project.....	79
5 Social responsibility	83
5.1 Legal and institutional security issues	84
5.1.1 Special legal norms of labor legislation.....	84
5.1.2 Organizational measures in the layout of the working area.....	84
5.2 Industrial safety	87
5.2.1 Analysis of hazardous and harmful industrial factors.....	87
5.2.2 Justification of measures to reduce the impact of harmful factors on the researcher.....	89
5.2.3 Justification of measures to reduce the impact of hazardous factors on the researcher.....	95
5.3 Environmental safety.....	99
5.4 Safety in emergency situation	100
5.4.1 Analysis of probable emergencies that may be initiated by the research object	100
5.4.2 Analysis of probable emergencies that may occur in the laboratory during research	101
5.4.3 Justification of measures to prevent emergencies and development of procedures in case of emergencies.....	101
Conclusion.....	103
References	104
Appendix A	111
Appendix B.....	113
Appendix C.....	114
Appendix D	116

Introduction

Nowadays sensors with single-molecule sensitivity can visualize in real-space the actual vibrations of individual molecules using surface- and tip-enhanced Raman spectroscopy, respectively. Moreover, beyond a wide range of applications from theranostics and sensors to energy harvesting, plasmonic nanostructures are being used in chemical synthesis and for pollutants decomposition. These applications are based on plasmon-induced photocatalysis that is attracting significant attention during recent years. A growing number of reports are demonstrating the ability of plasmonic nanostructures to catalyze energetically demanding chemical reactions [1–4].

In general, this can be explained by direct capture of hot electrons from the plasmonic nanostructure by molecules adsorbed on the nanostructures surface to drive chemical reactions or by separation of electron-hole pairs when hot electrons (holes) jump over the Schottky barrier and get injected into the semiconductor's conduction (valence) band. An additional contribution comes from the inelastic plasmon relaxation due to electron-electron and electron-phonon scattering that give rise to photothermal heating that promotes the photocatalytic reaction. Thus, both heat generation and hot electrons are the result of plasmon energy decay making metallic nanoparticles act as photothermal or photoelectric converters that can contribute to plasmon-induced photocatalysis. [5-8].

Among several reactions used, the conversion of nitro to amino groups can be considered as a standard system in plasmon-enhanced photocatalysis. In our previous research we investigated the plasmon-induced photocatalytic reaction with the conversion of 4-nitrobenzenethiol (4-NBT to 4-aminobenzenethiol (4-ABT)) [9]. We showed that localized heating contributes to the plasmonic photocatalysis of 4-NBT. Nevertheless, and despite recent progress in photocatalysis, the conditions necessary for the conversion of 4-NBT to 4-ABT and dimercaptoazonbenzene (DMAB) are still under debate [9, 10]. The physical mechanisms behind this reaction are believed to depend on the atomic scale catalytic active sites of metal, excitation wavelength, material (Ag vs. Au), LSPR energy, hotspots, electronic density of

states, substrate - molecule distance, and temperature [11, 12]. Thus, right now the community is broadly divided into two bands, those who claim that plasmonic heating is the sole and only contributor to plasmonic-driven photocatalysis, and those who claim that it is hot-electron transfer what dominates these reactions. This situation is not only for the photocatalytic reaction of 4-NBT but it is a general discussion intensively ongoing in the plasmonics and catalysis communities.

Object of the research: plasmon-induced photocatalytic reaction.

Subject matter of the research: competition of electromagnetic field enhancement and photo-chemical conversion in photocatalytic plasmon-induced reaction for theranostics of cancer tumours.

The purpose of this work: to investigate the correlation of electromagnetic enhancement and photo-chemical conversion effects in plasmon-induced photocatalytic reaction at the single nanoparticle level.

To achieve the purpose, it is necessary to solve a number of tasks:

- Writing a literature review on the topic;
- Research of existing solutions in this area;
- Planning of the experiment;
- Completing simulation experiment of this research;
- Completing experiment of this research;
- Investigation of the results and their interpretation;
- Evaluation of the feasibility of further in-vitro and in-vivo research;

1 Literature review

1.1 Physical and chemical fundamentals of plasmonics

1.1.1 Determination of plasmons

In physics, a plasmon is a quasiparticle corresponding to the quantization of plasma oscillations, which are collective vibrations of a free electron gas.

Plasmons largely determine the optical properties of metals and semiconductors. Electromagnetic radiation with a frequency below the plasma frequency of the material is well reflected from it because free electrons start to oscillate at the same frequency with the oscillations of the electromagnetic field of this radiation. But at a frequency above the plasma, the electrons can no longer oscillate fast enough, and electromagnetic radiation of such a high frequency can penetrate into the metal or semiconductor, pass through it or be absorbed by it [13, 14].

The plasmon frequencies of most pure metals occur in the ultraviolet region of the spectrum. These metals reflect radiation equally well and, therefore, look colorless and shiny in a visible range of wavelength. But copper and gold have electronic transitions at the frequencies of the visible spectrum. The light is more strongly absorbed by the metal at these frequencies rather than at others of the visible range. As a result, copper, silver and gold appear colored in the reflected light [15, 16].

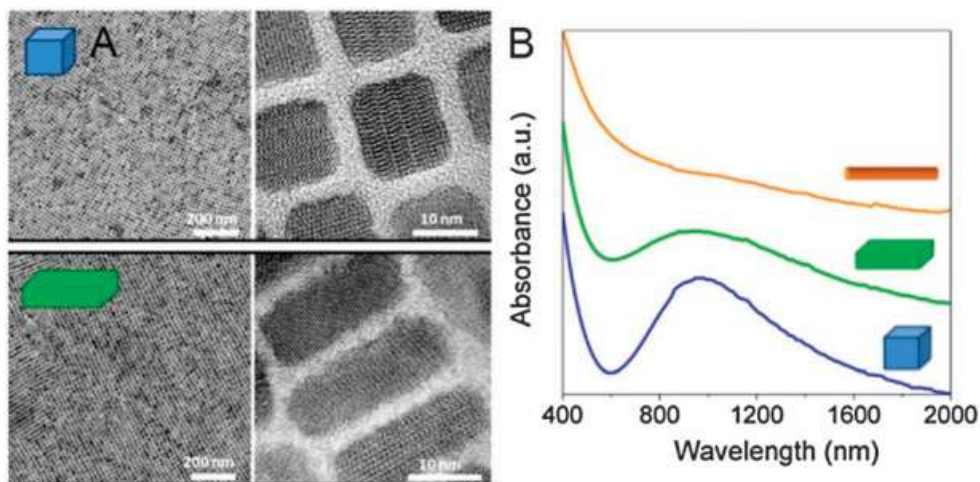


Figure. 1 (A) TEM and HRTEM images of Cu_{2-x}Te nanocubes (top) and nanoplates (bottom), and (B) UV/vis spectra of Cu_{2-x}Te nanorods (orange),

nanoplates (green) and nanocubes (blue). Adapted from Li et al.16 Copyright r 2013 ACS Publications [17].

In semiconductors, the plasmon frequency of the electrons of the valence band is usually in the far ultraviolet range but inter-level electronic transitions can be with the photon energies of visible light. Such a semiconductor will also selectively absorb the frequencies of visible light and appear colored [17, 18]. For highly doped nanoparticle-shaped semiconductors, the plasmon frequency may be in the near or mid-infrared range.

The classical physics approach can be used to describe plasmons. In this context free electrons in a metal are treated as a liquid entirely composed of electrons with a very high density (plasma). The fluctuations of density that appear on the surface of this material are called plasmons or surface plasmons. Each plasmon represents the quantization of classically oscillating plasma waves. This means that plasmons represent discrete values of an oscillating plasma wave. Therefore, most of their properties can be directly derived from Maxwell's equations.

The plasmon energy can be calculated in the model of almost free electrons as:

$$E_p = \hbar \omega_p = \hbar e \sqrt{\frac{n}{m \epsilon_0}}, \quad (1)$$

where n is the density of valence electrons, e is the elementary charge, m is the mass of the electron, and ϵ_0 is the vacuum permeability.

1.1.2 Surface plasmon resonance

Plasmon resonance is beginning to receive more recognition in the fields of chemistry, physics-, and materials science due to the wide variety of possible applications including optical sensing, data storage, light generation, biomedicine, and electronics. Due to its growing popularity it has become a topic of more research in order to try to understand its properties and how to harness and control its potential uses.

Surface plasmon resonance refers to the electromagnetic response that occurs when plasmons oscillate at the same frequency on the surface of the material. Since these plasmons oscillate at certain resonant frequencies, they move with periodic motive forces which can become large oscillation amplitudes when they interact. This phenomenon is stimulated by a light source. The frequency of light incidence must be equal to the natural frequency of the material otherwise resonance will not occur. These vibrations propagate on the surface between the material and the air and move in the direction of the surface of the negative dielectric material. Since these plasmons are located at this boundary they are very sensitive to changes in external stimuli such as energy absorption in the material. There are two popular configurations currently used to excite surface plasmon waves, the configurations of Otto and Kretschman [19].

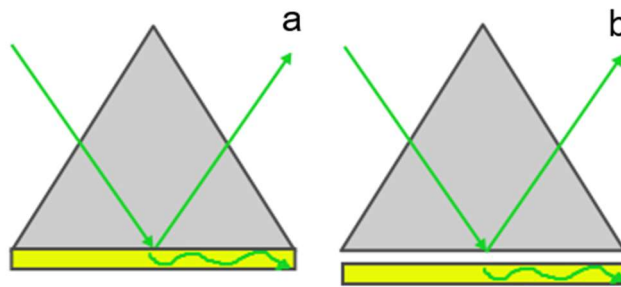


Figure 2. Otto (a) and Kretschman (b) configurations [19].

The Otto configuration shown in Figure 2a utilizes a light to illuminate a glass block or prism. The light wave is totally internally reflected and a thin metal film (typically gold or silver) is placed close enough so that the internally reflected light can interact with the plasmons on the surface and excite them. The Kretschmann configuration shown in Figure 2b is more commonly used and concerns cases when a thin metal film is evaporated onto the glass block as opposed to being separated. The wave of light passes through the glass block and the metal film excites the plasmons on the opposite side of the film (Figure 3) [19].

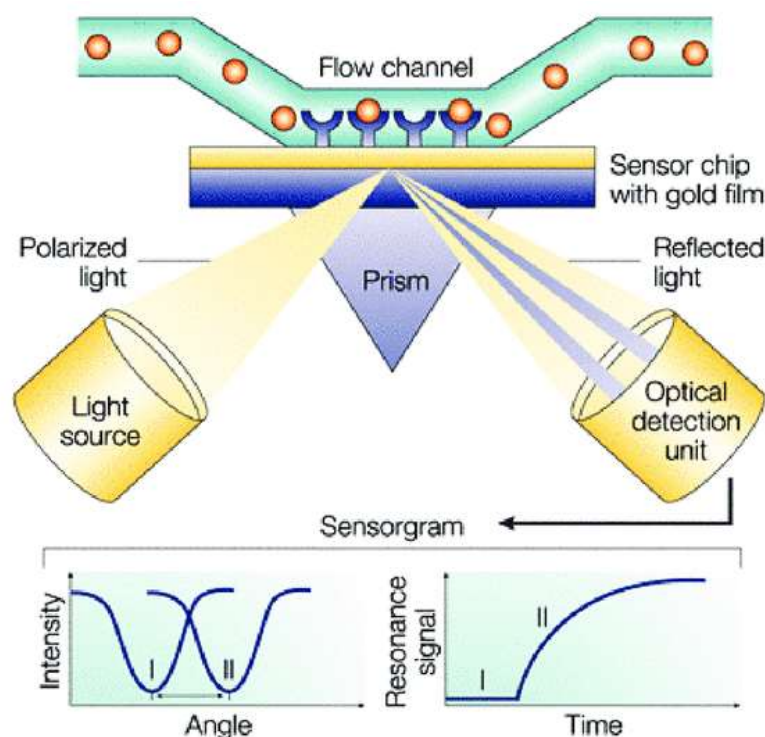


Figure 3. Surface plasmon resonance (SPR) detects changes in the refractive index in the immediate vicinity of the surface layer of a sensor chip. The SPR angle shifts (from I to II in the lower left-hand diagram) when biomolecules bind to the surface and change the mass of the surface layer. This change in resonant angle can be monitored non-invasively in real time as a plot of resonance signal (proportional to mass change) versus time [22].

Nanoparticles are of interest to the scientific community for a multitude of reasons including their large surface area to volume ratio which makes them very reactive to external stimuli quickly. The fact is that they operate on a quantum mechanics scale and that the nanoscale is the level at which many biological processes occur. Understanding how nanoparticles work helps researchers to be able to manipulate the properties of nanoparticles for desired outcomes [20].

One of the important properties of nanoparticles is that they exhibit SPR. When electric fields of light are directed at nanoparticles, the surface plasmons become excited and begin to resonate. This electric field also creates a separation of charge, which can be seen in Figure 4, that then forms a dipole oscillation in the same direction as the electric field of light. As the frequencies are the same, the SPR

allows a strong absorption of the incidence light while also allowing some scattering of light; these can be measured using a UV-VIs Spectrometer. The SPR band intensity and wavelength is dependent on the properties of the particle, including the shape, structure, metal type, size, and dielectric material surrounding the medium which can include air. The band intensity is strongest for metals Ag and Au. However, other metals like Cu have been used before. Au is most commonly used to observe this phenomenon as it is biologically compatible and inert even though Ag exhibits the strongest bands and sharpest peaks. At the nanoscale, SPR works the most efficiently and is capable of being observed through spectrometry [21].

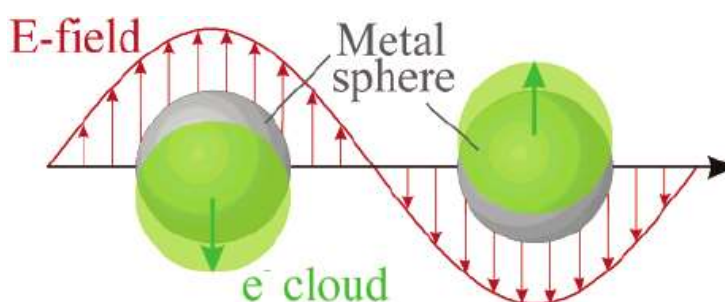


Figure 4. Schematic of plasmon oscillation for a sphere, showing the displacement of the conduction electron charge cloud relative to the nuclei [23].

1.1.3 Localized surface plasmon resonance

When a surface plasmon is confined to a particle of a size comparable to the wavelength of light, a nanoparticle, and the particle's free electrons participate in the collective oscillation, and it is termed a localized surface plasmon (LSP). The LSP has two important effects. First, electric fields near the particle's surface are greatly enhanced. This enhancement being greatest at the surface falls rapidly off with distance. Second, the particle's optical extinction has a maximum at the plasmon resonant frequency, which occurs at visible wavelengths for precious metals nanoparticles (Figures 4, 5). This extinction peak depends on the refractive index of the surrounding medium and is the basis for the sensing applications. To understand in depth how this localized surface plasmon resonance (LSPR) arises, we must turn to scattering theory [24].

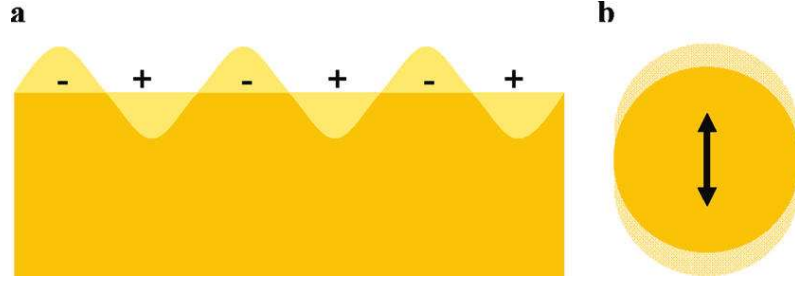


Figure 5. Illustrations of (a) surface plasmons and (b) a localized surface plasmon [24].

In 1908 Gustav Mie [25] explained the phenomena by solving Maxwell's equations for the absorption and scattering of electromagnetic radiation by spherical metallic particles. This theory has been used to calculate the spectra of particles smaller than the wavelength of light whose metallic dielectric function. In Mie's formulation, the extinction $E(\lambda)$ (scattering + absorption) of a sphere metal nanoparticle is related to the properties of the system by the equation [26]:

$$E(\lambda) = \frac{24\pi N_A a^3 \varepsilon_m^{\frac{3}{2}}}{\lambda \cdot \ln(10)} \left[\frac{\varepsilon_i}{(\varepsilon_r + \chi \varepsilon_m)^2 + \varepsilon_i^2} \right], \quad (2)$$

Where N_A is the areal density of nanoparticles, a is the radius of the metallic nanosphere, m is the dielectric constant of the medium surrounding the metallic nanosphere (assumed to be a positive real number independent from wavelength), λ is the wavelength of the absorbing radiation, ε_i is the imaginary portion of the metallic nanoparticle's dielectric function, ε_r is the real portion of the metallic nanoparticle's dielectric function, and χ is the term that describes the aspect ratio of the nanoparticle (equal to 2 for a sphere). It is evident from Equation (2) that the LSPR spectrum of a metallic nanosphere depends on the nanoparticle radius a , the nanoparticle material (ε_i and ε_r), the environment's dielectric constant (ε_m), and the shape of the nanoparticle (χ) [27].

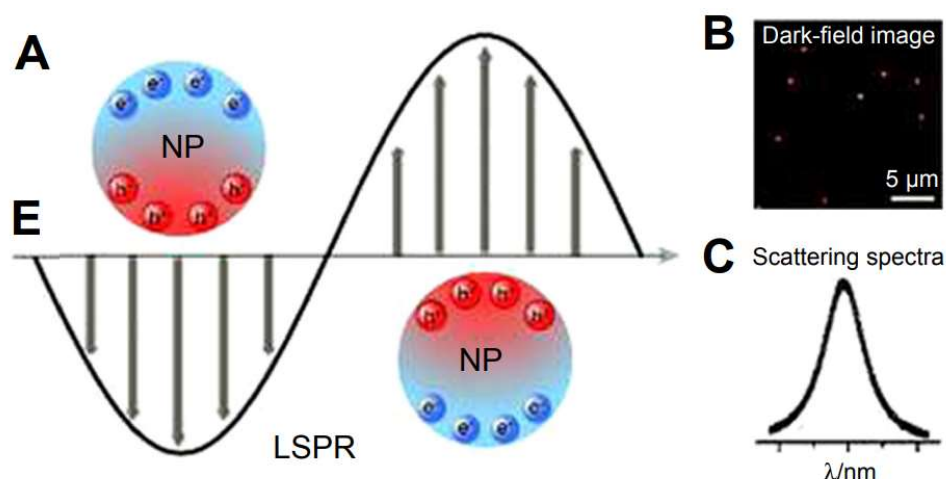


Figure 6. (A) Schematic description of localized surface plasmon resonance in metal NPs. (B) Dark-field image of NPs. (C) Scattering spectrum of a single NP [28].

The Mie's theory provides a deep understanding of the interactions of light with metal nanoparticles. But it has been developed for ideal systems and proved to be inadequate for most practical uses. A less rigorous approach is based on the assumption that the equations describing the extinction of the SPR of large metal surfaces hold also for the nanoparticles (Figure 6). In this case, in analogy with the SPR, the LSPR bands are expected to show a spectral shift ($\Delta\lambda$) [27].

Understanding of LSPR-based mechanisms of local EM field enhancement led to the development of a wide range of Raman spectroscopy methods including two important variants of Raman spectroscopy: surface-enhanced Raman spectroscopy (SERS) and tip-enhanced Raman spectroscopy (TERS).

1.2 Spectroscopy techniques

1.2.1 Raman spectroscopy

A spectroscopic technique typically used to determine vibrational modes of molecules is known as Raman spectroscopy. Rotational and other low-frequency modes of systems may also be observed in this technique. Providing a structural fingerprint by which molecules can be identified is the main usage of Raman spectroscopy in chemistry [29].

The main property of Raman spectroscopy is non-elastic scattering of photons known as Raman scattering. A source of monochromatic light used usually from a

laser ranges from visible to infrared or ultraviolet. Interaction of the laser with molecular vibrations results in chemistry shifting of the laser photons up or down. The energy shift provides the information about the vibrational modes in the system. Similarly, complementary information can be typically gained from infrared spectroscopy [30].

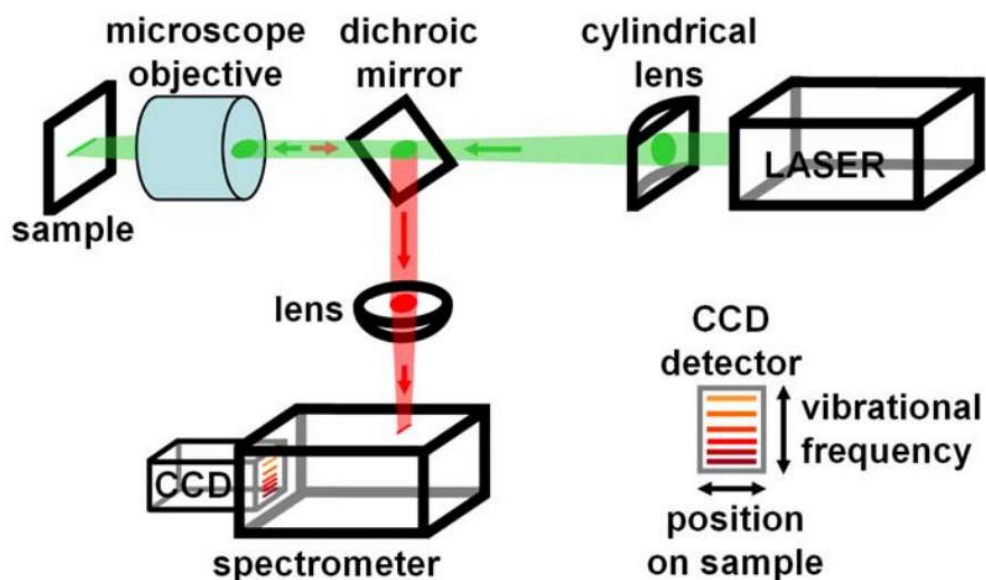


Figure 8. Schematic of Raman spectrometer [35].

Raman spectroscopy typically uses a laser wavelength of 532 nm (diode-pumped frequency doubled Nd:V) or 785 nm (AlGaAs diode) and can achieve a lateral resolution of better than half the wavelength (250–350 nm). This sub-cellular resolution is similar to that achieved in fluorescence imaging, and is far superior to the minimum resolution ($\sim 0.1\text{--}10\text{ mm}$) achievable with medical diagnostic techniques such as ultrasound, Magnetic Resonance Imaging, Positron Emission Tomography, or x-ray imaging. Some laser light which has lost energy after exciting one of the molecular vibrations is then red-shifted to a lower energy. This light goes through a spectrometer which disperses the light into a spectrum and records with a cooled CCD camera. A schematic of the apparatus is shown in Figure 8. Live cells can easily be studied in cell culture media, on a heated stage by an inverted microscope linked to a Raman spectrometer [35].

Such system requires both a high collection efficiency and a high-resolution spectrometer/CCD combination. It is highly beneficial to acquire a full high-

resolution Raman spectrum in one ‘shot’. So a CCD camera with a large number of pixels ($>1,000$) in the spectral axis is preferred. The difference between the frequency of the incident laser light and that of the red shifted light is equal to the frequency of the vibrational bond which has been excited. Each molecule has a unique ‘fingerprint’ of Raman peaks at well-defined frequencies [37] as biomolecules contain a variety of molecular bonds (e.g., C-H, C=C, O-H, aromatic ring) which are all excited. The spectrum senses the molecule(s) of interest of chemistry rather than performing elemental analysis – given that the information arises from the chemical bonds rather than from the nucleus. Frequency shifts are recorded in wavenumbers (cm^{-1}), and biological molecules have vibrations in the range $\sim 600\text{--}3,000\text{ cm}^{-1}$ [37].

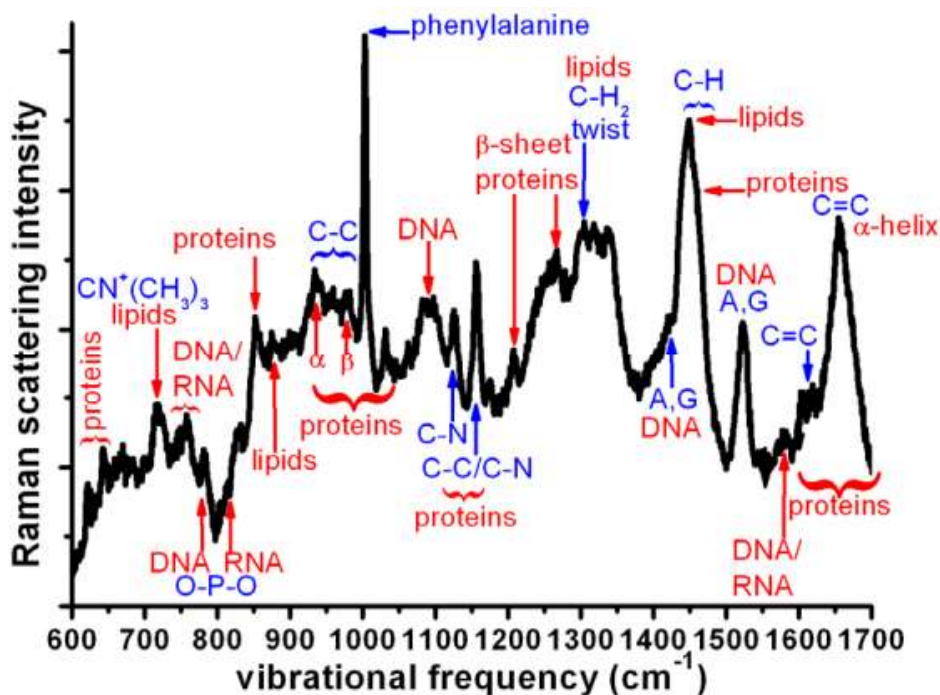


Figure 9. Unprocessed Raman spectrum of live MCF-7 breast cancer cells. 300 seconds acquisition time, 785 nm illumination, approximately 100 mW illumination power [35].

An example of Raman spectrum from a single live cell is displayed in Figure 9. The cell and the spectrum contain a very large number of different molecules which fall into the four major groups of nucleic acids, proteins, lipids and carbohydrates. The complex chemistry of the cell is projected into the Raman spectrum, and subtle changes to their function (hence the biochemistry) results in

changes to this spectrum. Therefore, Raman spectroscopy is a sensitive measure of biochemistry within live cells, tissues and bones [35].

Typically, a laser beam illuminates a sample. Lens collect electromagnetic radiation from the illuminated spot which is further sent through a monochromator. Elastic scattered radiation filtering is done at the wavelength corresponding to the laser line (Rayleigh scattering, Figure 10) by either a notch filter, edge pass filter or a band pass filter. The rest of the collected light is dispersed onto a detector [32].

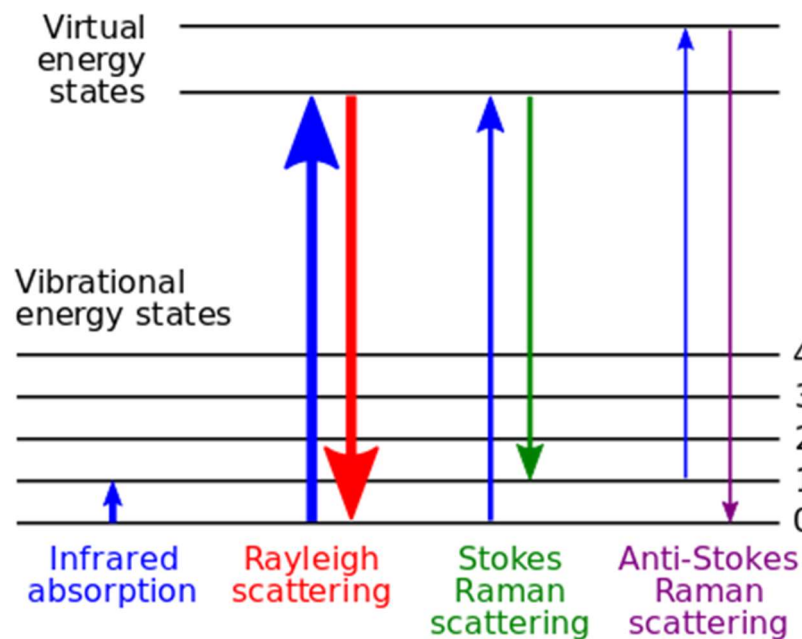


Figure 10. Raman scattering [32]

Raman spectroscopy is a totally non-invasive, label-free technique which excites vibrations of molecular bonds. Although infrared spectroscopy can excite these vibrational bonds it relies on low power sources and noisy detectors. Moreover, the used wavelengths are in the infrared range (3–15 μm) and cannot produce high resolution images of cells which are of the order of 10 μm in diameter. Infrared spectroscopy also suffers from an extremely low penetration depth in aqueous solution. So, it is not applicable in live cells unless attenuated total reflection is used to probe a shallow depth above the substrate [36].

The name "Raman spectroscopy" refers to vibrational Raman using laser wavelengths which are not absorbed by the sample (Figure 10). There are many other variations of Raman spectroscopy including surface-enhanced Raman, resonance

Raman, tip-enhanced Raman, polarized Raman, stimulated Raman, transmission Raman, spatially-offset Raman, and hyper Raman [33].

1.2.2 Surface Enhanced Raman Spectroscopy

Surface-enhanced Raman spectroscopy (SERS) is a highly sensitive and versatile analytical tool that is widely used in biosensing applications. In conventional Raman spectroscopy, molecules are detected by their characteristic scattering of laser light, but the sensitivity of the standard method is relatively low. By detecting the same Raman scattering from molecules adsorbed to rough metal surfaces, however, the sensitivity can be enhanced remarkably even enabling the detection of single molecules. Unfortunately, the mechanism of this enhancement is not well understood and is strongly dependent on the combination of surface and molecular target (Figure 11) [34].

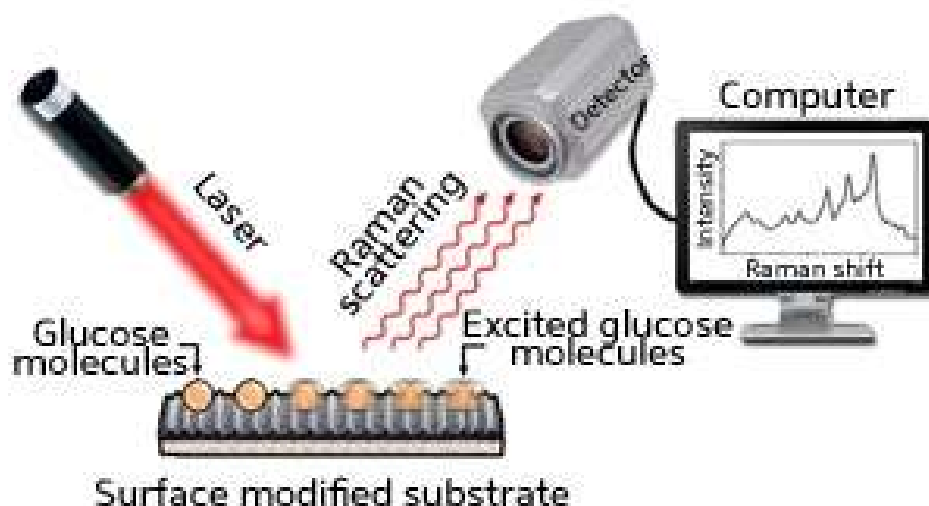


Figure 11. Schematic of SERS working principle [34].

In comparison to normal Raman spectroscopy SERS additionally requires the presence of metal nanostructures as an integral component. For SERS understanding, we therefore need to consider not only the interaction between light and molecules/matter but between light and metal nanostructures as well. The optical properties of metal nanostructures are the central topic of plasmonics [38].

Since the first observation of SERS spectra in 1974 [39] various physical and chemical enhancement mechanisms have been proposed to understand the SERS

mechanisms. Electromagnetic enhancement (EM) and chemical enhancement (CE) are the two most widely accepted mechanisms. It is well accepted that the EM mechanism contributes dominantly to the total SERS enhancement, showing enhancements from 4 to 11 orders of magnitude. Although CE is only 10–100 times. It can significantly modify the SERS features. Up to now the physical basis of EM is relatively clear and has been successfully applied to guide the experimental design of SERS to achieve a high detection sensitivity [40].

Electromagnetic enhancement factor

Surface-enhanced Raman scattering is a phenomenon that combines the light–metal interaction (plasmonic process, Figure 12b) and the light–molecule interaction (the vibrational spectroscopy, Figure 12a). It is necessary to understand the two interactions explicitly in order to understand the phenomenon. When the incident laser beam propagates onto the metal and dielectric interfaces the electromagnetic wave can drive the delocalized conduction electrons of the metal nanostructures into collective oscillation. When the frequency of the incident light matches with the inherent oscillation frequency of free electrons in the metal, SPR takes place. The resonance frequency depends on the size, shape, dielectric environment, and electron density of particles, the effective electron mass, etc. In metal nanostructures, the SPR can be highly localized to a specific position which is LSPR. The nanoparticles that are able to generate a strong LSPR effect are called plasmonic nanoparticles (PNP), which are usually Ag, Au, and Cu because they show strong SPR in the visible to near-infrared region [40].

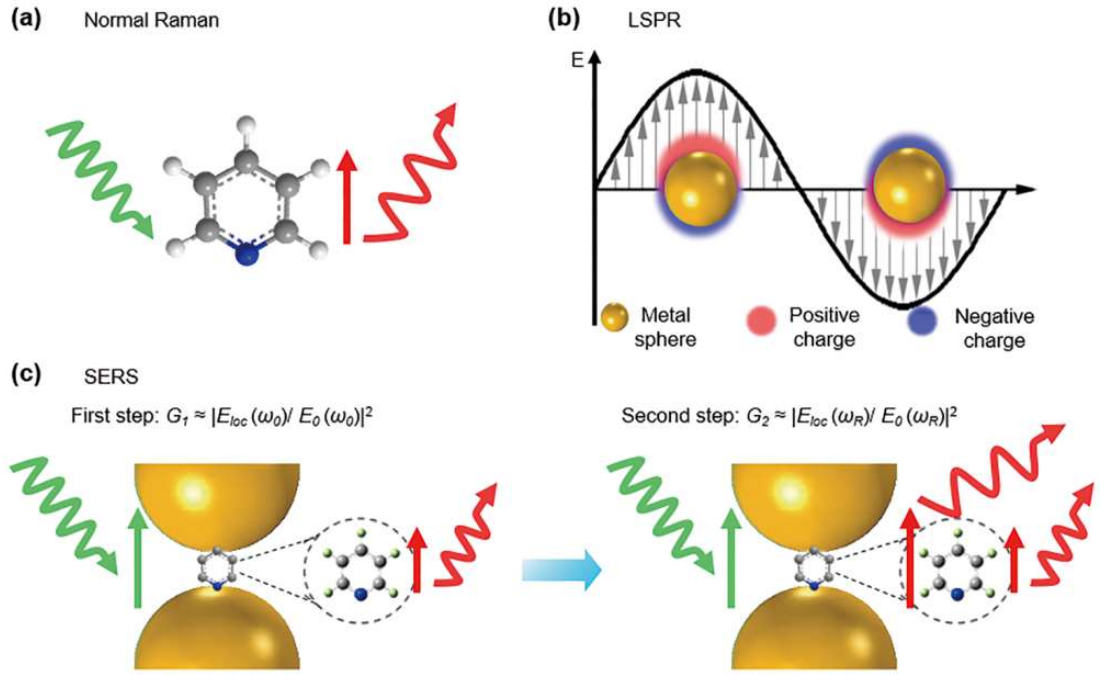


Figure 12. Schematics of (a) normal Raman, (b) localized surface plasmon resonance (LSPR), and (c) electromagnetic enhancement mechanism in SERS, including the two-step enhancements [41].

When molecules are placed near a plasmonic material the Raman process can be significantly enhanced leading to the so-called SERS process. The SERS process can be understood by a two-step enhancement process as shown in Figure 12c [41]. The first step results from the enhanced local field (near field) surrounding the PNPs (as receiving optical antennae) at the exciting wavelength (λ_{ex}): $E_{loc}(\lambda_{ex}) = G_1 E_0$, where G_1 is the enhancement factor of the electromagnetic field in the near field at λ_{ex} , and E_0 the exciting light with λ_{ex} . In the second step, the PNPs serve as transmitting optical antennae to transfer Raman signal from the near field to the far field, and the Raman signal is proportional to the enhanced local electric field at the Raman emission wavelength of λ_{em} : $E_{loc}(\lambda_{em}) = G_2 E_0$. Therefore, the overall SERS enhancement depends on the “exciting” and “emitting” field: $G_{SERS} \propto [E_{loc}(\lambda_{ex})/E_0]^2 [E_{loc}(\lambda_{em})/E_0]^2 = G_1^2 G_2^2$. The optimal SERS enhancement requires a delicate balance between exciting and emitting wavelengths with the plasmon peak of the metal nanostructure [40].

SERS Hot Spots

In most cases single PNP is not able to provide sufficient enhancement for practical applications. However, when two nanoparticles are brought close enough to each other they can create an extremely large SERS enhancement in the gap. Such a spatially much localized volume that exhibits extremely high electric field enhancement and produces strong SERS signal is called a hot spot. Hot spots are commonly found in the gaps between nanoparticle aggregates. Figure 13a shows a model to simplify the understanding of the highly enhanced EM field in the hot spot even without considering the LSPR effect [42].

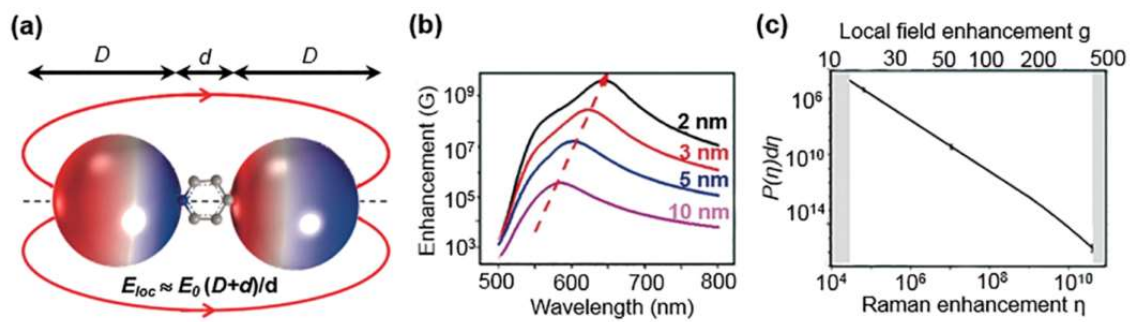


Figure 13. (a) Simplified model to understand the high electromagnetic field inside the gap of two nanoparticles. (b) Gap-size dependent SERS enhancement (G) of Au NPs dimer [43].

When two nanoparticles with a diameter of D and a gap distance of d are placed in a uniform electrostatic field E_0 gets polarized along the dimer axis. The local field in the gap can be estimated to be $E_{loc} = E_0 (D + d)/d$. The EF, i.e. $(D/d + 1)$, can be 6.7×10^6 for $D = 50$ nm and $d = 1$ nm, which is much higher than that obtained from a single particle even without considering the LSPR effect. Theoretical calculation of the enhancement factor of an Ag dimer with 2 nm gap ($\sim 10^9$) is about 10^4 larger than that of Ag sphere ($\sim 10^5$) (Figure 13b). A single dimer can produce a SERS signal equal to that of tens of thousands of single PNPs. The EF can reach 10^{11} with the further decrease of the gap size [44]. Such a high enhancement enables even single-molecule sensitivity for a variety of resonant and nonresonant molecules [45]. Therefore, it is highly important for bioanalytical SERS to design SERS substrates with effective coupling between nanostructures to offer

the highest sensitivity. A common strategy in bioanalytical SERS is to use the target molecules (e.g., antibody–antigen, protein, aptamer, and DNA [46-50]) to induce the aggregation or disaggregation, so that the SERS signal will turn on and off, respectively.

Although NIR lasers are preferred *in vivo* SERS applications Raman scattering of these long wavelengths is intrinsically weak. Therefore, a Raman reporter molecule that enhances SERS at these wavelengths (Figure 14) must be chosen along with selecting the most suitable metal substrate. A good SERS reporter molecule will produce a strong Raman signal and have an affinity for the metal surface. Therefore, Raman reporters often possess polarizable π electron systems within a molecule also bearing functional groups such as thiols, isothiocyanates or amines for surface attachment. In addition, further enhancement can be obtained by incorporating a chromophore as the Raman reporter and selecting a laser excitation wavelength that matches an electronic transition of the chromophore. These can result in surface enhanced resonance Raman scattering (SERRS) signals increased by a factor of up to 10^6 [51].

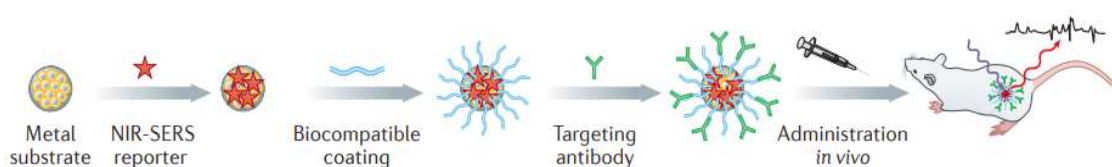


Figure 14. Preparation and administration of *in vivo* SERS nanobiosensors [51].

The recent high demand for a sensitive and simultaneous detection of multiple targets *in vivo* has led the researchers to the use of nanoparticle (NPs) based on SERS technique. In most cases, such sensing modality is realized by anchoring strong Raman active molecule (also known as reporter molecule, RM) on to the surface of metal NPs which can be further conjugated with molecular recognition motifs to render specific targeting. Such nanoprobes are termed as SERS nanotags and their sensitivity will inherently depend on the signal intensity generated by the Raman reporter molecules. SERS nanotags have shown significant advantages over conventional fluorescence-based NPs such as quantum dots [52].

In most of the afore-mentioned SERS tags-based detection techniques, the amount of target molecule is quantitatively analyzed according to the intensity of SERS signal. In an entirely different way, Olivo et al. observed that the Raman frequencies of an antibody conjugated SERS-active molecule can be affected when binding to its target antigen. The frequency shifts were attributed to structural deformations of the reporter molecule as a result of the binding event, which means that a single antibody-conjugated SERS reporter molecule could behave as a nanomechanical biosensor (Figure 15) [53].

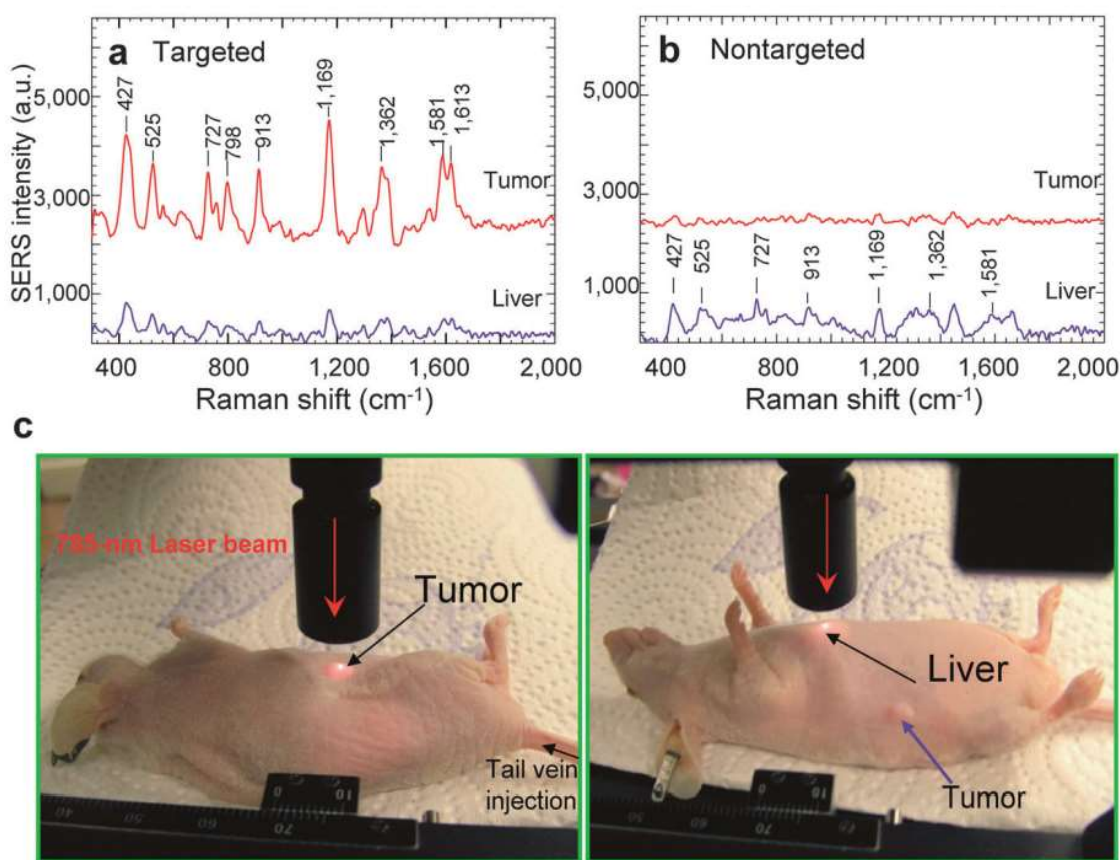


Figure 15. In vivo cancer marker detection using surface-enhanced Raman with antibody conjugated gold nanoparticles that recognize the tumor marker. (a) SERS spectra obtained from the tumor (red) and liver (blue) by using targeted nanoparticles and (b) non-targeted nanoparticles. (c) Pictures showing a laser beam focusing on tumor or liver sites. In vivo SERS spectra were obtained with a 785 nm laser at 20 mW and 2s integration [51].

SERS has become a powerful vibrational spectroscopic and imaging technique over the last decades and its applications in chemical, material and, in particular, biomedical fields are rapidly increasing.

1.2.3 Tip-Enhanced Raman Spectroscopy

Tip-enhanced Raman scattering (TERS) combines surface enhanced Raman spectroscopy (SERS) with Raman-AFM analysis. The goal of this exciting research area is to offer true nanometer scale spatial resolution for Raman.

The principles of TERS are simple although the practical use of TERS is complex and requires considerable expertise in terms of spectroscopy and optics.

Surface enhanced Raman scattering (SERS) can provide orders of magnitude increases in Raman signal intensity. If the tip of an atomic force microscope (AFM) made SERS active (by coating with a SERS active metal or metal nanoparticles), the SERS effect would be expected to occur only within the immediate vicinity of the tip. Since the tip has dimensions typically <100 nm the spatial resolution of such a measurement would depend upon the tip itself and would similarly be <100 nm [54].

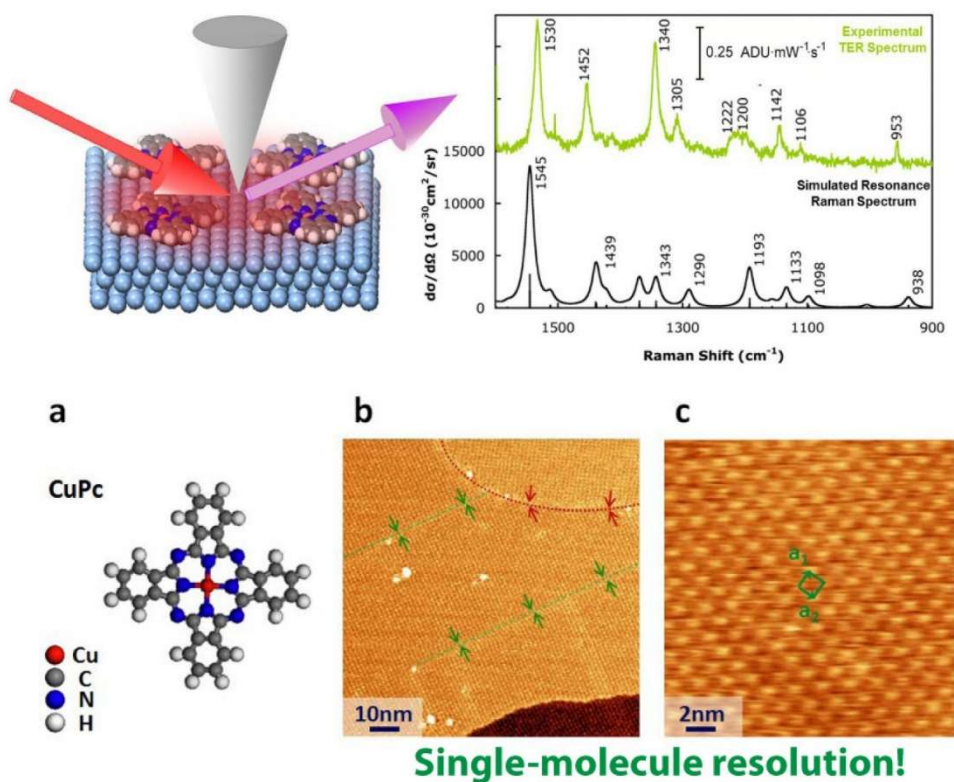


Figure 16. Example of TERS spectra and resolution [55].

A TERS experiment usually involves focusing the excitation laser beam through standard microscope objectives to yield a diffraction limited $\sim 0.5 - 1 \mu\text{m}$ spot size (depending on objective and laser wavelength). The SERS active tip is then brought into contact with the sample within the laser spot.

There will be two main Raman scattering processes: ‘normal’ Raman scattering from the $0.5 - 1 \mu\text{m}$ diffraction limited laser spot and surface enhanced Raman scattering (SERS) from the tip (e.g., tip enhanced Raman scattering). Since SERS can give increases of intensity by factors up to 10^{14-15} , the practical achievement of nanometer scale Raman analysis depends on the intensity of TERS being of a similar or greater magnitude than the ‘normal’ Raman signal. This is not guaranteed since there are concomitant orders of magnitude decreases in the number of molecules being sampled in TERS compared with ‘normal’ Raman [54].

Successful TERS measurements have been made on a range of sample types but achieving such results is not trivial and cannot be expected for every possible sample.

The sensitivity and spatial resolution of Raman spectroscopy can be markedly improved by employing the localized surface plasmon resonance (LSPR) effect in which a high-intensity and localized electric field is generated at the surface of a metal nanoparticle illuminated by light matching its natural plasmon frequency. This phenomenon is exploited in TERS, which has emerged as a powerful nanoanalytical tool for nanoscale chemical characterization over the past years [56–59]. TERS harnesses a combination of LSPR and the lightning rod effect to generate an enhanced electromagnetic (EM) field at the tip of a sharp metallic scanning sample microscopy (SPM) probe positioned in the focal spot of an excitation laser (Figure 17a) [60].

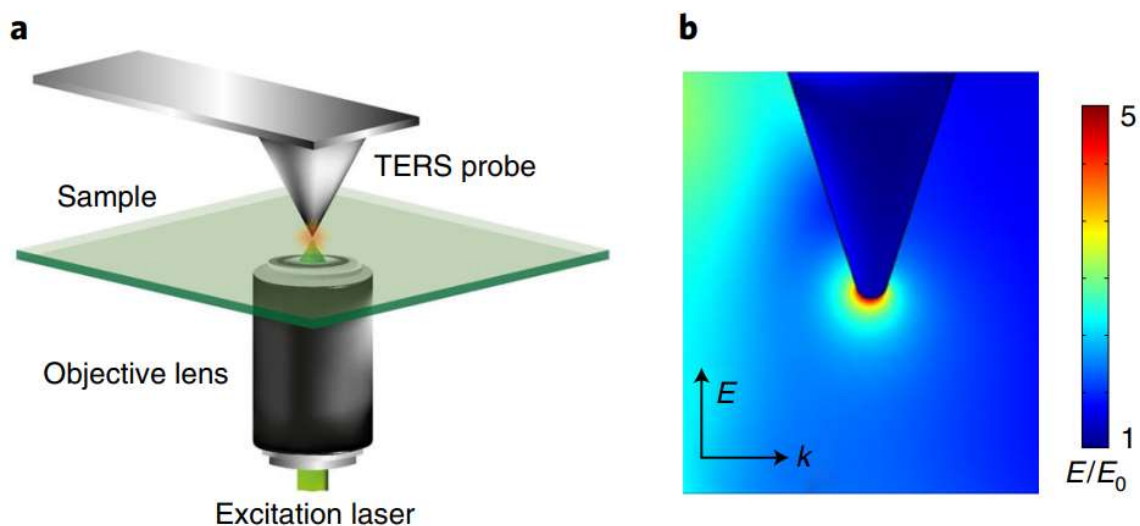


Figure 17. TERS principle. a), Schematic diagram illustrating the principle of TERS, combining the chemical sensitivity of SERS and the high lateral resolution of SPM. b), simulated electric field amplitude map of an Ag TERS probe tip irradiated with a laser of 532-nm wavelength with an electric field parallel to the probe axis calculated using COMSOL Multiphysics [61].

This EM field enhancement can reach several orders of magnitude and is localized to a region similar in dimensions to the probe tip (typically <50 nm) as demonstrated by the simulated map shown in Figure 17b [56]. Together with chemical enhancement effects in some cases, these phenomena result in an increase in Raman scattering signal intensity from molecules present in the vicinity of the probe tip and allow TERS to overcome the diffraction and sensitivity limitations of conventional Raman spectroscopy [61].

Thus, TERS combines the high chemical sensitivity of SERS and the high spatial resolution of SPM (Figure 18) providing nondestructive and label-free surface chemical imaging at nanometer length scales.

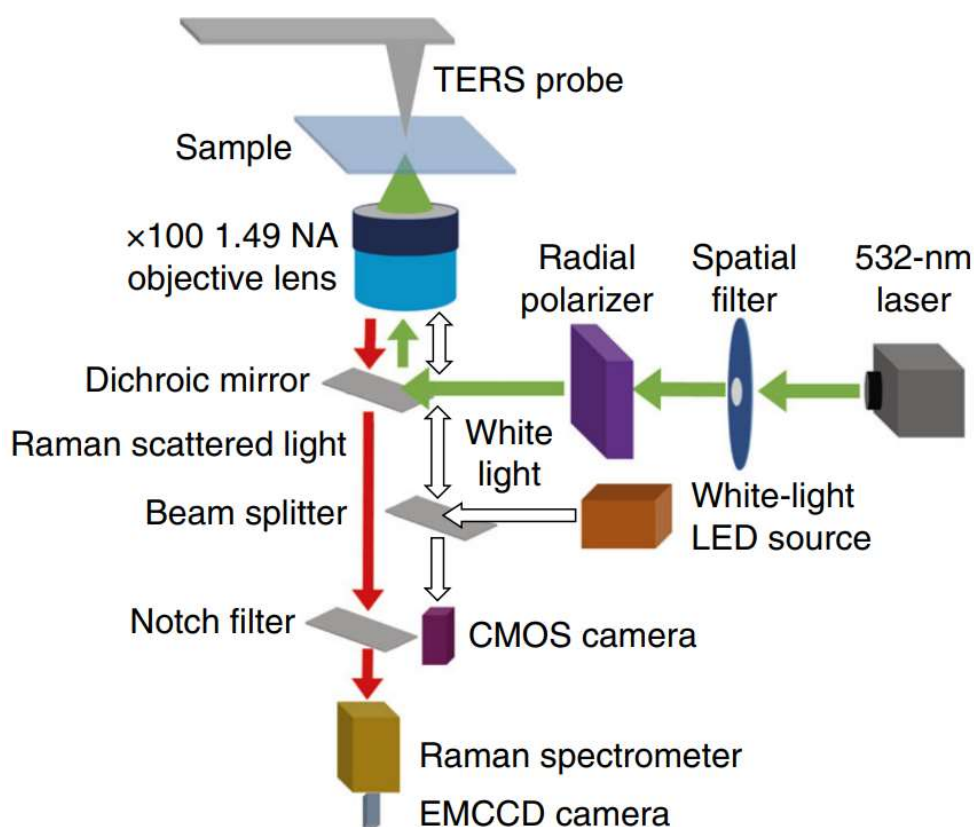


Figure 18. Optical configuration of the TERS system. A schematic diagram depicting the optical configuration of the transmission-mode AFM-TERS microscope. CMOS, complementary metal-oxide semiconductor; EMCCD, electron-multiplying charge-coupled device; LED, light-emitting diode [61].

1.3 Plasmon-induced photocatalytic reaction

1.3.1 Photocatalysis

Photocatalysis is the acceleration of a photoreaction in the presence of a catalyst. In catalyzed photolysis, light is absorbed by an adsorbed substrate. In photogenerated catalysis, the photocatalytic activity (PCA) depends on the ability of the catalyst to create electron–hole pairs, which generate free radicals (e.g. hydroxyl radicals: $\bullet\text{OH}$) able to undergo secondary reactions. Its practical application was made possible by the discovery of water electrolysis by means of titanium dioxide (TiO_2) [62].

In the development of new photocatalysts, many candidates with higher photocatalytic activities than TiO_2 have been studied, most featuring wide bandgaps and only active under UV lights [63].

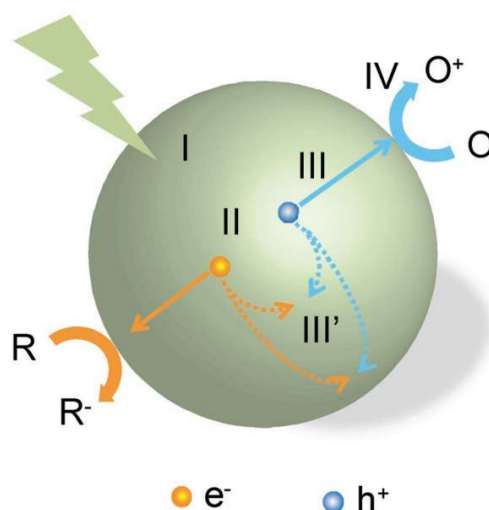


Figure 19. Steps in photocatalytic reaction process. R: chemicals in reductive reactions, O: chemicals in oxidative reactions. (I) light absorption to generate electron-hole pairs; (II) separation of excited charges; (III) transfer of electrons and holes to the surface of photocatalysts; (III') recombination of electrons and holes; (IV) utilization of charges on the surface for redox reactions [64].

Photocatalysis, while varying in details in terms of reactions and mechanisms, may be described by four important steps (shown in Figure 19): (I) light absorption to generate electron-hole pairs; (II) separation of excited charges; (III) transfer of electrons and holes to the surface of photocatalysts; and (IV) utilization of charges on the surface for redox reactions. For the third step, a large portion of electron-hole pairs recombine, either en route to the surface or on the surface sites [65].

The recombination dissipates the harvested energy in the form of heat (nonradiative recombination) or light emission (radiative recombination). The long-lived photogenerated charges on the surface have the potential to promote different redox reactions, the details of which depend on the donor or acceptor properties of the surface absorbed species [66].

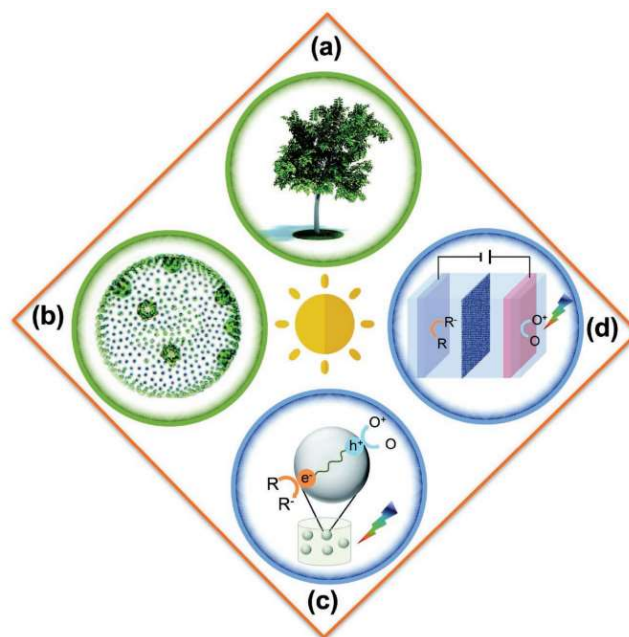


Figure 20. Types of photocatalytic reactions. a) Natural photosynthesis in plants, b) photosynthesis by microalgae, c) nanoparticles photocatalysis, d) photoelectrocatalysis [64].

In an effort to categorize existing approaches of photocatalysis, presented in Figure 6 four classes of reactions. In the first category (Figure 20a), we see the most successful photocatalysis, natural photosynthesis. An ingenious result of billions of years of evolution by Nature, the process has been the main source of our energy supply. Carbohydrates are the key products of these reactions [67]. A variation of this reaction is shown in Figure 20b, where microalgae perform reactions similar to those in plants but synthesize unique chemicals such as H_2 or other valuable chemicals (e.g., ethanol, butanol, glycerol, and isoprene) [67]. When it comes to artificial photosynthesis systems, a great number of variations exist. They may be grouped into two general types as summarized in Figure 6c and 6d. When the reduction and oxidation reactions are not intentionally separated (Figure 20c), a system with the benefit of inherently low cost is obtained. Note that reactions involving both heterogeneous and homogeneous catalysts can be included in this category. A competing strategy is to physically separate the reduction and oxidation sites. A wired version of the last strategy is shown in Figure 20d.

But the wire is not essential here. A back-to-back wireless configuration falls in the same category, as well. A key distinguishing feature of Figure 6c and 6d is

whether the reduction and oxidation sites are physically separated by a reasonable distance (greater than a few hundred nanometers) [64].

1.3.2 Plasmon-induced hot electrons

Metal–semiconductor heterogeneous nanorods (NRs) can greatly enhance and trap light mainly by scattering photons, plasmon resonance energy transfer, and plasmon-induced hot electrons from metal nanostructures [68]. Diverse metal–semiconductor heterogeneous nanostructures have recently been of significant interest both in the fundamental light–matter interaction mechanism and technological applications, including photovoltaics, photocatalysis, and spectroscopic applications, particularly in SERS, on account of the advantages of broad spectral tunability, large absorption cross sections, and long-term stability of plasmonic metal nanostructures. By exploring the chemical enhancement of semiconductor nanostructures along with electromagnetic enhancement of plasmonic metal nanostructures, many research efforts have been focused on the pursuit of more sensitive SERS-active substrates, possibly extending to the level of single molecule detection sensitivity (Figure 21) [69].

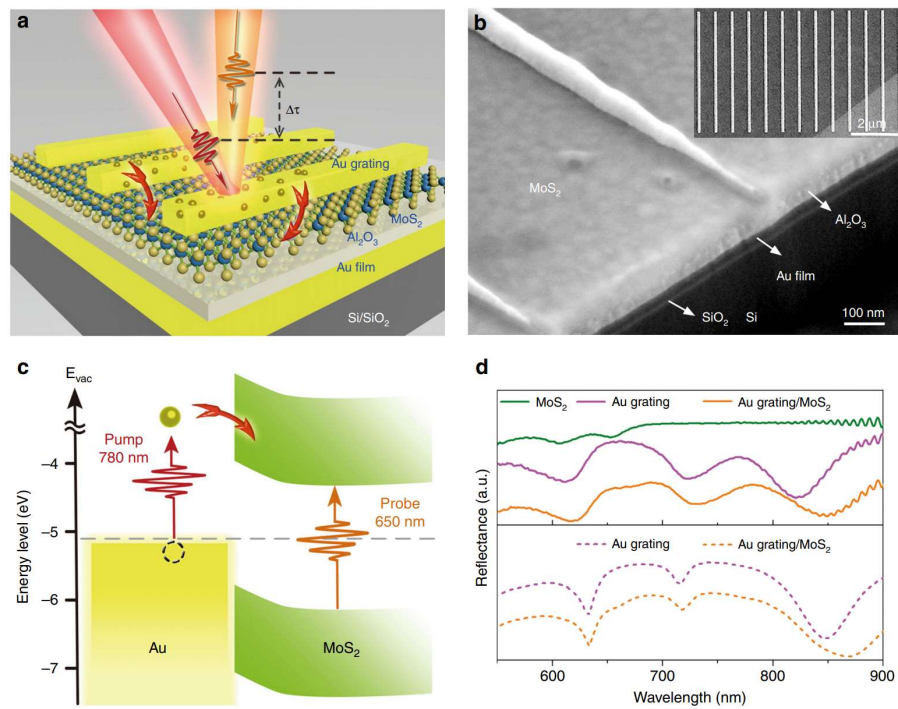


Figure 21 Characterizations of the heterostructure, including an SEM image, a band alignment diagram and reflectance spectra and schematic of plasmonic hot electrons pumping [70].

Since chemical enhancement is mostly related to the CT between the absorbate molecules and semiconductor, the highly-efficient injection of plasmon-induced hot electrons into the semiconductor has become a key problem [69].

For now, there are two different plasmon-induced hot electron injection mechanisms. One is the plasma-induced hot electron transfer mechanism (PHET), which refers to the transfer of hot electrons formed by the plasmon decay of metal nanostructures into a coupled semiconductor, and the other is the plasmon-induced metal-to-semiconductor interfacial charge-transfer transition (PICCT) mechanism, which refers to the direct generation of an electron in the coupled semiconductor and an electron hole in the plasmonic metal in the decay process of plasmons. The PICCT mechanism was first reported to have a highly efficient plasmon-induced electron hole pair separation in Au–CdSe NRs with Au tips at both the ends of CdSe NRs. CdSe is a narrow band gap semiconductor with a band gap of 1.76 eV and the Schottky barrier of Au–CdSe is 0.64 eV [69].

2 Materials and methods

2.1 The name of the research

Investigation of plasmon-induced photocatalytic reaction at the single nanoparticle level.

2.2 Objectives of the research

The purpose of the work is to investigate plasmon-induced reaction with different spectroscopic methods such as: Raman, SERS, TERS at a single nanoparticle with high resolution and 3D physical model creation which allows us to understand how to drive and control this type of reaction for photochemistry, nanobiosensors, theranostics of cancer tumor.

Research objectives:

1. To investigate plasmon-induced photocatalytic reaction mechanism with comparing Raman spectra of bulk 4-NBT absorbed on glass, and monolayer absorbed on plasmonic nanoparticles;
2. To make SERS measurements with Au/Ag nanocages and nanorods covered with monolayer of 4-NBT at $\lambda=532$ nm, 638 nm, 785 nm laser irradiation. To study

the obtained SERS spectra for the presence of photocatalytic activity and the intensity of this activity.

3. To evaluate the role of temperature in plasmon-induced photocatalytic reaction by increasing the temperature from 25 to 200 °C with a 20 °C step. To investigate how the intensity ratio NO_2/NH_2 changes and how many 4-NBT molecules turn into 4-ABT by comparing SERS spectra peaks specific for these molecules at a particular Raman shift distance.

4. To make TERS measurements with Au/Ag nanocubes covered with 4-NBT at $\lambda=638$ nm laser irradiation. To investigate at the particular nanoparticle the obtained TERS spectra for the presence of photocatalytic activity and the intensity of this activity.

5. To investigate purely photon influence on photocatalytic reaction by increasing power density and photon intensity with focus changing without external heating;

6. To create 3D physical model of TERS experiment in COMSOL Multiphysics wave-optics module. First to make a model with single Au (Johnson&Christy, 1972) spherical nanoparticle, next to make a model with Ag (Johnson&Christy, 1972) cube nanoparticle and Au tip above, and with Si substrate with Au tip above.

7. To create 3D physical model of photothermal heating during TERS in COMSOL Multiphysics Joule-heating module with Ag cube nanoparticle and Au tip above, and with Si substrate, Au tip above.

8. To compare all results, to process the data and to make a conclusion of this work.

2.3 Places of research

Academic building of TPU «Since park», labs № 203, 303;

University of Technology of Troyes labs;

Chemnitz University of Technology labs;



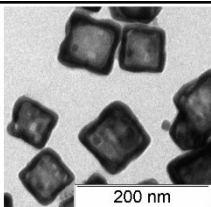
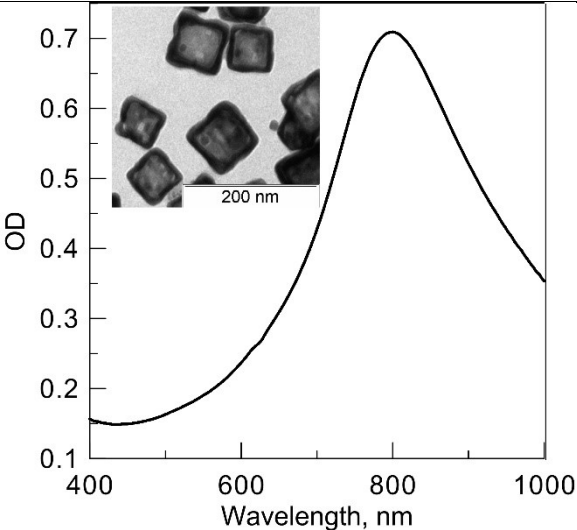
Saratov State University labs.

2.4 Test substances

2.4.1 Information about the objects of the research

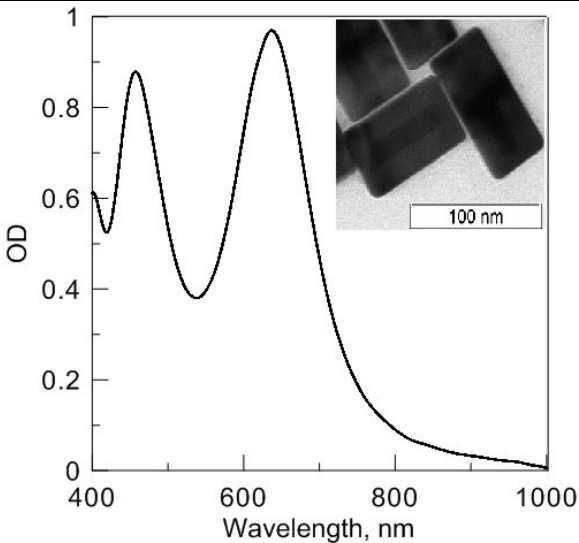
Investigated substances is Au/Ag nanocages, nanocubes, nanorods covered with monolayer of 4-NBT which is restored up to 4-ABT and DMAB:

Au/Ag nanocages

Structural formula:
<div style="display: flex; justify-content: space-around; align-items: center;"><div style="text-align: center;"> Au</div><div style="text-align: center;"> Ag</div></div>
SEM picture and absorption spectrum:
<div style="display: flex; align-items: center;"><div style="flex: 1;"></div><div style="flex: 2;"></div></div>
IUPAC: Gold/Silver nanocages
Chemical name: Au/Ag nanocages
Gross formula: [Au]/[Ag]
Molecular mass: 196.97/107.87 g/mol
CAS № 7440-57-5/ 7440-22-4
Storage conditions: at room temperature, protected from water and direct light in clean, dry, inert atmosphere, in sealed bag

Au and Ag nanocages are a solution of green and blue colors (because of their optical properties). Such type of particles can be produced by reacting silver nanoparticles with chloroauric acid (HAuCl_4) in boiling water.

Au/Ag nanorods

Structural formula:
<div style="display: flex; justify-content: space-around; align-items: center;">AuAg</div>
SEM picture and absorption spectrum:

IUPAC: Gold/Silver nanorods
Chemical name: Au/Ag nanorods
Gross formula: [Au]/[Ag]
Molecular mass: 196.97/107.87 g/mol
CAS № 7440-57-5/ 7440-22-4
Storage conditions: at room temperature, protected from water and direct light in clean, dry, inert atmosphere, in sealed bag

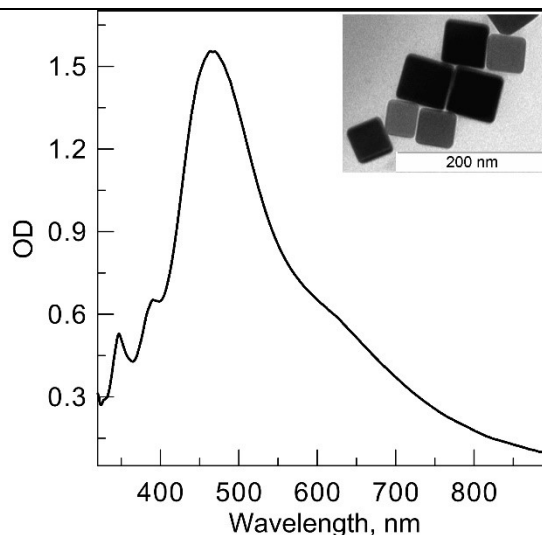
Au and Ag nanorods are a solution of violet and deep blue colors (because of their optical properties). The seed-mediated growth method is the most common and achieved method for synthesizing high-quality gold/silver nanorods. A typical growth protocol involves the addition of citrate-capped gold/silver nanospheres, served as seeds, to the bulk HAuCl_4 growth solution.

Ag nanocubes

Structural formula:

Ag

SEM picture and absorption spectrum:



IUPAC: Silver nanocubes

Chemical name: Ag nanocubes

Gross formula: [Ag]

Molecular mass: 107.87 g/mol

CAS № 7440-22-4

Storage conditions: at room temperature, protected from water in clean, dry, inert atmosphere, in sealed bag

Ag nanocubes are a solution of yellow color (because of their optical properties). Silver nanocubes can be synthesized using ethylene glycol as a reducing agent and PVP as a capping agent, in a polyol synthesis reaction (vide supra). A typical synthesis using these reagents involves adding fresh silver nitrate and PVP to a solution of ethylene glycol heated at 140 °C.

Si wafer (substrate)

Structural formula:

Si

IUPAC: Silicon wafer

Chemical name: Si wafer

Gross formula: [Si]

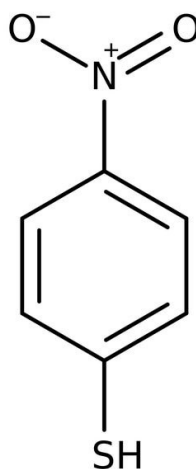
Molecular mass: 28.09 g/mol

CAS № 7440-21-3

Storage conditions: should be stored at temperature between 18°C and 24°C, relative humidity of less than 30%, and in clean, dry, inert atmosphere (e.g. Nitrogen), and in a vacuum sealed bag

4-nitrobenzenthioi, 4-NBT

Structural formula:



IUPAC: 4-nitrobenzene-1-thiol

Chemical name: 4-nitrobenzenethiol, 4-NBT

Gross formula: $\text{C}_6\text{H}_5\text{NO}_2\text{S}$

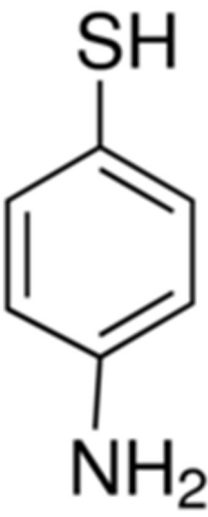
Molecular mass: 155.17 g/mol

CAS № 1849-36-1

Storage conditions: at room temperature, protected from water in clean, dry, inert atmosphere, in sealed bag

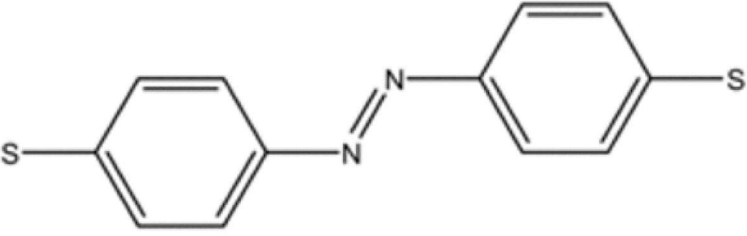
4-NBT is a yellow powder, it dissolves only slightly in water and will evaporate to air. It is produced on a large scale from benzene.

4-aminobenzenthion, 4-ABT

Structural formula:

IUPAC: 4-aminobenzene-1-thiol
Chemical name: 4-aminobenzenethiol, 4-ABT
Gross formula: C ₆ H ₇ N ₁ S ₁
Molecular mass: 127.15 g/mol
CAS № 477741-48-3
Storage conditions: at 2-8°C of temperature, protected from water in sealed bag

4-ABT only occurs from 4-NBT in the process of photocatalytic reaction. Color is couldn't be identified.

4,4-dimercaptoazobenzene, DMAB

Structural formula:

IUPAC: 4,4'-dithiobis(benzene)
Chemical name: 4,4-dimercaptoazobenzene, DMAB

Gross formula: C ₁₂ H ₁₂ N ₂ S ₂
Molecular mass: 248.4 g/mol
CAS -
Storage conditions: at 2-8°C of temperature, protected from water, in sealed bag

DMAB as well as 4-ABT only occurs from 4-NBT in the process of photocatalytic reaction. Color couldn't be identified.

2.4.1.1 Preparing the substance for use

Solutions and depositions of substances at Si wafer for research were prepared in the laboratory one day before the experiment. Pure glassware was used to prepare the water solutions of 4-NBT. All chemicals were obtained commercially and used without further purification.

2.4.1.2 Actions with residues

The remains of ready-made solutions of substances were disposed of according to the rules established by SanPiN 2.1.7.2790-10 and GOST 30772-2001. The primary packaging of the studied substances, as well as disposable inventory used to work with solutions of the studied substances, were disposed of as food and household waste in the prescribed manner.

2.5 Research methods

2.5.1 Fabrication of Ag Nanocubes and Au Nanocages.

NPs were prepared by a protocol previously reported by Skrabalak et al. [71], with a minor modification [72]. In the first step, Ag nanocube templates samples) were prepared by mixing 30 mL of EG, a sodium sulfide solution in EG (0.35 mL, 3 mM), a PVP solution in EG (7.5 mL, 20 g/L), and a silver nitrate solution in EG (2.5 mL, 48 g/L) under argon flow at a temperature of 150 °C. The resultant Ag nanocubes were washed by centrifugation (12000g, 30 min) and redispersed in 40 mL of ethanol. The isolated Ag nanocubes were converted into Au nanocages via the galvanic replacement reaction [72]. To this end, 2 mL of the as-prepared nanocube suspension was added to the PVP water solution (100 mL, 1 g/L). The mixture was heated at 100 °C under magnetic stirring, followed by the dropwise

addition of 10 mL of 1 mM HAuCl₄. The resulting nanocages were washed by centrifugation (12000g, 20 min) and were redispersed in 4 mL of water.

2.5.2 Au/Ag Nanocuboids synthesis

First, Au nanorods were prepared by a seed-mediated growth in a binary surfactant mixture as described elsewhere [73, 74]. Then, 100 μ L of 100 mM AgNO₃ solution was added to a mixture of 4 mL of Au nanorods and 12 mL of 20 mM CTAC, followed by the addition of 400 μ L of 100 mM ascorbic acid as a reductant.³⁴ The mixture was incubated and unstirred at 70 °C for 3 h. After that, the obtained Au/Ag nanocuboids were washed and finally redispersed in 4 mL of water.

2.5.3 Characterization of plasmonic nanoparticles

Extinction spectra were measured with a SPECORD 250 spectrophotometer (Analytik, Jena, Germany). Transmission electron microscope (TEM) images were obtained with a Libra-120 TEM (Carl Zeiss, Jena, Germany) at the “Simbioz” Center in Saratov for the Collective Use at IBPPM RAS.

2.5.4 Experimental setup and measurement technique

We performed Raman spectroscopy, SERS and TERS measurements on aggregates and individual NPs at 3 different wavelengths. Micro-Raman spectroscopy experiments were performed within the spectral range 1000–1700 cm⁻¹ using the 532 (green), 638 (red), and 785 (IR) nm lines of solid-state lasers in a XploRA Raman spectrometer (Appendix A). A LabRAM HR800 system (Appendix B) was used for the temperature dependent SERS measurements under green and red laser illumination, 514.7 and 633 nm, respectively. Both spectrometers were coupled to an optical microscope Olympus BX-40. A 100 \times objective (N.A. 0.9) was used to illuminate the sample and to collect the Raman signal in the backscattering geometry. A long working distance objective was used (50 \times LWD, N.A. 0.5) for the temperature-dependent experiments. The experiments at different focus distances (power density) were realized using a piezoelectric scanner that varied the laser focus (with a 100 LWD objective, N.A. = 0.7) below and above the sample plane.

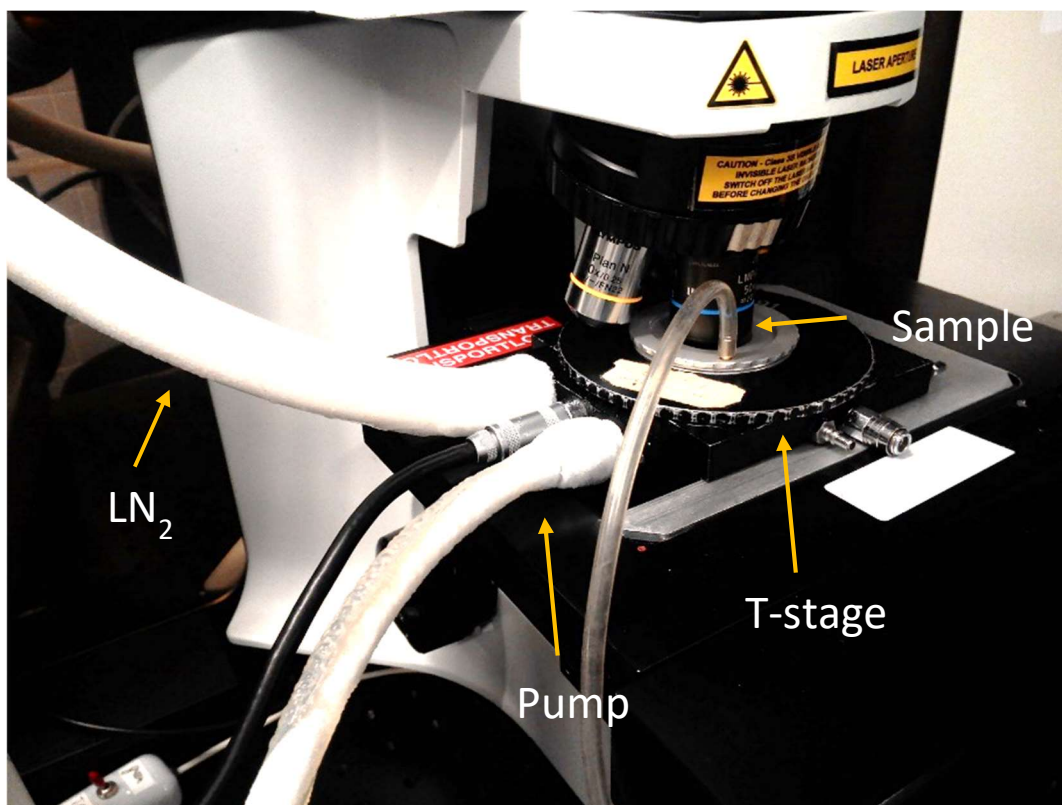


Figure 22. TERS system.

A charge-coupled device was used for the detection of the Raman signal using a diffraction grating of 600 lines per millimeter, a spectral resolution of at least 4 cm^{-1} , and an acquisition time of 1 s. The laser power was limited to the range 0.5–2 mW to avoid unintended modifications of the molecular layers.

The colloids of Au and Ag NPs were first dropcasted on a Si surface and dried in air. 4-NBT molecules were dissolved in ethanol and used as a stock solution for the functionalization of the metal NPs deposited on Si wafers. The NP-coated silicon wafer was immersed in the 4-NBT solution overnight to ensure the formation of a monolayer of 4-NBT on the surface of NPs. Afterward, the sample was taken out, rinsed gently with ethanol to remove possible physically absorbed molecules, and finally dried under N_2 flow.

Two different setups were used in the side illumination/collection configuration: a home-coupled TERS system (Figure 22) with an Agilent 5420 AFM (Appendix D) and a LabRam HR800 Raman spectrometer, and a dedicated TERS system OmegaScope-R (Appendix C) from AIST-NT Inc. coupled to an Xplora Raman spectrometer. Raman spectroscopy was performed under red (633 nm and

638 nm) and green (514.7 nm) laser excitations. The light of 1 mW power was focused with a 50x LWD objective (N.A. 0.42) in the Agilent-HORIBA system, and 160 μ W focused with a 100x LWD objective (N.A. 0.7) in the AIST-NT-Xplora HORIBA system. The power density was 105 and 133 W/mm² for the two experimental setups. A grating of 600 l/mm was used to disperse the scattered light on CCD detectors.

2.5.5. Finite element method in COMSOL Multiphysics for creation of 3D simulation model

For physical part (EM field and temperature) computation of our experimental results we decided to create a 3D model of electromagnetic wave scattering by NP in electromagnetic waves, frequency domain and Joule-heating modules at commercial software COMSOL Multiphysics. COMSOL allows to use Finite element method (FEM) to solve the wave Maxwell equation in particular edges and points of the model with mesh (Figure 23). Laser beam propagation was approximated by a plane electromagnetic wave with an electric field component $E=1$ V/m. Two different meshes was created. For PMLs it was triangular surface mesh with 5-layer sweep. For all other model objects (air, NPs, substrate, tip) it was tetrahedral mesh. Mesh also was adapted and more precise at the regions of interest such as shown in Figure 23. All obtained intensities of the electric field are presented in $V/m \cdot 10^4$.

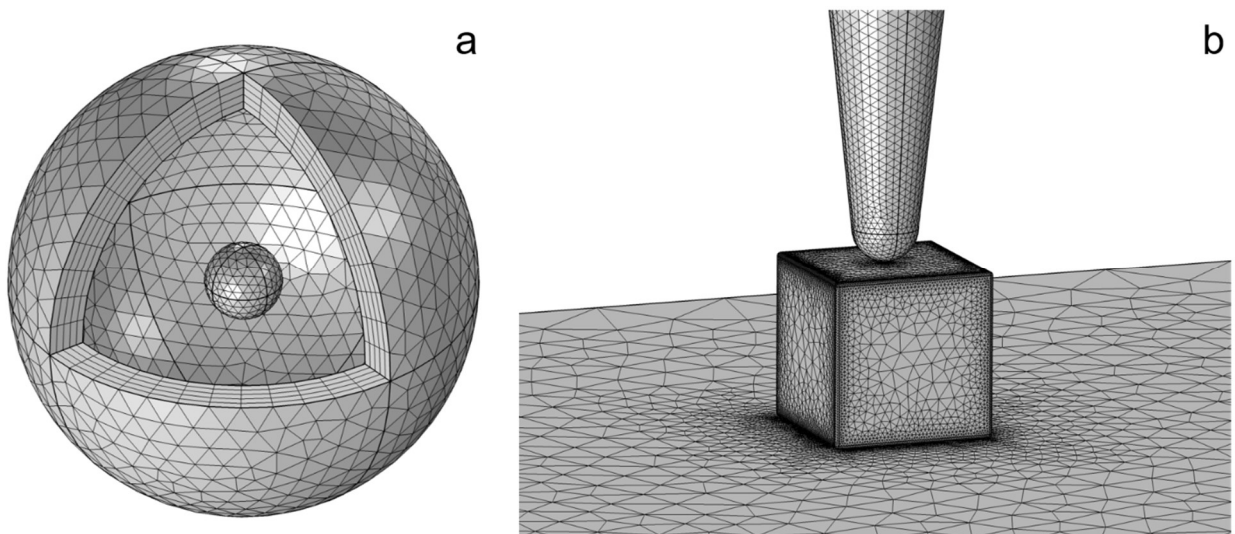


Figure 23. FEM mesh in COMSOL Multiphysics: a) spherical NP, b) cubic NP.

Two shapes of nanoparticles were investigated: a sphere and a cube. Electromagnetic wave scattering of spherical shape is a well-known process and is needed to be checked in COMSOL Multiphysics to find out if we can reach the real condition of the experiment. In our research we perform wavelength parametric sweep from 100 to 900 nm with 20 nm step of incident plane parallel wave from side in vertical polarization along Z axis and from top in horizontal polarization along X axis. Size of sphere also was swept from 10 to 100 nm. Material of nanosphere was «Au Johnson&Christy, 1972» chosen in COMSOL library. Perfectly matched layer (PML) was used for definition of boundary condition and had a spherical shape (Figure 23a)

Next, we performed simulation of Ag nanocube, Au tip «Au/Ag Johnson&Christy, 1972» and Si substrate «Si Green, 2008». All materials were taken from COMSOL library. Model components had the following parameters: 100x100 nm cube with 2 nm radius fillet; 20 nm radius of Au tip with visible length of 300 nm; 1x1 μm Si substrate. Distances ‘the substrate - the tip’ and ‘nanocube – tip’ were 2 nm. Incident 638 nm plane parallel wave propagates from a side with 60 degrees to horizontal X axis. PML for boundary condition in this case was cubical shape to visualize scattering from flat facer of model components (Figure 23b).

The next step was evaluation and visualization of temperature by applying electric potential, value of which was converted from electric field intensity acquired at the previous step. It was applied between model components the same as at previous case but now in different Joule – heating COMSOL module.

3 Results and discussion

3.1 Raman spectroscopy insights on plasmon-induced photocatalysis

We performed SERS to 4-NBT adsorbed on two different substances, bulk 4-NBT on galss (a) and monolayer on Ag NPs (b). Figure 24a shows that there are no any changes in a region of interest at 1432 cm^{-1} where NH_2 peak related to 4-ABT molecule should be. 3 wavelengths (532, 638 and 785 nm) were used, but we

did not see any photocatalytic activity. This makes it possible to say that photocatalysis doesn't occur despite the huge amount of 4-NBT. Meanwhile in Figure 24b, only monolayer is adsorbed on Ag nanocubes while we can see a strong photocatalytic conversion from 4-NBT to 4-ABT and high intensity ratio between NO_2/NH_2 peaks.

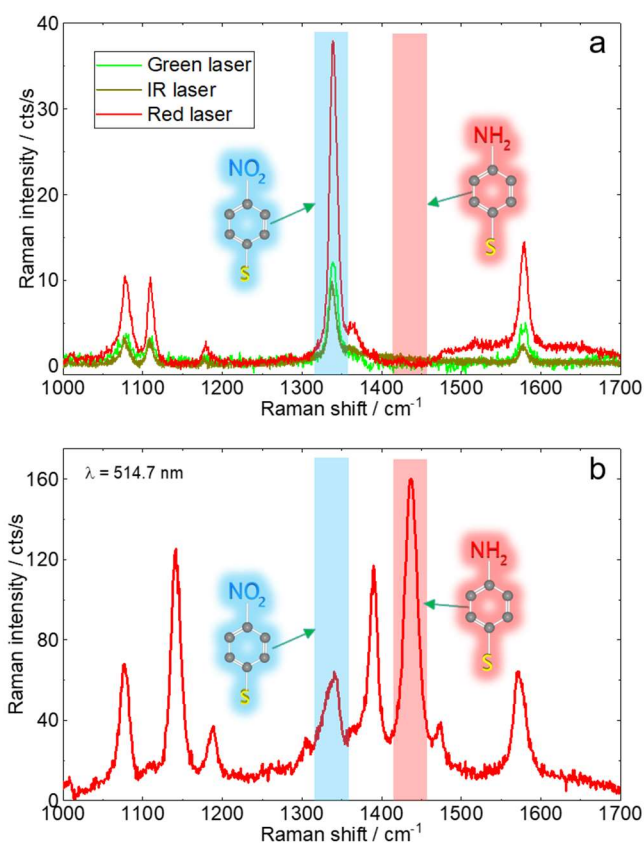


Figure 24. Raman spectra of: a) bulk 4-NBT adsorbed on glass, measured with 532 (green) 638 (red), and 785 (IR) nm wavelength laser irradiation; b) monolayer of 4-NBT adsorbed on Ag nanocubes at Si substrate with 514.7 nm wavelength laser irradiation.

It is known that plasmon-induced photocatalytic reaction may occur due to the excitation of electrons on the surface of plasmonic nanoparticles. This happens because of «hot electron» transfer from plasmon nanocubes molecules to 4-NBT, which induced such conversion. Plasmon-induced photocatalytic reaction occurs due to the following reasons: so-called «hot electrons» transfer mechanism, charge transfer, hybridization metal – molecule and high temperature. In case of «hot

electrons» transfer, after laser irradiation is applied to sample with plasmonic NPs and photocatalytic active molecule, enough energy is communicated to the electrons to transfer from the valence band to the conduction band as shown at Figure 25. After that the two electrons come to Nitrogen (N) molecule and a series of reactions begins.

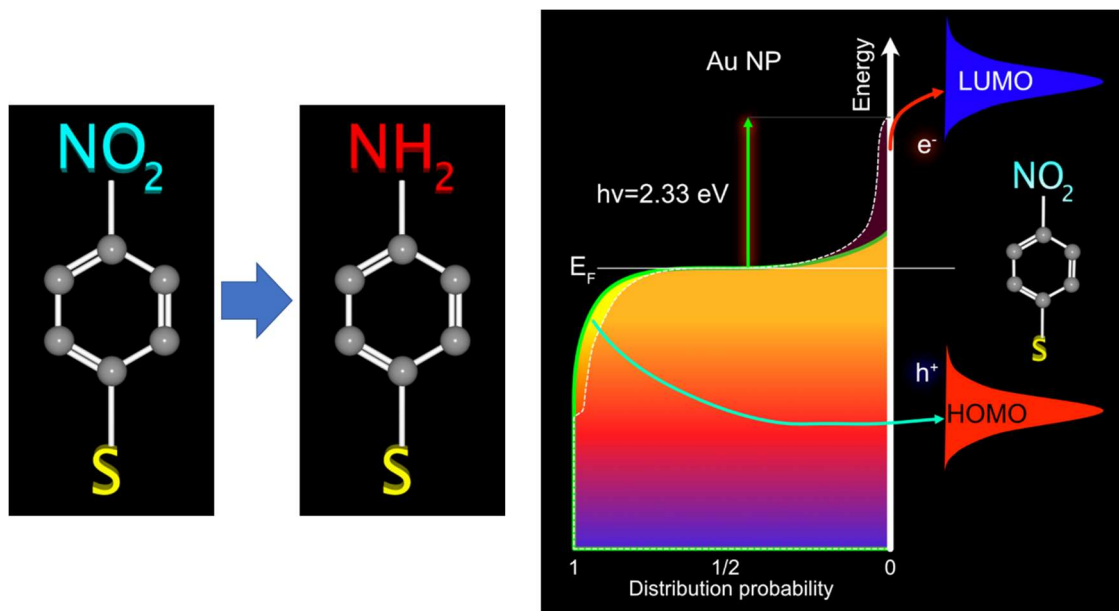


Figure 25. Schematic of 4-NBT to 4-ABT conversion due to electron transfer from HOMO (valance band) to LUMO (conduction band).

As a result of these reactions, the degree of N oxidation changes from +5 to +3 since the electrons are negatively charged particles. The nitro group is replaced by an amino group.

3.2 SERS spectra comparison of 4-NBT on Au/Ag nanocages and Au/Ag nanorods. Influence from LSPR

Using the same SERS technique, we obtain a few more SERS spectra of 4-NBT but in this case it was adsorbed on Ag/Au nanocages and nanorods. If we look at Figure 26a, low photocatalytic activity can be observed at 532 nm wavelength, which completely unrelated to plasmon resonance peak. It also noticeable that maximum Raman intensity is only $0.5 \text{ ctss}^{-1}\text{mW}^{-1}$.

However, red and infrared wavelengths which are closer to LSPR were used but no photocatalytic reaction was observed. In Figure 26b we can see only NO_2

peak at 1339 cm^{-1} with high Raman intensity. This led us to the question: Is LSPR excitation enough for plasmon photocatalysis?

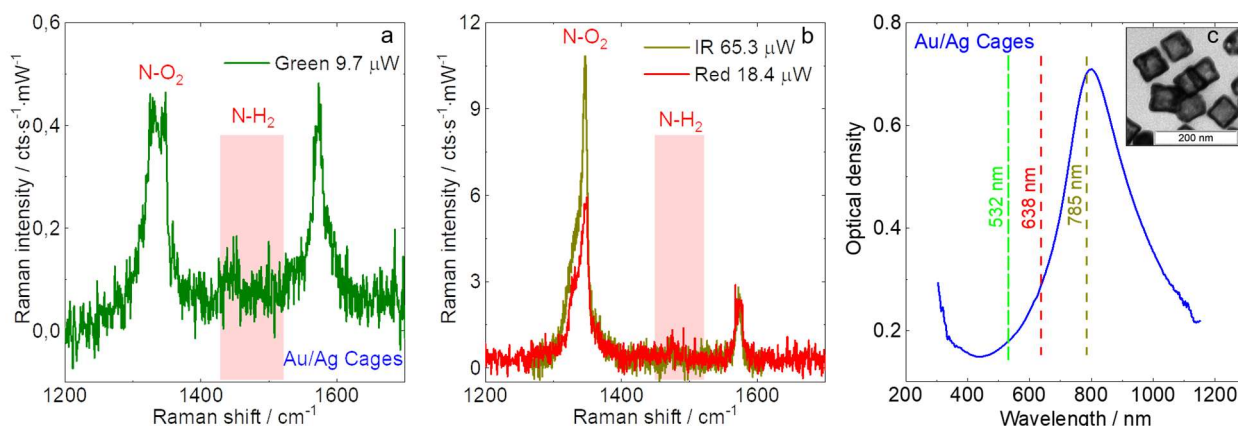


Figure 26. SERS spectra of Au/Ag nanocages on Si wafer with monolayer of 4-NBT adsorbed on NPs: a) at 532 nm green wavelength, b) at 638 and 785 nm wavelengths, c) optical density characteristic of Au/Ag nanocages.

Our investigation of Au/Ag nanorods (Figure 27) shows that even at a wavelength far from LSPR peaks with low Raman intensity we can observe strong conversion of NO_2 to NH_2 which means higher photocatalytic activity.

In Figure 27a all three-laser wavelengths were used (IR, red, green), and we can see high enhancement of Raman signal from the sample at 638 nm wavelength which is obvious due to LSPR peaks of Au/Ag nanorods and other IR. Green wavelengths results are almost unseen because of a large scale for red one. But if we look at Figure 27b where rescaled SERS spectra for green and IR wavelengths is presented – much higher photocatalytic intensity ratio of 4-NBT to 4-ABT can be observed.

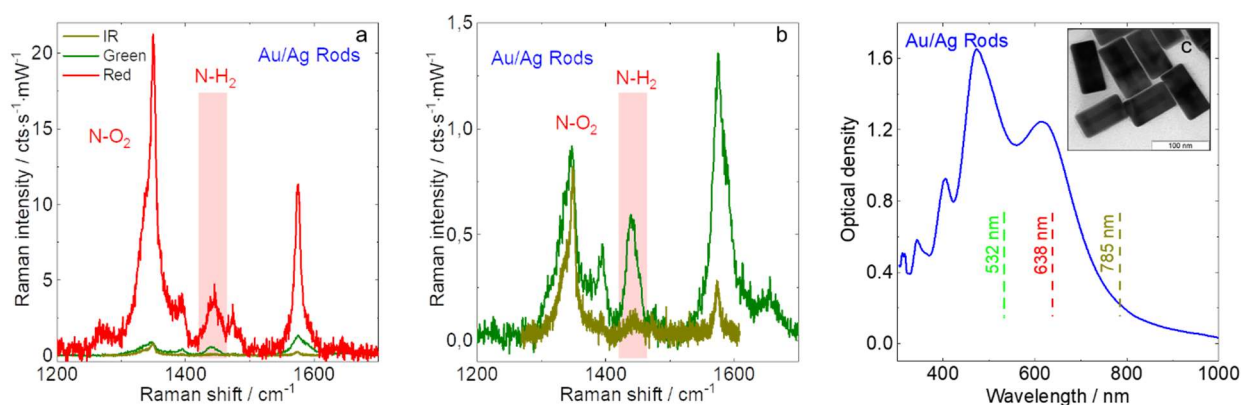


Figure 27. SERS spectra of Au/Ag nanorods on Si wafer with monolayer of 4-NBT adsorbed on NPs: a) at 532, 638 and 785 nm wavelengths, b) at 532 and 785 nm wavelengths, c) optical density characteristic of Au/Ag nanorods.

To sum up, it is possible to claim that high SERS signal intensity caused by local surface plasmon resonance does not correlate with the high photocatalytic activity of a 4-NBT molecule.

3.3 Temperature influence on photocatalytic activity

All previous SERS measurements were performed at the room temperature (25 °C). Next, temperature was increased up to 200 °C. SERS spectra measurements were performed at every 20 °C as shown at Figure 28b.

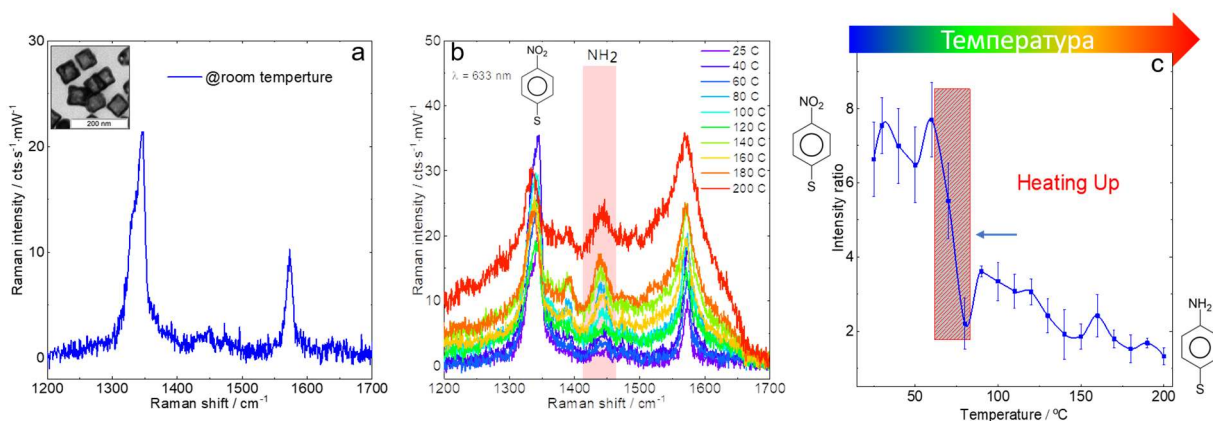


Figure 28. SERS spectra of 4-NBT adsorbed on Au/Ag nanocages on Si substrate: a) SERS spectra at room (25 °C) temperature, b) SERS spectra at 25-200 °C temperatures with a 20 °C step, c) Intensity ratio of NO₂/NH₂ at 25-200 °C temperatures.

In Figure 28a no any photocatalytic activity is observed. However, if we increase the temperature from 25 °C to 200 °C as presented in Figure 28b, according to the Arrhenius law the next tendency can be seen: the more temperature is, the more 4-NBT molecules became 4-ABT and we get more intensive photocatalysis:

$$\ln \left(g \cdot \text{Int.} \frac{4ABT}{4NBT} \right) = -\frac{E_a}{R} \left(\frac{1}{T} \right) + \ln(A), \quad (3)$$

where E_a – activation energy; R – gas constant; T – temperature; A – preexponential factor; $\left(g \cdot \text{Int.} \frac{4ABT}{4NBT} \right) = k$ – speed of reaction.

Figure 28c shows intensity ration between reagent and product (NO_2/NH_2) which is significantly decreased with temperature rising. Particularly large drop of intensity ratio is observed at the temperature of 80 °C.

Thus, we can say that the temperature has a high effect on the intensity of the photocatalytic reaction and can drive it.

3.4 TERS maps with HR insights of individual plasmonic nanoparticles

TERS measurements were performed at the Ag nanocubes in Figure 29. Here we can clearly see an individual nanoparticle with high resolution (Figure 29b) and its corresponding TERS intensity maps (Figure 29c).

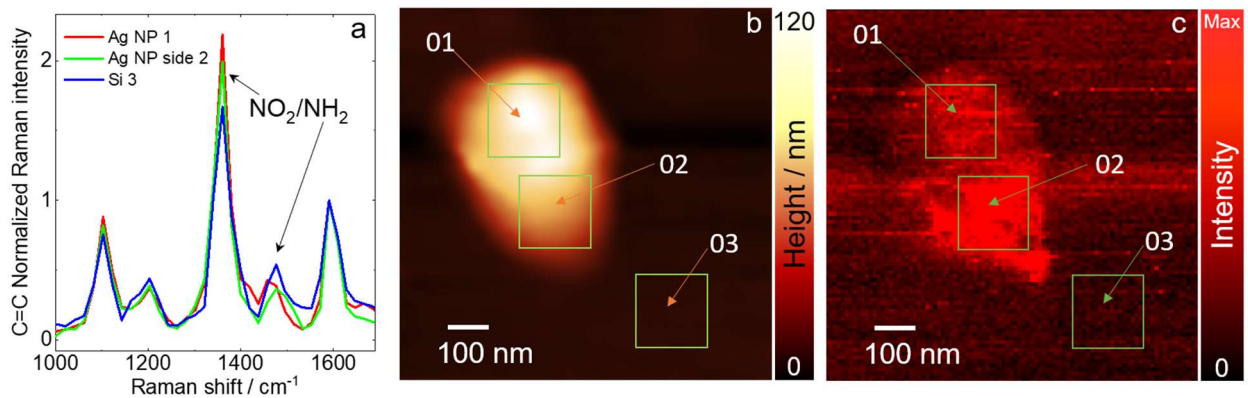


Figure 29. TERS performed on Ag nanocube with size of 100x100 nm, 4-NBT adsorbed on Ag NPs and Si wafer, wavelength of laser irradiation 638 nm: a) Normalized C=C TERS spectra from 3 regions: on Ag nanocube, on a side of Ag nanocube and on Si substrate, b) AFM topography image of individual Ag

nanocube with maximum height of 120 nm, c) TERS intensity map of Ag NP and Si wafer.

According to the map data and intensity spectra we can identify the 3 places of interest where the most intense photocatalytic activity is observed. Comparison of the AFM and TERS maps topography images allows us to speak about the phenomenon of temperature drift of a nanoparticle. In this case, the effect of temperature drift is weakly expressed and manifests itself only in the presence of a certain “shadow” of the nanoparticle thereby not interfering with the analysis of the result (Figure 29b).

Considering the spectra obtained from 3 points, we can judge the maximum amplification of the Raman signal in the first region, which is located on the nanoparticle. The second largest gain region is located at the interface between the nanoparticle and the substrate, and the last region on the Si substrate (Figure 29a). However, if we consider the ratio of NO_2 and NH_2 peaks, the maximum photocatalytic conversion is observed in the third region on Si substrate.

We have two possible cases. On the one hand, we can observe the conversion of 4-NBT to 4-ABT. On the other hand, nitrogen can create connection with nitrogen of another 4-NBT molecule and become 4,4-dimer-capto-azo-benzen or DMAB as shown in Figure 30. We have investigated two regions – on Si and on Ag NP. If we compare AFM image and TERS intensity map, we will notice that the most intensive place is on Ag NP (Figure 30a, b).

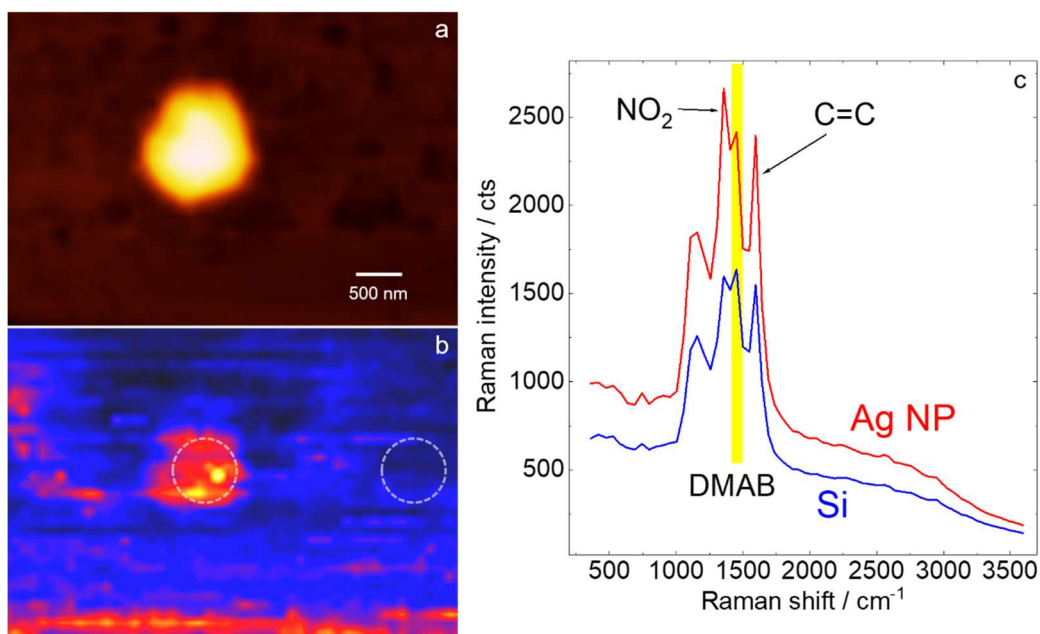


Figure 30. TERS on individual Ag nanocube with 4-NBT adsorbed on Ag NPs and Si wafer, wavelength of laser irradiation 638 nm: a) AFM topography image, b) TERS intensity map, c) Normalized C=C TERS spectra from 2 regions: on Ag NP and on Si substrate.

However, like in previous TERS experiment with 4-NBT to 4-ABT conversion, we can observe TERS spectra in Figure 30c. By comparing the TERS intensity peaks that relate to NO_2 and DMAB, respectively, we can say that 4-NBT is converted to DMAB more in the region on Si. Though TERS intensity is higher on Ag NP photocatalytic activity is lower than in the region on Si.

Based on the above facts, we can conclude that a higher intensity of the TERS signal does not correlate with a higher photocatalytic activity of the molecule. This phenomenon was also observed in previous studies with the SERS technique.

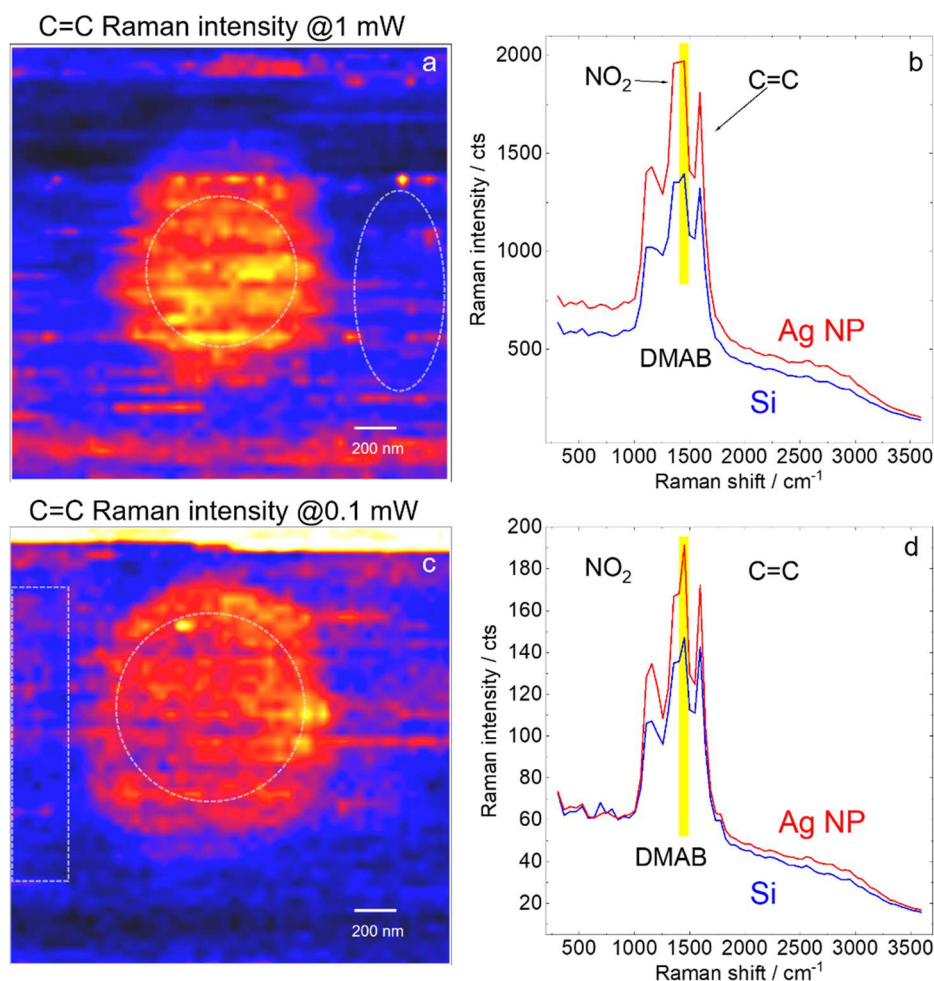


Figure 31. TERS measurement on individual Ag NP and Si wafer covered with 4-NBT, wavelength of laser irradiation 638 nm: a) TERS intensity map of Ag nanocube and Si wafer covered with 4-NBT with increased scan density, b) Normalized C=C TERS spectra from regions on Ag NP and Si substrate with increased scan density, c) TERS intensity map of Ag nanocube and Si wafer covered with 4-NBT with normal scan density, d) Normalized C=C TERS spectra from regions on Ag NP and Si substrate with normal scan density.

We increased the TERS scan density. Results under such condition are shown in Figure 31a, b. Intensity ratio of NO_2/DMAB is decreased on Ag nanocube and Si substrate respectively compared to the results in Figure 30. Although the intensity of the transition of 4-NBT to DMAB is still higher in the region of the Si substrate, the photocatalytic activity in the region of the Ag nanocube increased more than on the Si substrate (Figure 31b) in comparison with the results before the

increase in scan density (Figure 30c). All this indicates that longer irradiation and scan density promote photocatalytic 4-NBT reaction.

It should be noted that with a further decrease in the scanning density, laser power, and laser exposure time, the photocatalytic reaction continued with high intensity (Figure 31c, d). More and more 4-NBT molecules reacted and converted to DMAB. From which we can conclude that this photocatalytic reaction of 4-NBT is irreversible.

3.5 Photons influence on the photocatalytic reaction

Next measurements were performed with a power density decrease and increase of the laser beam, as shown in Figure 32. The increase and decrease in power density occurred by focusing of laser beam using lenses. The focus position have been increased from 2.7 to 6.7 μm , thereby we were able to achieve an increase in photon intensity (Figure 32b).

If we compare intensity peaks of NO_2 and NH_2 at 2.7 and 6.7 μm from Figure 32a it will become obvious that NO_2/NH_2 intensity ratio is higher at 6.7 μm and therefore photocatalytic activity is higher as well. This experiment was carried out without external heating, which suggests that catalytic conversion of 4-NBT to 4-ABT also occurs by increasing photon intensity.

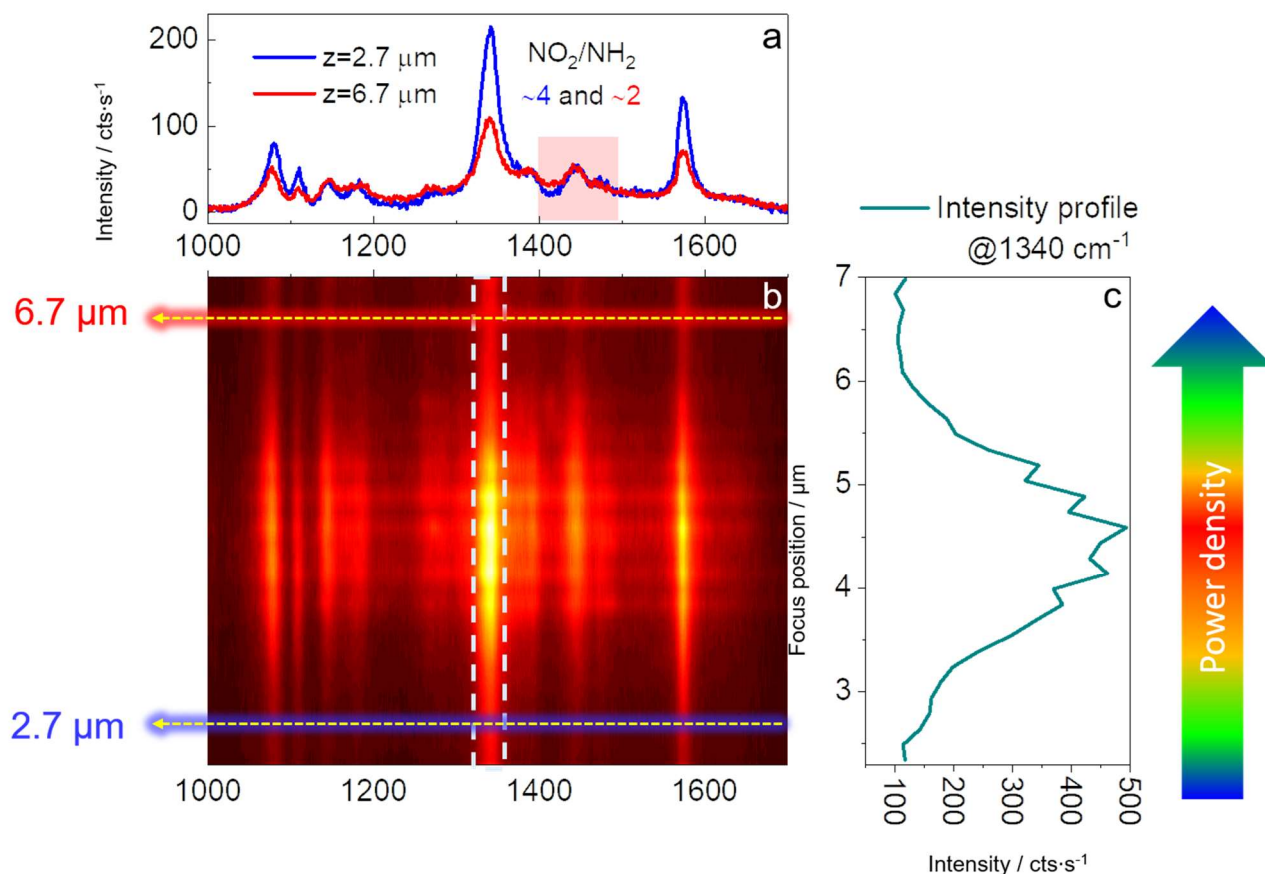


Figure 32. Raman intensity with different laser power density: a) Spectra of 4-NBT with focus position of 2.7 and 6.7 μm , b) Intensity map at different focus position from 2 to 7 μm , c) Intensity profile at 1340 cm^{-1} with focus position from 2 to 7 μm .

3.6 Simulation model of Au nanosphere in COMSOL Multiphysics

In order to accurately describe the model of our TERS experiment with a silver nanocube, silicon substrate and gold tip it was decided to first make a simpler model of a gold nanoparticle of a spherical shape, make a parametric scan of the size and length of a plane-parallel wave, and then move on to a more complex model. This simulation was performed in electromagnetic waves, frequency domain module.

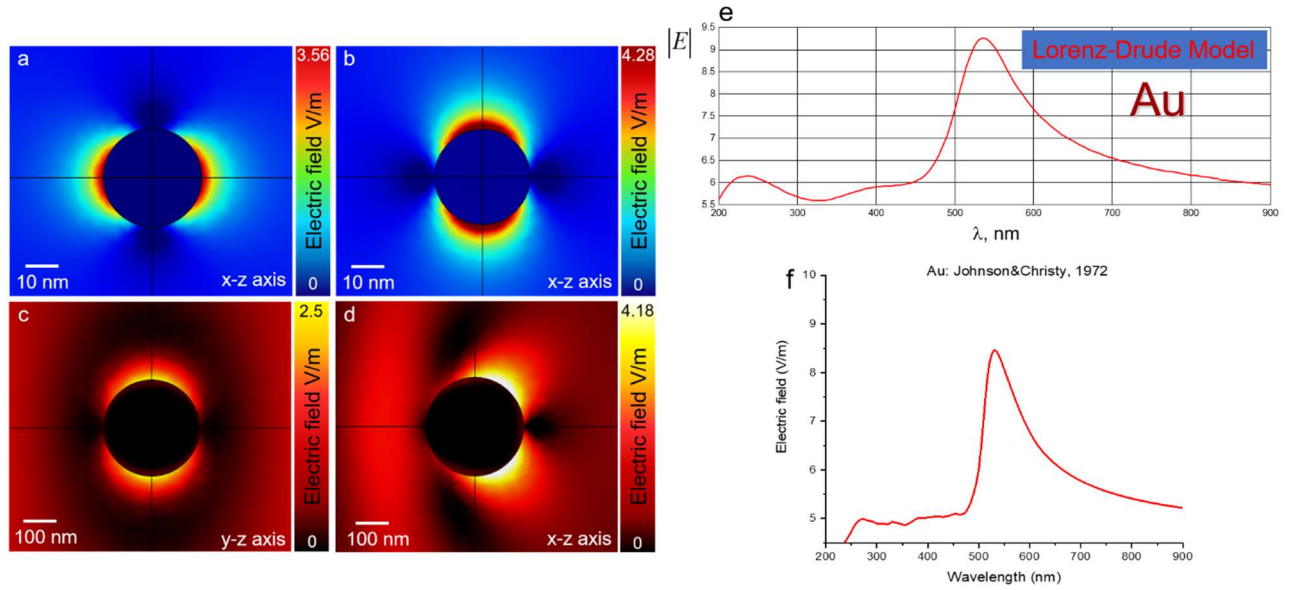


Figure 33. Model of «Au Johnson&Christy, 1972» nanosphere with external EF field of 1 V/m: a) Scattered electric field enhancement, horizontal polarization, size of nanosphere is 10 nm; b) vertical polarization; c) size of nanosphere increased up to 100 nm, vertical polarization; d) horizontal polarization; e) «Lorenz-Drude Au» nanosphere model, electric field intensity in absolute at 200-900 nm wavelength of plane-parallel wave; f) experimental model of «Au Johnson&Christy, 1972» nanosphere, electric field intensity in absolute at 200-900 nm wavelength of plane-parallel wave.

Using the commercial environment of COMSOL Multiphysics, we built a nanosphere model of electromagnetic waves scattering. This resulted in a local increase in the intensity of the electromagnetic field due to plasmon resonance. The dependence of the intensity modulus of the scattered electric field by a nanoparticle at wavelengths from 200 to 900 nm was obtained as shown in Figure 33f. We can say that we were able to accurately recreate the classical Lorentz-Drude model (Figure 33e) using the library built into COMSOL Multiphysics. It is possible to observe the coincidence of the peaks of the electric field intensities of the two model's data with a small error which is probably associated with errors in the calculation during iterations.

Also, there is a very noticeable change in the shape and intensity of the electric field when comparing Figure 33a, b and Figure 33c, d images. In (c) and (d)

pictures, there is a slight decrease in the intensity of the electric field and a change in the dipole angle, which approaches 45 degrees. This phenomenon is associated with an increase in the size of the nanoparticles from 10 to 100 nm and is well studied at present. This also proves the correctness of our model work.

3.7 Simulation model of TERS experiment in COMSOL Multiphysics

The next step was to create a physical research model using the TERS methodology, for comparison with a real experiment.

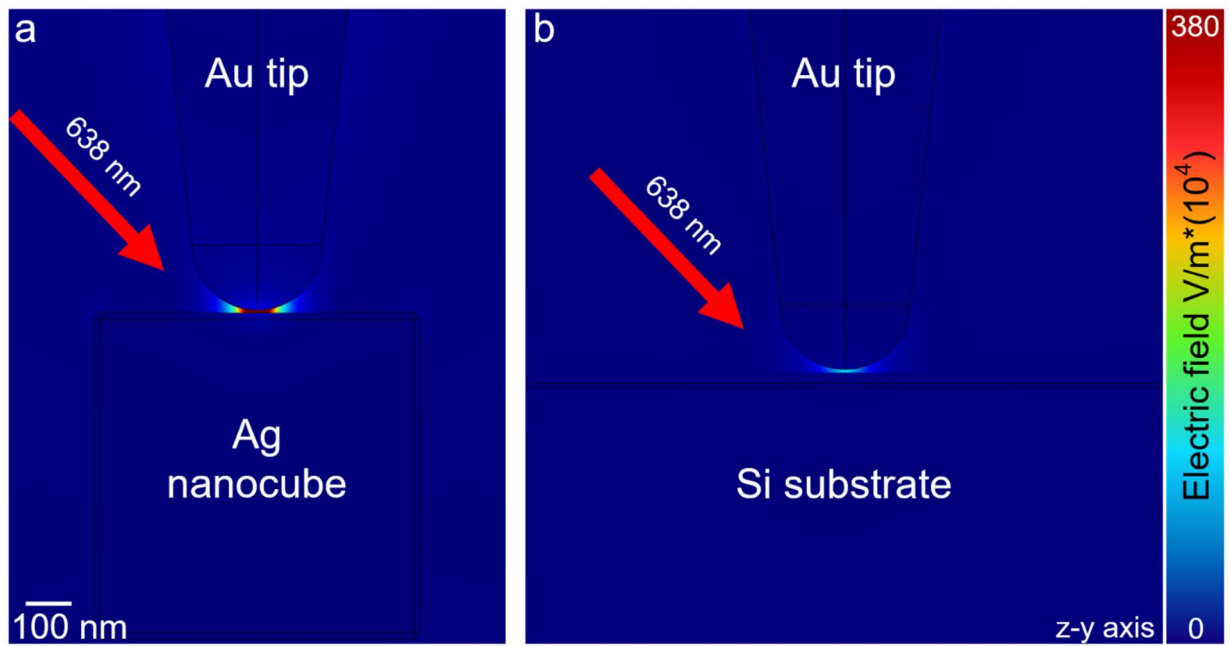


Figure 34. COMSOL simulation images of EF enhancement due to 638 nm under 60 degrees to X axis plane parallel wave scattering: a) between Ag nanocube 100x100 nm, 2 nm fillet radius and 20 nm radius Au tip 2 nm above, b) between Si substrate piece and 20 nm radius Au tip 2 nm above.

This simulation model (Figure 34) is a comparison of field amplification for cases with an Ag nanocube and Si substrate. In case of a nanoparticle from Figure 34a, there is an increase in the intrusiveness of the electric field up to 380 V/m. While in the case of the silicon substrate depicted in Figure 34b we can observe EF enhancement only to approximately 50 V/m. This phenomenon is associated with the LSPR.

This is connected with noble metals (gold and silver in this case). Their electrons begin to oscillate intensively due to irradiation with a certain wavelength

such as 638 nm and create electron clouds while silicon is not capable of this phenomenon. In Figure 34a, we observe simultaneous plasmon resonance of an Ag nanoparticle and an Au tip. But in Figure 34b we can only see amplification from the tip.

This effect confirms our results obtained in a real TERS experiment in which the same tendency was observed.

3.8 Simulation model of temperature evaluation in COMSOL Multiphysics.

After obtaining positive results for the previous electromagnetic wave scattering model in the form of a local field enhancement, it was decided to obtain the results of estimating the maximum local temperature which we can obtain using only a physical model.

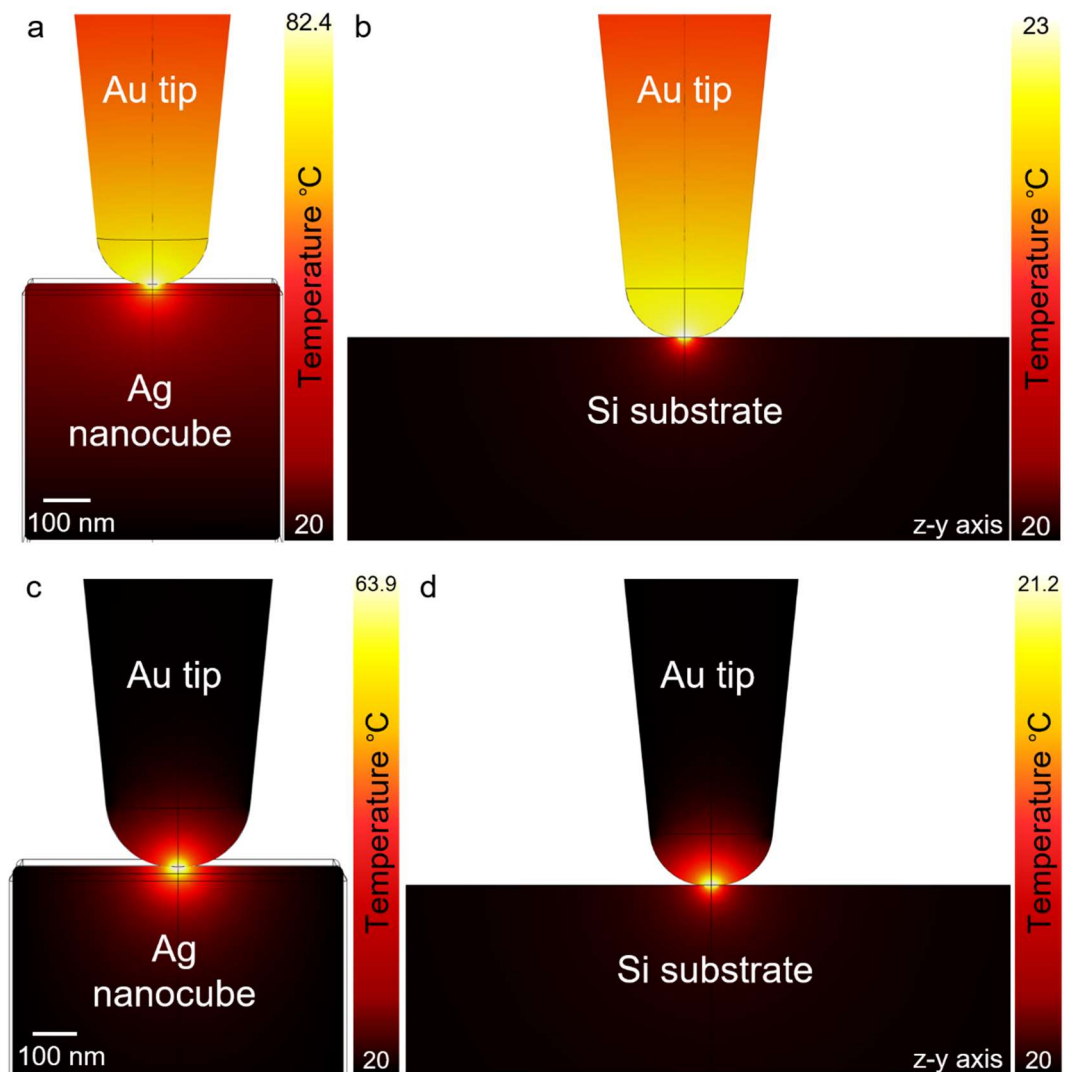


Figure 35. COMSOL simulation pictures of temperature increase and distribution from Joule-heating module: a) temperature distribution with a maximum of 82.4°C between Ag nanocube and Au tip, b) temperature distribution with the maximum of 23°C between Si substrate and Au tip, c) hotspot local temperature distribution with a maximum of 63.9°C between Ag nanocube and Au tip, d) hotspot local temperature distribution with a maximum of 21.2°C between Si substrate and Au tip.

To achieve the objective, in the Joule heating module, we applied a potential equal to the electric field intensity obtained in the electromagnetic wave module and multiplied by the length of the region where this field intensity was observed. The obtained potential value was 0.0296 and 0.0072 V. It was applied between the nanoparticle and the tip as well as between the substrate and the tip, respectively.

All temperature changes are presented with respect to reference temperature equal to 20°C. As presented in Figure 35a maximum temperature of 82.4°C can be observed in the hottest point between tip and Ag NP. Meanwhile the temperature of 23°C was observed for a small region between the substrate and the tip. However, in Figure 35a,b, heat diffusion and dissipation into the tip and a nanoparticle are very noticeable. For us it is important to obtain the maximum temperature of hotspots. So it was decided to subtract from some areas of the model objects in order to see the local temperatures which are presented in Figure 35c,d and equal to 63.9°C for (c), and 21.2°C for (d).

It is obvious that the temperature between Au tip and Ag nanocube is much higher than between Si substrate and Au tip due to the higher applied potential as well as the electrical conductivity 61.6e6[S/m] and thermal conductivity 429[W/(m·K)] of silver, which is much higher than that of silicon (electrical conductivity 1000[S/m], thermal conductivity 34[W/(m·K)]).

The results obtained from the simulation model tell us that we get a sufficient hot spot temperature equal to 63.9°C maximum only due to the LSPR effect. This temperature is sufficient for some applications of nanoparticles in medicine such as

photothermal therapy of cancer tumors where the destruction of cancer cells occurs by increasing the temperature up to 42°C or more.

4 Financial management, resource efficiency and resource saving

The purpose of this section discusses the issues of competitiveness, resource efficiency and resource saving, as well as financial costs regarding the object of study of Master's thesis. Competitiveness analysis is carried out for this purpose. SWOT analysis helps to identify strengths, weaknesses, opportunities and threats associated with the project, and give an idea of working with them in each particular case. For the development of the project requires funds that go to the salaries of project participants and the necessary equipment, a complete list is given in the relevant section. The calculation of the resource efficiency indicator helps to make a final assessment of the technical decision on individual criteria and in general.

4.1 Competitiveness analysis of technical solutions

In order to find sources of financing for the project, it is necessary, first, to determine the commercial value of the work. Analysis of competitive technical and methodical solutions in terms of resource efficiency and resource saving allows to evaluate the comparative effectiveness of scientific development. This analysis is advisable to carry out using an evaluation card.

First of all, it is necessary to analyze possible technical solutions and choose the best one based on the considered technical and economic criteria.

Evaluation map analysis presented in Table 1. The position of our TERS methodology and competitors SERS and Raman thermometry is evaluated for each indicator on a five-point scale, where 1 is the weakest position and 5 is the strongest. The weights of indicators in the amount should be 1. Analysis of competitive technical solutions is determined by the formula:

$$C = \sum W_i \cdot P_i, \quad (4)$$

C - the competitiveness of research or a competitor;

W_i – criterion weight;

P_i – point of i-th criteria.

TERS technique with an AFM system was used as a main methodic in this master thesis. Moreover using 2 modules (electromagnetic wave, frequency domain and Joule-heating, stationary domain) from commercial software COMSOL Multiphysics a few physical simulation models of real TERS experiments was created (P_f).

Competitors usually implements the following methods with some simulation in relative programs: SERS (P_{il}) and Ultrafast Raman thermometry (P_{i2}).

Table 1. Evaluation card for comparison of competitive technical solutions.

Evaluation criteria	Criterion weight	Points			Competitiveness Taking into account weight coefficients		
		P_f	P_{il}	P_{i2}	C_f	C_{il}	C_{i2}
1	2	3	4	5	6	7	8
Technical criteria for evaluating resource efficiency							
1. Energy efficiency	0.05	2	5	4	0.1	0.25	0.2
2. Reliability	0.2	4	3	4	0.8	0.6	0.8
3. Safety	0.15	5	5	5	0.75	0.75	0.75
4. Functional capacity	0.1	4	2	3	0.4	0.2	0.3
5. Measurements accuracy	0.2	5	3	4	1	0.6	0.8
Economic criteria for performance evaluation							
1. Development cost	0.05	3	4	2	0.15	0.2	0.1
2. Scientific developments market penetration rate	0.15	5	3	5	0.75	0.45	0.75
3. Methodology perspectives	0.1	5	3	4	0.5	0.3	0.4
Total	1	33	28	31	4.45	3.65	4.1

As we can see after competitiveness analysis the highest competitiveness points is for our TERS (C_{if}) methodology and equal 4.45 in total, meanwhile for SERS (C_{il}) total points equal 3.65 and Ultrafast Raman thermometry (C_{i2}) equal 4.1. Most of the points TERS methodology received for functionality, measurement

accuracy, methodology perspective and scientific developments market penetration rate.

However, despite the fact that our methodology bypasses the other two in total, there are some problems with energy consumption and the cost of equipment and operation, which is a little high. In terms of cost and energy efficiency, it is most acceptable to use the SERS or Raman thermometry methods, but these techniques will not give the most accurate result and are not the latest in scientific community.

4.2 SWOT analysis

Complex analysis solution with the greatest competitiveness is carried out with the method of the SWOT analysis: Strengths, Weaknesses, Opportunities and Threats. The analysis has several stages. The first stage consists of describing the strengths and weaknesses of the project, identifying opportunities and threats to the project that have emerged or may appear in its external environment. The second stage consists of identifying the compatibility of the strengths and weaknesses of the project with the external environmental conditions. This compatibility or incompatibility should help to identify what strategic changes are needed.

Table 2. SWOT analysis

	Strengths: S1. The results obtained with this TERS methodology are quite accurate. S2. The functionality of this technique allows to compare the results with the results obtained using already known and new techniques. S3. TERS methodology permit to obtain more in-depth information about the process of plasmon photocatalysis, not studied previously. S4. The equipment used for the TERS methodology is not narrowly targeted and can be used for other studies and experiments.	Weaknesses: W1. High cost of equipment. W2. It takes a lot of time to synthesize and prepare the necessary reagents, set up the equipment and process the results. W3. Some materials are not located in Tomsk and they need to be ordered or synthesized. W4. Equipment are constantly used by other researchers and engineers.
Opportunities:	<i>Using our technique, which includes the simultaneous usage of TERS maps of Raman</i>	<i>The equipment, reagents and materials that we use in TERS experiments are a little</i>

<p>O1. Get information of plasmon photocatalysis at the level of a single nanoparticle.</p> <p>O2. The ability to simultaneously obtain an AFM topography image and a TERS map of an individual nanoparticle</p> <p>O3. The ability to control the time of the experiment, the power density of the laser, the density of the scanned area.</p> <p>O4. Possibility of heating and cooling the sample.</p> <p>O5. An experiment performed using the TERS methodology can be simulated in COMSOL Multiphysics</p>	<p><i>signal amplification by increasing the electromagnetic field intensity and obtaining AFM images of the topography of the studied surface, we obtain detailed information about all processes of the plasmon-induced photocatalytic reaction on single nanoparticles with high accuracy. While currently, most techniques do not allow to obtain similar results with high resolution on the nanoscale. The functionality of the equipment used will allow us to vary the parameters we need over a wide range and observe how they affect the photocatalytic conversion of 4-NBT to 4-ABT and DMAB. The results of this technique can be compared with the simulation physical model made in COMSOL Multiphysics.</i></p>	<p><i>expensive and the experiments themselves with their description take a lot of time. However, they help to obtain very precise and reliable data that can be reproduced in any other laboratory in the world with the same or similar equipment using our methodology. Equipment is constantly used by other researchers. Therefore, to reduce costs and lead time it is necessary to schedule our time of usage and to obtain as many experimental data as possible while the equipment is at our disposal. Since the materials are mainly custom-made or synthesized in Germany and France and then brought to Tomsk, it is necessary to plan what and how many specific materials we need, and then make an order in advance.</i></p>
<p>Threats:</p> <p>T1. Since our methodology takes a long time, other scientists can get other results, process them and publish faster than we do.</p> <p>T2. The equipment used in the classic SERS and Raman techniques has been studied in more detail and is not so expensive.</p> <p>T3. Due to the fact that the scientific community is developing quite fast, it is likely that new methods will soon appear for studying the process of plasmon photocatalysis, which may exceed ours.</p> <p>T4. After the publication of our results, disputes may arise with other scientific researchers who use other methods.</p>	<p><i>The technique that we use requires a lot of time to get good and accurate results and we can't do anything about it. However, we can speed up the process of describing and interpreting experimental data, as well as the process of preparing material for publication in scientific journals. Although, the published results may be controversial with existing researches of plasmon photocatalysis, we should publish our studies. As they are important not only for photochemical processes but can be used in theranostics of cancer tumors and the development of new nanobiosensors.</i></p>	<p><i>Speaking about the weaknesses and threats to our research, time is the determining factor. With constantly evolving technologies, new techniques appear every year. To accelerate the spread of our methodology and not to miss its relevance, we can delegate the synthesis of the materials and reagents we need, the preparation of the corresponding finished samples with substrates to companies involved in such developments. Thus, we will take ready-made samples and examine them using our TERS methodology without wasting time on their preparation. For the speedy publication of our results, we can attract more scientists competent in the reaction of plasmon catalysis.</i></p>

4.3 Project Initiation

The initiation process group consists of processes that are performed to define a new project or a new phase of an existing one. In the initiation processes, the initial purpose and content are determined and the initial financial resources are fixed. The internal and external stakeholders of the project who will interact and influence the overall result of the research project are determined.

Table 3. Stakeholders of the project

Project stakeholders	Stakeholder expectations
RSCABS TPU University of Technology of Troyes Chemnitz University of Technology Saratov State University	Published articles in scientific journals with a high impact factor. The results obtained using the TERS methodology are used and taken into account in the scientific community for the processes of photochemistry, the creation of nanobiosensors, theranostics of cancerous tumors.

Table 4. Purpose and results of the project

Purpose of project:	To investigate and show the role of temperature, time of exposure and laser power density in plasmon photocatalysis at the single nanoparticle level using TERS technique
Expected results of the project:	The results show that the photocatalytic reaction proceeds more intensively (the conversion of 4-NBT to 4-ABT, DMAB) and drivable by temperature with our TERS methodology.
Criteria for acceptance of the project result:	Results are repeatable and interpretable.
Requirements for the project result:	Intensity ratio of NO_2/NH_2 is decreased with temperature increase

	High resolution of plasmon photocatalysis of a single nanoparticle is obtained
	The results are interpreted, processed and published.
	An assessment of the possibility of conducting <i>in-vivo</i> clinical trials is given.

The organizational structure of the project

It is necessary to solve some questions: who will be part of the working group of this project, determine the role of each participant in this project, and prescribe the functions of the participants and their number of labor hours in the project.

Table 5. Structure of the project

№	Participant	Role in the project	Functions	Labor time, hours (working days (from table 7) × 6)
1	Andrey Alekseevich Averkiev	Researcher/engineer	Experimentation, Model simulations, Data processing, Papers writing, Report writing	498
2	Raul David Rodriguez Contreras	Researcher/Project leader	Experimentation, Hardware Setup, Data processing, Planning, Communication, Papers writing, Report checking	246

Project limitations

Project limitations are all factors that can be as a restriction on the degree of freedom of the project team members.

Table 6. Project limitations

Factors	Limitations / Assumptions
3.1. Project's budget	1000000 rubs
3.1.1. Source of financing	RSCABS TPU
3.2. Project timeline:	
3.2.1. Date of approval of plan of project	27.01.2020
3.2.2. Completion date	25.05.2020

Project Schedule

As part of planning a science project, you need to build a project timeline and a Gantt Chart.

Table 7. Project Schedule

Job title	Duration, working days	Start date	Date of completion	Participants
Literature review	6	3.02.2020	8.02.2020	A.A. Averkiev
Research planning	6	10.02.2020	15.02.2020	R.D. Rodriguez/ A.A. Averkiev
Data processing of experimental results	11	17.02.2020	29.02.2020	R.D. Rodriguez/ A.A. Averkiev
Experiment modelling and simulation in COMSOL Multiphysics	22	17.02.2020	14.03.2020	A.A. Averkiev
Results discussion	6	16.03.2020	21.03.2020	R.D. Rodriguez/ A.A. Averkiev
Consultation with colleges	6	16.03.2020	21.03.2020	R.D. Rodriguez
Scientific manuscript writing	12	23.03.2020	4.04.2020	A.A. Averkiev/ R.D. Rodriguez

Report writing	31	6.04.2020	16.05.2020	A.A. Averkiev
Report checking and corrections	6	18.05.2020	23.05.2020	R.D. Rodriguez


Total duration of working time – 89 days

A Gantt chart, or harmonogram, is a type of bar chart that illustrates a project schedule. This chart lists the tasks to be performed on the vertical axis, and time intervals on the horizontal axis. The width of the horizontal bars in the graph shows the duration of each activity.

Table 8. A Gantt chart

№	Activities	Participants	T _c , days	Duration of the project											
				February			March			April			May		
				1	2	3	1	2	3	1	2	3	1	2	3
1	Literature review	A.A. Averkiev	6	■											
2	Research planning	R.D. Rodriguez/ A.A. Averkiev	6		■										
3	Data processing of experimental results	R.D. Rodriguez/ A.A. Averkiev	11			■									
4	Experiment modelling and simulation in COMSOL Multiphysics	A.A. Averkiev	11			■	■	■							
5	Results discussion	R.D. Rodriguez/ A.A. Averkiev	6						■						
6	Consultation with colleges	R.D. Rodriguez	6						■						
7	Scientific manuscript writing	A.A. Averkiev/	11							■	■	■			

		R.D. Rodriguez													
8	Report writing	A.A. Averkiev	31												
9	Report checking and corrections	R.D. Rodriguez	6												

A.A. Averkiev -  R.D. Rodriguez - 

4.4 Scientific and technical research budget

The amount of costs associated with the implementation of this work is the basis for the formation of the project budget. This budget will be presented as the lower limit of project costs when forming a contract with the customer.

To form the final cost value, all calculated costs for individual items related to the manager and the student are summed.

In the process of budgeting, the following grouping of costs by items is used:

- Material costs of scientific and technical research;
- costs of special equipment for scientific work (Depreciation of equipment used for design);
- basic salary;
- additional salary;
- labor tax;
- overhead.

Calculation of material costs

The calculation of material costs is carried out according to the formula:

$$C_m = (1 + k_T) \cdot \sum_{i=1}^m P_i \cdot N_{consi}, \quad (5)$$

where m – the number of types of material resources consumed in the performance of scientific research;

N_{consi} – the amount of material resources of the i -th species planned to be used when performing scientific research (units, kg, m, m², etc.);

P_i – the acquisition price of a unit of the i -th type of material resources consumed (rub. /units, rub. /kg, rub. /m, rub. /m², etc.);

k_T – coefficient taking into account transportation costs.

Prices for material resources can be set according to data posted on relevant websites on the Internet by manufacturers (or supplier organizations).

Table 9. Material costs

Name	Unit	Amount	Price per unit, rub.	Material costs, rub.
Ag nanocubes	10 ml	1	156000	79000
Au/Ag nanorods	25 ml	1	50000	21500
4-NBT	25 g	1	37000	8400
Si substrate, N-type, 2 in. × 0.5 mm	1 ea	5	17500	58500
Total				167400

Costs of special equipment

This point includes the costs associated with the acquirement of special equipment (instruments, stands, devices and mechanisms) necessary to carry out work on a specific topic.

Table 10. Costs of special equipment and software

№	equipment and software identification	Quantity of equipment	Price per unit, rub.	Total cost of equipment, rub.
1.	COMSOL Multiphysics	1	126000	126000
2.	COMSOL Multiphysics, electromagnetic waves module	1	66500	66500
3.	COMSOL Multiphysics,	1	66500	66500

	Joule-heating module			
--	----------------------	--	--	--

Calculation of the depreciation

If you use available equipment, then you need to calculate depreciation:

$$A = \frac{C_{\text{непб}} \cdot H_a}{100} \quad (6)$$

A - annual amount of depreciation;

$C_{\text{непб}}$ - initial cost of the equipment;

$H_a = \frac{100}{T_{\text{сл}}}$ - rate of depreciation;

$T_{\text{сл}}$ - life expectancy.

№	equipment identification	Quantity of equipment	Total cost of equipment, rub.	Life expectancy, year	Depreciation for the duration of the project, rub.
1.	XploRA Raman spectrometer	1	8592000	10	35800
2.	LabRAM HR800 system	1	6609000	10	27538
3.	OmegaScope-R	1	5500000	10	22917
4	Agilent 5420 AFM	1	750000	10	3125
5.	PC	1	127000	5	4233

Total for the title "Costs of special equipment" – 93613 rubles.

Basic salary

This point includes the basic salary of participants directly involved in the implementation of work on this research. The value of salary costs is determined based on the labor intensity of the work performed and the current salary system

The basic salary (S_b) is calculated according to the formula:

$$S_b = S_d \cdot T_w, \quad (7)$$

where S_b – basic salary per participant;

T_w – the duration of the work performed by the scientific and technical worker, working days;

S_d - the average daily salary of a participant, rub.

The average daily salary is calculated by the formula:

$$S_d = \frac{S_m \cdot M}{F_v}, \quad (8)$$

где S_m – monthly salary of an participant, rub.;

M – the number of months of work without leave during the year:

at holiday in 48 days, $M = 11.2$ months, 6 day per week;

F_v – valid annual fund of working time of scientific and technical personnel (244 days).

Table 11. The valid annual fund of working time

Working time indicators	
Calendar number of days	365
The number of non-working days	
- weekend	52
- holidays	14
Loss of working time	
- vacation	48
- isolation period	7
- sick absence	
The valid annual fund of working time (F_d)	244

Monthly salary is calculated by formula:

$$S_{month} = S_{base} \cdot (k_{premium} + k_{bonus}) \cdot k_{reg}, \quad (9)$$

where S_{base} – base salary, rubles;

$k_{premium}$ – premium rate;

k_{bonus} – bonus rate;

k_{reg} – regional rate.

Table 12. Calculation of the base salaries

Performers	S_{base} , rubles	$k_{premium}$	k_{bonus}	k_{reg}	S_{month} , rub.	W_d , rub.	T_p , work days	W_{base} , rub.
A.A. Averkiev Engineer	17 890	0.6	0.55	1,3	26746	1228	83	101924
R.D. Rodriguez Professor	49141				73466	3372	41	138252

Total for the title "Basic salary" - 240176 rubles.

Additional salary

This point includes the amount of payments stipulated by the legislation on labor, for example, payment of regular and additional holidays; payment of time associated with state and public duties; payment for work experience, etc.

Additional salaries are calculated on the basis of 10-15% of the base salary of workers:

$$W_{add} = k_{extra} \cdot W_{base} , \quad (10)$$

where W_{add} – additional salary, rubles;

k_{extra} – additional salary coefficient (10%);

W_{base} – base salary, rubles.

$W_{add} (A.A. Averkiev) = 10192 \text{ rubles};$

$W_{add} (R.D. Rodriguez) = 13825 \text{ rubles};$

Total for the title "Additional salary" – 24017 rubles.

Labor tax

Tax to extra-budgetary funds are compulsory according to the norms established by the legislation of the Russian Federation to the state social insurance (SIF), pension fund (PF) and medical insurance (FCMIF) from the costs of workers.

Payment to extra-budgetary funds is determined of the formula:

$$P_{social} = k_b \cdot (W_{base} + W_{add}) \quad (11)$$

where k_b – coefficient of deductions for labor tax.

In accordance with the Federal law of July 24, 2009 No. 212-FL, the amount of insurance contributions is set at 30%. Institutions conducting educational and scientific activities have rate - 27.1%.

Table 13. Labor tax

	Project leader (R.D. Rodriguez)	Engineer (A.A. Averkiev)
Coefficient of deductions	0.271	
Salary (basic and additional), rubles	152077	112116
Labor tax, rubles	41213	30383

Total for the title "Labor tax" – 71596 rubles.

Overhead costs

Overhead costs include other management and maintenance costs that can be allocated directly to the project. In addition, this includes expenses for the maintenance, operation and repair of equipment, production tools and equipment, buildings, structures, etc.

Overhead costs account from 30% to 90% of the amount of base and additional salary of employees.

Overhead is calculated according to the formula:

$$C_{ov} = k_{ov} \cdot (W_{base} + W_{add}) \quad (12)$$

where k_{ov} – overhead rate.

Table 14. Overhead

	Project leader (R.D. Rodriguez)	Engineer (A.A. Averkiev)
Overhead rate	0.3	
Salary, rubles	152077	112116
Overhead, rubles	45623	33635

Total for the title "Overhead costs" – 79258 rubles.

Other direct costs

Energy costs for equipment are calculated by the formula:

$$C = P_{el} \cdot P \cdot F_{eq}, \quad (13)$$

where

P_{el} – power rates (5.8 rubles per 1 kWh);

P – power of equipment, kW;

F_{eq} – equipment usage time, hours.

C (*XploRA Raman spectrometer*) = 418 rubles;

C (*LabRAM HR800 system*) = 626 rubles;

C (*OmegaScope-R*) = 835 rubles;

C (*Agilent 5420 AFM*) = 209 rubles;

C (*PC*) = 950 rubles.

Total for the title "Other direct costs" – 3038 rubles.

Formation of budget costs

The calculated cost of research is the basis for budgeting project costs.

Determining the budget for the scientific research is given in the table 15.

Table 15. Items expenses grouping

Name	Cost, rubles
1. Material costs	167400
2. Equipment costs	352613
3. Basic salary	240176
4. Additional salary	24017
5. Labor tax	71596
6. Overhead	79258
7. Other direct costs	3038
Total planned costs	938098

4.5 Evaluation of the comparative effectiveness of the project

Determination of efficiency is based on the calculation of the integral indicator of the effectiveness of scientific research. Its finding is associated with the definition of two weighted average values: financial efficiency and resource efficiency.

The integral indicator of the financial efficiency of a scientific study is obtained in the course of estimating the budget for the costs of three (or more) variants of the execution of a scientific study. For this, the largest integral indicator of the implementation of the technical problem is taken as the calculation base (as the denominator), with which the financial values for all the options are correlated.

The integral financial measure of development is defined as:

$$I_f^d = \frac{C_i}{C_{max}}, \quad (14)$$

where I_f^d – integral financial measure of development;

C_i – the cost of the i-th version;

C_{max} – the maximum cost of execution of a research project (including analogues).

The obtained value of the integral financial measure of development reflects the corresponding numerical increase in the budget of development costs in times (the value is greater than one), or the corresponding numerical reduction in the cost of development in times (the value is less than one, but greater than zero).

Since the development has one performance, then $I_f^d = 1$.

The integral indicator of the resource efficiency of the variants of the research object can be determined as follows:

$$I_m^a = \sum_{i=1}^n a_i b_i^a, \quad I_m^p = \sum_{i=1}^n a_i b_i^p, \quad (15)$$

where I_m – integral indicator of resource efficiency for the i-th version of the development;

a_i – the weighting factor of the i-th version of the development;

b_i^a, b_i^p – score rating of the i-th version of the development, is established by an expert on the selected rating scale;

n – number of comparison parameters.

The calculation of the integral indicator of resource efficiency is presented in the form of table 17.

Table 16 – Evaluation of the performance of the project

Criteria	Weight criterion	Points
1. Energy efficiency	0.05	2
2. Reliability	0.15	4
3. Safety	0.15	5
4. Functional capacity	0.1	4
5. Measurements accuracy	0.15	5
Economic criteria for performance evaluation		
1. The cost of development	0.05	2
2. Market penetration rate	0.15	5
3. Expected life	0.1	4
4. After-sales service	0.1	3
Total	1	34

Integral indicator of resource efficiency:

$$I_m = 0.05 \cdot 2 + 0.15 \cdot 4 + 0.15 \cdot 5 + 0.1 \cdot 4 + 0.15 \cdot 5 + 0.05 \cdot 2 + 0.15 \cdot 5 + 0.1 \cdot 4 + 0.1 \cdot 3 = 4.15;$$

The integral indicator of the development efficiency (I_e^p) is determined on the basis of the integral indicator of resource efficiency and the integral financial indicator using the formula:

$$I_e^p = \frac{I_m^p}{I_f^d}, I_e^a = \frac{I_m^a}{I_f^a} \text{ and etc.} \quad (16)$$

$$\text{Since the development has one performance: } I_e^p = \frac{4.15}{1} = 4.15;$$

Comparison of the integral indicator of the current project efficiency and analogues will determine the comparative efficiency. Comparative effectiveness of the project:

$$E_c = \frac{I_e^p}{I_e^a} \quad (17)$$

Thus, the effectiveness of the development is presented in table 18.

Table 18 – Efficiency of development

№	Indicators	Points
1	Integral financial measure of development	1
2	Integral indicator of resource efficiency of development	4.15
3	Integral indicator of the development efficiency	4.15

Comparison of the values of integral performance indicators allows us to understand and choose a more effective solution to the technical problem from the standpoint of financial and resource efficiency.

Conclusion of financial management section

Thus, in this section was developed stages for design and create competitive development that meet the requirements in the field of resource efficiency and resource saving.

These stages include:

- development of a common economic project idea, formation of a project concept;
- organization of work on a research project;
- identification of possible research alternatives;
- research planning;
- assessing the commercial potential and prospects of scientific research from the standpoint of resource efficiency and resource saving;
- determination of resource (resource saving), financial, budget, social and economic efficiency of the project.

This section shows that our methodology based on the use of TERS together with AFM and subsequent modeling in COMSOL Multiphysics has a high cost. However, this technique competitive advantage is possibility to obtain very accurate and repeatable results related to the study of the plasmon-induced photocatalytic reaction of the 4-NBT to 4-ABT and DMAB reduction with a high resolution in the nanoscale at the single nanoparticle level.

5 Social responsibility

Introduction

The object of the research in this Master's thesis is a plasmon-induced photocatalytic reaction. This work is characterized by working in laboratory to investigate plasmon photocatalysis based on 4-NBT conversion to 4-ABT and DMAB due to LSPR, temperature, time of laser exposure and laser power density using our TERS coupled with AFM methodology. After experiments, processing the data and on PC, as well as model creation of real experiment in COMSOL Multiphysics environment.

If security measures are not followed, SERS, TERS and AFM have an in-built low power laser with adjustable power, which cause unpleasant consequences: temporary or permanent blindness. Also, this work is related to the synthesis and use of certain chemicals and materials, such as: gold and silver nanoparticles, 4-NBT, silicon substrates, solutions of silver nitrate. Although these materials themselves are practically harmless to humans, some other chemicals in laboratories, if they come into contact with the eyes and respiratory tract, can cause irritating effects. Therefore, it is necessary to provide conditions that will satisfy the established rules and minimize the negative impact on laboratory technicians.

In relation to large data process and simulation using a personal computer (PC), it can be concluded that there is a need to organize a workplace behind a computer in accordance with the standards. Research work were carried out in an educational institutions of University of Technology of Troyes laboratories; Chemnitz University of Technology laboratories, and in TPU RSCBT laboratories № 205, 303 of Science park.

The purpose of this section is to analyze the objects of study in order to identify the main technospheric hazards, and to assess their impact on humans and the environment.

5.1 Legal and institutional security issues

5.1.1 Special legal norms of labor legislation

According to the Labor Code of the Russian Federation, N 197-FZ, an employee of laboratory rooms 205 and 303 of TPU Science park has the right:

- to have a workplace that meets labor protection requirements;
- to have compulsory social insurance against industrial accidents and occupational diseases in accordance with federal law;
- to refuse to perform work in case of danger to his life and health as a result of violation of labor protection requirements with the exception of cases provided for by federal laws until such danger is eliminated;
- to be provided with the means of individual and collective protection in accordance with the requirements of labor protection at the expense of the employer;
- to undergo an urgent medical examination in accordance with medical recommendations while keeping his place of work (position) and average earnings during the said medical examination.

5.1.2 Organizational measures in the layout of the working area

The workplace in laboratory rooms 205 and 303, Science park of the TPU must meet the requirements of GOST 12.2.032-78 and GOST 12.2.033-78. It should occupy the area of at least 5 m². The height of the room should be at least 4 m, and the volume should be at least 20 m³ per person. The height above the floor of the working surface at which the operator works must be 720 mm. The optimal size of the table surface is 1600x1000 mm². Under the table there should be legroom with the depth of 650 mm. The work table should also have a footrest at the angle of 15° to the surface of the table. Stand length is 400 mm, width is 350 mm. The distance between the keyboard and the edge of the table should be no more than 300 mm, which will provide convenient support for the forearms. The distance between the

operator's eyes and the video display screen should be 40 – 80 cm. The desk should be stable, have uniform non-metallic coating that does not have the ability to accumulate static electricity. The chair should have a design that excludes numbness of the body due to circulatory disorders during prolonged work in the workplace.

The design of the experimental equipment and the organization of the workplace should ensure the optimal position of the worker, which is achieved by the following regulation: there should be footrests under the working surface.

In cases where it is impossible to regulate the working surface height and the footrest, it is allowed to design and manufacture equipment with an unregulated height of the working surface and footrest. In this case, the numerical values of the working surface height are determined according to table 17.

Table 17. The numerical values of the working surface height.

Work Category	The height of the working surface, mm, when organizing the workplace		
	Female	Male	Female and male
Easy	990	1060	1025
Average	930	980	955
Hard	870	920	895

The employee workplace in the laboratory rooms 205 and 303, TPU Science park meets GOST 12.2.032-78 and GOST 12.2.033-78 requirements. The total area of the laboratory 205 is 48.7 m², the volume is 145.8 m³ (length A = 8.1 m, width B = 6 m, height C = 3 m). The total area of the laboratory 303 is 24 m², the volume is 72 m³ (length A = 6 m, width B = 4 m, height C = 3 m).

The placement of Microscopes, spectrometers and chemical equipment and the organization of workplaces takes place according to the PND F 12.13.1-03, SanPiN 5804-91 and GOST R-50723-94. In order to ensure safety, it is necessary to perform a number of measures:

- All chemicals and materials should be stored at room temperature, protected from water in clean, dry, inert atmosphere, in sealed bag;

- As a floor material, special linoleum or wood should be used to eliminate the accumulation of static electricity;
- The composition of the furniture should not be synthetic fibers;
- The matte finish on the walls and ceiling prevents the reflection of laser radiation;
- Non-combustible materials should be used as a wall and ceiling covering;
- Mirror coatings should be excluded;
- The location of the elements of the workplace should be organized rationally, taking into account the speed, power and physiological personal capabilities;
- It is necessary to allocate a separate place for the means used during work (gloves, napkins, glasses, etc.);
- Observe the ventilation of the room, which provides a three-fold exchange of air per hour.
- Safety precautions, first-aid kits, first aid instructions, a fire extinguisher in the workplace and campaign information should be required in case of an emergency.
- Laboratory room should be marked with special chemical hazard mark:



Figure 22 – Chemical hazard sign

- Almost all used equipment has in-built laser and a laser hazard sign. Therefore, a laser hazard sign should hang on the laboratory door:



Figure 23 – Laser hazard sign

5.2 Industrial safety

This section analyzes the harmful and hazardous factors that may arise when synthesizing of Au/Ag NPs, samples preparing and investigating the sample with laser hazard equipment.

5.2.1 Analysis of hazardous and harmful industrial factors

Industrial safety is the system of organizational measures and technical means that prevent or reduce the likelihood of exposure to working personnel of the dangerous traumatic factors that arise in the working area during work.

Further selection of factors is made using GOST 12.0.003-2015 “Hazardous and harmful industrial factors. Classification”. The selection results are shown in table 18.

Table 18 – Harmful and hazardous factors when working with a chemical, equipment with in-built laser and PC.

The source of the factor, the name of the type of work	List of factors (according to GOST 12.0.003-2015)		Normative document
	Harmful	Hazardous	
1) Execution of works for the chemicals.	1) Eyes and respiratory tract contact with chemicals; 2) decrease in illumination of the room; 3) microclimate deviations.	1) chemical hazard; 2) fire hazard.	GOST 12.1.007-76; GOST 12.1.005-88; SanPiN 2.2.4.3359-16; SP 60.13330.2016; SP 52.13330.2016; SN 2.1.8.566–96.
2) Execution of works for the	1) decrease in illumination of the room;	1) laser irradiation in equipment.	GOST 12.1.030-81; GOST 12.1.038-82; GOST 12.1.045-84;

equipment with in-built laser.	2) adverse electromagnetic environment; 3) microclimate deviations.	2) High voltage value in the electrical circuit. 3) fire hazard.	GOST 12.1.006-84; SP 52.13330.2016; SP 60.13330.2016; SP 51.13330.2011; SniP 2125—80; SN 2.1.8.562–96; SN 2.1.8.566–96. R 2.2.2006-05;
3) Data processing, results description and model simulation on a personal computer.	1) decrease in illumination of the room; 2) adverse electromagnetic environment; 3) microclimate deviations.	1) High voltage value in the electrical circuit. 2) fire hazard.	SanPiN 2.4.1340–03; SanPiN 2.2.4.548-96; GOST 12.1.019-2017; GOST 12.1.003-83; GOST 12.1.005-88; GOST 12.1.006-84; SP 51.13330.2011. SN 2.1.8.566–96.

Since the execution of the work steps occurs at the use of chemicals, equipment with in-built laser and PC, we exclude psychophysiological and biological harmful and hazardous factors.

Physical hazards, as a rule, include:

- 1) high concentration of chemicals in the air when improperly handled;
- 2) electromagnetic (laser) radiation;
- 3) increased air temperature;
- 4) insufficient illumination of the working area;
- 5) increased noise level in the room and other factors.

The greatest influence on the human body have chemicals and equipment with in-built lasers (electromagnetic radiation). Chemicals can hit in the eyes and respiratory tract which cause short-term visual impairment and difficulty breathing, coughing. Since the lasers built into the equipment are not too powerful, they can only be dangerous for eyes. However, prolonged exposure to electromagnetic radiation can cause serious visual impairment, short-term or permanent blindness.

5.2.2 Justification of measures to reduce the impact of harmful factors on the researcher

Chemical hazard

The most dangerous factor when working in a chemical laboratory is the presence of other chemicals, since the chemicals we work with are practically harmless.

GOST 12.1.007-76 states what requirements are applied to a workplace with a possible chemical hazard:

1. Maximum permissible concentrations (MPC) of harmful substances in the air of the working area are mandatory sanitary standards for use in the industrial buildings design, technological processes, equipment and ventilation, as well as for preventive and routine sanitary surveillance.

2. The content in the body of harmful substances entering it in various ways (by inhalation, through the skin, through the mouth), should not exceed the biological maximum permissible concentrations (MPC).

3. For the period preceding the design of production, approximate safe exposure levels (SLE) should be temporarily established by calculation according to physicochemical properties or by interpolation and extrapolation in series similar in structure of compounds or in acute hazard indicators.

4. In some cases, in agreement with the state sanitary inspection authorities, it is allowed to use SECS of at least 1 mg/m GOST 12.1.007-76 Occupational Safety Standards System (OSSS) when designing production. Harmful substances. Classification and general safety requirements (with Amendments N 1, 2) in the air of the working area (moderately and low hazard substances). In other cases, shoe should not be used in the production design;

5. SLE should be reviewed two years after their approval or replaced by MPC taking into account the accumulated data on the ratio of the workers health with working conditions.

6. In accordance with the established MPC or SEC of harmful substances, methods for their control in the air of the working area should be developed.

7. Basic requirements for controlling the harmful substances content in the air of the working area

8. Control over the harmful substances content in the air of the working area should be carried out in accordance with the requirements of GOST 12.1.005.

Electromagnetic environment

The main sources of the electromagnetic field at the workplace are wiring, equipment with in-built laser and PC.

The normalized parameter of the electric field is the electric field (E) in kV/m, the magnetic field is the magnetic field (H) in A/m or the magnetic field (B) in μT , in accordance with the requirements of GOST 12.1.006-84 «SSBT. Electromagnetic fields of radio frequencies. General safety requirements». And SanPiN 2.2.1340-03.

The electric field strength should be:

- in the frequency range 5Hz ... 2kHz -25V/m;
- in the frequency range 2kHz ... 400kHz – 2.5V m.

The magnetic flux density should be:

- in the frequency range 5Hz ... 2kHz – 250nTl;
- in the frequency range 2kHz ... 400kHz – 25nTl.

To reduce the electromagnetic fields effects, observe the optimal ground loop design of the equipment; optimal wiring; competent layout of the laboratory and the working room; if possible, avoid the presence of unused equipment creating a strong electromagnetic field in the working room; Periodically carry out wet cleaning, this will decrease the effect of static electricity.

Deviation and calculation of room illumination

An important parameter for continuous work both in the laboratory and in the office is the lighting of the room. Quite a lot of accidents occur due to poor

lighting and by workers mistakes in low light conditions. Thus, good lighting of the workplace avoids many potential problems, including the workers' health.

When lighting, sanitary and hygienic working conditions improve, visual and general fatigue decreases, and occupational eye diseases are prevented.

The following types of lighting are distinguished:

a) natural lighting, which is more favorable for vision and more economical. In this workshop, the type of natural lighting is lateral. The visual work category in SP 52.13330.2011 "Natural and artificial lighting" – according to the degree of accuracy – medium accuracy. For this production, the natural illumination coefficient $NIC = 0.5\%$. The production room provides natural lighting through window openings.

b) artificial lighting is used at any time of the day. In medium-precision work, artificial illumination with a combined lighting system is 200 lux, with a total system of 150 lux. Luminaires with fluorescent lamps are used.

According to SP52.13330.2011 "Natural and artificial lighting" with combined lighting for the visual work category of medium accuracy, the illumination value standard at workplaces is 200 lux.

A normal working posture should be considered one in which the employee does not need to lean forward by more than $10 \dots 15^\circ$, tilting back and forth is not desirable, the main requirement for a working posture is direct posture.

A significant influence on the operator's performance is made by the correct choice of the type of organs placement to control machines panels and mechanisms. The dashboards should be positioned so that the planes of the indicators front parts are perpendicular to the lines of the operator's gaze, and the necessary controls are within reach. The most important controls should be located in front and to the right of the operator.

To better distinguish the controls, they should be different in shape and size, painted in different colors or have a marking or corresponding inscription. The use of foot control makes it possible to reduce the load on the hands and thus reduce the overall operator fatigue.

Choosing the fixtures location must be guided by two criteria:

- high-quality lighting provision, limiting blinding and the necessary directivity of light to the workplace;

- The most economical creation of standardized lighting.

The most favorable relative distance between the fixtures is determined by the formula [75]:

$$\lambda = \frac{L}{h}, \quad (17)$$

where L is the distance between the lamps, m;

h – the height of the lamp suspension above the working surface, m, determined by the formula: $h = H - h_p$.

Then we get: $h = 4 - 1 = 3m$.

Recommended value [75], numerically equal to: $\lambda = 1.2$.

From here we define L , we get: $L = 1.2 \cdot 3 = 3.6m$.

The distance from the walls of the room to the extreme lights, it is recommended to choose [75]:

$$R = \frac{L}{3} = \frac{3.6}{3} = 1.2m. \quad (18)$$

The light field length A_{cn} is determined by the formula:

$$A_{cn} = A - 2R = 7.5 - 2 \cdot 1.2 = 5.1m. \quad (19)$$

The light field width B_{cn} is determined by the formula:

$$B_{cn} = B - 2R = 4 - 2 \cdot 1.2 = 1.6m. \quad (20)$$

We define the lamp characteristics we need. The characteristics of the selected lamp are presented in table 19.

Table 19 - Characteristics of the lamp

Lamp type	LD 40-2
Lamp power, w	40
Length A_{cb} , mm	1235
Width B_{cb} , mm	215
High H_{cb} , mm	184
Efficiency, %	75

Using the coefficient of use method, it is possible to determine the luminous lamps flux necessary to create a given illumination of a horizontal surface, taking into account the light reflected by walls, ceilings, or vice versa to find the illumination at a given flux. The utilization method is used only when calculating the total uniform illumination [75].

The laboratory 205 total area, S is 48.7 m^2 , the volume is 145.8 m^3 (length $A = 8.1 \text{ m}$, width $B = 6 \text{ m}$, height $C = 3 \text{ m}$). The laboratory 303 total area, S is 24 m^2 , the volume is 72 m^3 (length $A = 6 \text{ m}$, width $B = 4 \text{ m}$, height $C = 3 \text{ m}$).

The room index is determined by the formula [75]:

$$\text{For laboratory 205 } i=\eta=\frac{S}{(A+B)h_n}=\frac{48.7}{3\times(8.1+6)}=1.15, \quad (21)$$

$$\text{For laboratory 303 } i=\eta=\frac{S}{(A+B)h_n}=\frac{24}{3\times(6+4)}=0.8,$$

where S is the area of the room, m^2 ;

h - the height of the lamp suspension above the working surface, m

The number of lamps in the room is determined by the formula [75]:

$$\text{For laboratory 205 } n=\frac{E \cdot k \cdot S \cdot z \cdot 100}{F \cdot \eta}=\frac{7.4 \cdot 1.5 \cdot 48.7 \cdot 1.2 \cdot 100}{1520 \cdot 1.15}=37.1 \Rightarrow 37 \text{ a.u.},$$

$$\text{For laboratory 303 } n=\frac{E \cdot k \cdot S \cdot z \cdot 100}{F \cdot \eta}=\frac{7.4 \cdot 1.5 \cdot 24 \cdot 1.2 \cdot 100}{1520 \cdot 0.8}=26.3 \Rightarrow 26 \text{ a.u.}$$

where $F = 1520$ - minimum illumination, lux [75];

k - safety factor;

η - utilization of light flux, fraction of units;

$z = (z_p)^{-1} = 1.1^{-1} = 1.2$ - coefficient of unevenness [75].

As a result of this calculations it was found that 37 lamps are needed in laboratory 205, therefore, 9 illuminators. 26 lamps are needed in laboratory 303, therefore, 7 illuminators.

In the laboratory rooms 205 and 303, the TPU Science park completely meet the requirements for lighting, and even more then they have a larger number of lamps than the calculated value.

Microclimate deviations

Optimal microclimatic conditions are established according to the criteria of the optimal thermal and functional a person state. They provide a general and local sensation of thermal comfort during an 8-hour shift with minimal stress of thermoregulation mechanisms, do not cause deviations in the health state, create the prerequisites for a high level of performance and are preferred at workplaces.

In accordance with SanPiN 2.2.4.548-96, the optimal microclimate parameters at workplaces should correspond to the values given in Tables 20, 21, as applied to the performance of various categories work in the cold and warm periods.

Work in the laboratory with equipment and work in the office at the computer for energy costs coincide with categories IIa and Ib, respectively.

Table 20 – Optimal values of microclimate indicators at workplaces of industrial premises

Period of the year	Category of works by energy consumption levels, kcal/h	Air temperature, C°	Surface temperature, C°	Relative air humidity, %	Air flux speed, m/s
Cold	Ib (140-174)	21-23	20-24	60-40	0.1
	IIa (175-232)	19-21	18-22		0.2
Warm	Ib (140-174)	22-24	21-25		0.1
	IIa (175-232)	20-22	19-23		0.2

Table 21 – Permissible values of microclimate indicators at workplaces of industrial premises

Period of the year	Category of works by energy consumption levels, kcal/h	Air temperature, C°		Surface temperature, C°	Relative humidity, % air	Speed, m/s	
		The range below optimum values	The range above the initial values			below the optimum values, no more than	higher than optimal values, not more than
Cold	Ib (140-174)	19.0-20.9	23.1-24.0	18.0-25.0	15-75	0.1	0.2
	IIa (175-232)	17.0-18.9	21.1-23.0	16.0-24.0	15-75	0.1	0.3
Warm	Ib (140-174)	20.0-21.9	24.1-28.0	19.0-29.0	15-75	0.1	0.3
	IIa (175-232)	18.0-19.9	22.1-27.0	17.0-28.0	15-75	0.1	0.4

The normalization of the industrial premises' microclimate is carried out through the following measures:

- Buildings and premises equipment with heating systems;
- Stationary and mobile heating points installation;
- Installation and repair of ventilation and air conditioning systems;
- Humidifiers use;
- Air-showering of working places;
- Protecting the facade of the building (except the north) with sun protection devices etc.

5.2.3 Justification of measures to reduce the impact of hazardous factors on the researcher

Chemical safety

In the laboratory we carried out work on our harmless chemicals, there were also quite harmful chemicals in contact with skin and eyes.

By the degree of exposure to the body, harmful substances are divided into four hazard classes:

- 1st — extremely hazardous substances;
- 2nd — highly hazardous substances;
- 3rd — moderately hazardous substances;
- 4th — low-hazard substances.

According to GOST 12.1.007-76, the hazard class of harmful substances is established depending on norms and indicators indicated in table 22.

Table 22. Hazard class standards and indicators.

Name of indicator	Norms for hazard class			
	1st	2nd	3rd	4th
Maximum allowable concentration (MPC) of harmful substances in the air of the working area, mg/m ³	Less than 0.1	0.1-1.0	1.1-10.0	More than 10.0
The average lethal dose when introduced into the stomach, mg/kg	Less than 15	15-150	151-5000	More than 5000
The average lethal dose when applied to the skin, mg/kg	Less than 100	100-500	501-2500	More than 2500

The average lethal concentration in air, mg/m ³	Less than 500	500-5000	5001-50000	More than 50,000
Coefficient of possibility of inhalation poisoning (CPIP)	More than 300	300-30	29-3	Less than 3
Acute area	Less than 6.0	6.0-18.0	18.1-54.0	More than 54.0
Chronic area	More than 10.0	10.0-5.0	4.9-2.5	Less than 2.5

Based on the data in table 22, the substances we worked with and the other substances in the laboratory are suitable for the 4th hazard class, i.e. low hazard.

To reduce the effect of chemically harmful substances, it is necessary to observe several precautions: wear special clothing (bathrobe and gloves); before carrying out any work - wear safety glasses and a mask; do not approach stands with potentially hazardous chemicals; present in laboratory only for the necessary time to complete experiments; perform work in the presence of a senior research fellow. It is important that all chemicals must be placed in containers appropriate for them and put into special cabinets with a constant temperature.

Electrical Safety

Electrical safety is a system of organizational and technical measures and means that protect people from the harmful and dangerous effects of electric current, electric arc, electromagnetic field and static electricity (GOST 12.1.009-76).

The most common reason is approaching a certain distance or direct human contact with exposed live parts.

This can happen due to several factors:

- malfunction of devices or wiring;
- insufficient user qualifications, lack of basic safety standards knowledge;
- non-compliance and inconsistency of measures to temporarily turn on and off contact groups and conductive elements during operation, prevention or equipment repair or power plants;
- insulation damage or lack of grounding.

To avoid this, it is necessary to strictly observe the electrical safety basic requirements at the factory when working with electrical equipment (operating

instructions for electrical appliances). There is a special classification of electrical equipment and personnel according to the electrical hazard degree. To a greater extent, the hazard class from 1 to 5 depends on the voltage (up to 1000 volts or more) and the type of performed work.

The laboratory rooms 205 and 303 of TPU science park refers to premises without increased danger in which there are no conditions creating an increased or special danger, since the AFM, TERS and SERS nominal voltage installation corresponds to 220 V. All current-carrying parts of the installation are isolated, in a protective casing and grounded.

Additional electrical protective equipment in electrical installations. Additional insulating electrical protection means include dielectric gloves, boots, rubber mats and walkways, insulating supports on porcelain insulators and portable groundings. The release of the affected current can be done in several ways to install up to 1000 V:

1. The electrical installation is disconnected using the nearest switch, switch or other shutdown device, as well as by removing or removing the fuses (plugs), plug connector.

2. If for some reason it is not possible to quickly disconnect the electrical installation manually due to the remoteness or inaccessibility of the switch, it is possible to break the current circuit through the victim by breaking the wires using an axe with a dry wooden handle or nippers, pliers and other tools with insulating handles. Cutting should be done to each wire separately, so as not to cause a short circuit between the wires, as a result of which an electric arc can occur, which can cause serious body burns and eye damage.

Laser safety

Lasers are highly hazardous devices. Although there are several risk factors associated with laser installations, laser safety refers to methods of protection against factors directly related to laser radiation.

Even the lasers of the lowest power (a few milliwatts) can be hazardous to vision. When it gets into the eye, the laser beam focuses in a spot of very small size, which can lead to burns of the retina, partial or complete irreversible loss of vision in a split second. More powerful lasers can cause eye damage, even with scattered radiation. Direct and, in some cases, scattered radiation from such a laser can cause skin burns (up to complete destruction) and is a fire hazard.

This hazard degree is determined by biological effects and is regulated by special norms and standards developed by relevant national and international organizations. These norms and standards establish the maximum permissible levels of energy exposure (in J/cm²) of tissues laser irradiation depending on the radiation wavelength, exposure time, irradiated area, repetition frequency and pulse duration.

Safety rules for the manufacture and laser systems operation should provide such low levels of exposure to laser radiation that they, obviously, in any situations in the laser system operation, are below the maximum permissible levels. The laser system operation should not pose any threat to the personnel health.

According to the degree of the generated radiation danger, technological lasers are classified into 5 classes, which are shown in table 23.

Table 23. Laser safety classes.

Safety class	Laser power	Annotation
Class I	Less than 0.39 mW	Safe for predictable applications
Class II	Less than 1 mW	Applies to visible lasers only. Eye protection is common, for example, an eye wash reflex. Do not use at head level.
Class IIIA (3R)	Less than 5 mW	Direct eye contact is dangerous, especially through optical instruments (binoculars, telescope, theodolite, level, telescope, lenses). Qualified workers and specialists should be used.
Class IIIB	More than 5 mW but less than 0.5 W	
Class IV	More than 0.5 W	Very dangerous, especially when used in open areas.

In built lasers in AFM, TERS and SERS equipment belong to the first and second safety classes - that is, they are generally safe if technician follows the instructions for use and wear safety glasses. Therefore, before starting the experiment, it is necessary to correctly plan all operations carried out with the laser and not allow the situation in which the laser head will be at the level of the engineer's head.

Security Organizational Measures:

- the laser system should only be used for its intended purpose. In addition, on this system it is unacceptable to carry out any work that could endanger safety.
- the operation, commissioning and repair of the laser system may only be carried out by specially trained personnel.
- personnel should be provided with laser-protective glasses, protective clothing, gloves and a special tool for removing processed parts.
- before starting the system, the operator must make sure that there are no people in the danger zone.

5.3 Environmental safety

Environmental safety (ES) is an acceptable level of natural and anthropogenic environmental hazards negative impact on the environment and humans.

This paragraph considers the impact of this study on the environment and atmosphere. When working with plasmonic nanoparticles and 4-NBT molecules, no evaporation and emission into the lithosphere occurs. When working with SERS, TERS, AFM equipment with an integrated laser and PC, there is also no negative impact on the environment.

It is necessary to consider the procedure for the equipment disposal that is no longer suitable for use and cannot fulfill its functions.

The disposal procedure consists of two main steps:

Stage 1. Write-off

Write-off by the organization of available on the balance sheet and obsolete computer and electronic equipment.

Stage 2. Disposal

This stage is completely carried out by us on the basis of the certificates we have on special registration, licenses for the collection, use, disposal, transportation, disposal of hazardous waste, and the sanitary and epidemiological conclusion. It includes the following procedures:

- providing us with a preliminary list of utilized equipment and agreeing on the cost of disposal services.
- conclusion of an Agreement for the disposal of decommissioned hardware.
- providing to the Customer for independent filling out the forms of the Certificate of Acceptance of the Vehicle.
- dismantling, vehicles removal and Act of completion signing.
- payment by the customer for disposal services.

5.4 Safety in emergency situation

5.4.1 Analysis of probable emergencies that may be initiated by the research object

An emergency situation is a situation in a certain territory that has arisen as a result of an accident, natural hazard, catastrophe, natural or other disaster that could result in or result in human casualties, damage to human health or the environment, significant material losses and violation of people's living conditions according to GOST R 22.0.01-2016 and GOST R 22.3.03-94.

In Russia, the decision to introduce an emergency regime depending on the scale of the situation is made by the Government, the Russian Ministry for Emergencies or the relevant emergency commissions.

Our research of plasmon-induced photocatalysis takes place at the nanoscale level using safe substances, such as: silicon substrates, gold and silver nanoparticles, and 4-NBT molecules. All these substances and manipulations with them are not able to cause or provoke an emergency situation.

5.4.2 Analysis of probable emergencies that may occur in the laboratory during research

Laboratory emergencies can be mostly caused by technogenic nature.

Emergency stations can occur for the following reasons:

- damage to storage facilities with bulk chemicals;
- severe voltage drops that may lead to failure of the security system and equipment;
- breakage of power wires, ground faults and other damage;
- work on malfunctioning equipment;
- failure to comply with the instructions for safe handling of equipment and chemicals;
- Fire in the laboratory and in the entire scientific institution.

Each of the above incidents can entail a threat to the health of engineers, as well as failure, equipment breakdown. However, the most dangerous is the fire occurrence in the premises, which can entail a big number of casualties among employees, equipment losses and possible destruction of the building.

5.4.3 Justification of measures to prevent emergencies and development of procedures in case of emergencies

1. In case of power wire breakage, ground fault and other damage, the burning appearance, immediately turn off the power and report an emergency to the supervisor;

2. Do not start to work until troubleshooting;

3. In case of chemicals depressurization:

- a) wear personal protective equipment if they have not been worn before;
- b) warn nearby employees of an accident;
- c) leave the laboratory immediately and exit the building;
- d) move fast, but do not run and do not pick up dust;
- e) do not touch walls and surrounding objects of the building;

3. In case of fire or/and smoke:

a) immediately report by phone "01" in the fire Department, alert working, to inform the head of Department, to report the fire at the guard post.

b) to open the emergency exits from the building, disconnect the power supply, close the Windows and shut the door.

c) proceed to extinguish the fire with primary fire extinguishing means, if it does not involve a risk to life.

d) arrange a meeting of the fire brigade.

e) leave the building and be in the evacuation zone.

4. In case of accident:

a) immediately organize first aid to the victim and, if necessary, its delivery in the medical organization;

b) take urgent measures to prevent the development of an emergency and the traumatic factors impact on others;

c) to preserve the situation as it was at the time of the accident before the beginning of accident investigation, if it does not threaten the life and health of other people and does not lead to a catastrophe, accident or other extraordinary circumstances. If it is impossible to preserve it – to fix the situation (to draw up schemes, to carry out other measures).

Conclusion of social responsibility section

This section provided the description of the social responsibility that accompanies the master thesis performance.

Industrial and environmental safety were described. Various harmful and hazardous factors and methods of struggle against them were revealed. In addition, a measures list to reduce threats in case of emergencies was given, as well as legal and security organizational issues. The most important aspects of organizational activities in the design and working area illumination were presented.

Conclusion

In this work, plasmon-induced photocatalytic reaction at the single plasmonic nanoparticles level has been investigated. Using the TERS coupled with AFM technique, we were able to obtain maps on which the topography of single Au/Ag nanoparticles and TERS intensities are clearly visible.

We showed that plasmon photocatalysis can occur not only due to local enhancement of the electromagnetic signal (LSPR), but also with an increase in temperature, laser radiation power density, irradiation time, and scanning density of the sample. Moreover, according to the Arrhenius law, we have shown that the mechanism of 4-NBT to 4-ABT and DMAB conversion is more dependent on temperature than on LSPR, which is evidenced by the intensity ratios.

The results of this investigation can be used to create a single-component system for theranostics of cancer tumors, and the results are of great importance for the processes of photochemistry and nanobiosensorics.

Further research on plasmon photocatalysis will be aimed at improving the simulation model, calculations and surface chemistry of AuAg & AuPd alloys.

References

1. Zhang, J. et al. Engineering the Absorption and Field Enhancement Properties of Au–TiO₂ Nanohybrids via Whispering Gallery Mode Resonances for Photocatalytic Water Splitting. *ACS Nano* 10, 4496–4503 (2016).
2. Sousa-Castillo, A. et al. Boosting Hot Electron-Driven Photocatalysis through Anisotropic Plasmonic Nanoparticles with Hot Spots in Au–TiO₂ Nanoarchitectures. *The Journal of Physical Chemistry C* 120, 11690–11699 (2016).
3. Li, Z. et al. Reversible Modulation of Surface Plasmons in Gold Nanoparticles Enabled by Surface Redox Chemistry. *Angewandte Chemie* 127, 9076–9079 (2015).
4. Zhang, N. et al. Near-field dielectric scattering promotes optical absorption by platinum nanoparticles. *Nature Photonics* 10, 473–482 (2016).
5. Zhao, A. (2005). Controlling the Kondo Effect of an Adsorbed Magnetic Ion Through Its Chemical Bonding. *Science*, 309(5740), 1542–1544.
6. Kim, M., Lin, M., Son, J., Xu, H., & Nam, J.-M. (2017). Hot-Electron-Mediated Photochemical Reactions: Principles, Recent Advances, and Challenges. *Advanced Optical Materials*, 5(15), 1700004.
7. Hou, W., & Cronin, S. B. (2012). A Review of Surface Plasmon Resonance-Enhanced Photocatalysis. *Advanced Functional Materials*, 23(13), 1612–1619.
8. Zeng, Z.-C., Wang, H., Johns, P., Hartland, G. V., & Schultz, Z. D. (2017). Photothermal Microscopy of Coupled Nanostructures and the Impact of Nanoscale Heating in Surface-Enhanced Raman Spectroscopy. *The Journal of Physical Chemistry C*, 121(21), 11623–11631.
9. Golubev, A. A., Khlebtsov, B. N., Rodriguez, R. D., Chen, Y. & Zahn, D. R. T. Plasmonic Heating Plays a Dominant Role in the Plasmon-Induced Photocatalytic Reduction of 4-Nitrobenzenethiol. *The Journal of Physical Chemistry C* 122, 5657–5663 (2018).

10. Keller, E. L. & Frontiera, R. R. Ultrafast Nanoscale Raman Thermometry Proves Heating Is Not a Primary Mechanism for Plasmon-Driven Photocatalysis. *ACS Nano* 12, 5848–5855 (2018).
11. Pozzi, E. A. et al. Evaluating Single-Molecule Stokes and Anti-Stokes SERS for Nanoscale Thermometry. *The Journal of Physical Chemistry C* 119, 21116–21124 (2015).
12. Boerigter, C., Aslam, U. & Linic, S. Mechanism of Charge Transfer from Plasmonic Nanostructures to Chemically Attached Materials. *ACS Nano* 10, 6108–6115 (2016).
13. Burdick, Glenn. Energy Band Structure of Copper. *Physical Review*. (1963), Vol. 129. P. 138–150.
14. S. Zeng. A review on functionalized gold nanoparticles for biosensing applications // *Plasmonics*, (2011). Vol. 6, iss. 3. P. 491–506.
15. Kittel, C. *Introduction to Solid State Physics*. 8th. John Wiley & Sons, (2005). P. 403.
16. Böer, K. W. *Survey of Semiconductor Physics*, 2nd. John Wiley & Sons, (2002). Vol. 1. P. 525.
17. Liu, Xin; Swihart, Mark T. Heavily-doped colloidal semiconductor and metal oxide nanocrystals: an emerging new class of plasmonic nanomaterials // *Chem. Soc. Rev.*, (2014). Vol. 43. P. 3908–3920.
18. Pi, Xiaodong; Delerue, Christophe. Tight-binding calculations of the optical response of optimally P-doped Si nanocrystals: a model for localized surface plasmon resonance // *Physical Review Letters*, (2013). Vol. 111. P. 177402.
19. Garcia, Guillermo, Evan Runnerstrom, Anna Llordes, Andre Anders, Delia J. Millron, Thomas J. Richardson, Rafaella Buonsanti, and Rueben J. Mendelsberg. "Surface Plasmon Resonance Sensors." *Nano Letters* (2011): A-F. Lawrence Berkeley Lab. American Chemical Society Publications, 28 July 2011.
20. Huang, Xiaohua, and Mostafa A. El-Sayed. "Gold Nanoparticles: Optical Properties and Implementations in Cancer Diagnosis and Photothermal Therapy."

Gold Nanoparticles: Optical Properties and Implementations in Cancer Diagnosis and Photothermal Therapy. Ministry of Science & Technology, Egypt, 12 Feb. 2010.

21. Long, Yi-Tao, and Chao Jing. Localized Surface Plasmon Resonance Based Biosensors. Shanghai: Springer, 2014. Google Books. Springer, 10 Apr. 2014.

22. Cantale, Vera. (2011). Towards label-free biosensors based on localized surface plasmon resonance.

23. K. Lance Kelly, Eduardo Coronado, Lin Lin Zhao, and George C. Schatz. The Optical Properties of Metal Nanoparticles: The Influence of Size, Shape, and Dielectric Environment. J. Phys. Chem. B, Vol. 107, No. 3, 2003.

24. Mayer, K. M., & Hafner, J. H. (2011). Localized Surface Plasmon Resonance Sensors. Chemical Reviews, 111(6), 3828–3857.

25. O. Taratula, E. Galoppini, R. Mendelsohn, P. I. Reyes, Z. Zhang, Z. Duan, J. Zhong, Y. Lu. Stepwise functionalization of ZnO nanotips with DNA. Langmuir. 2009, 25(4), 2107-2113.

26. D. Erts, B. Polyakov, H. Olin, E. Tuite. Spatial and mechanical properties of dilute DNA monolayers on gold imaged by AFM. The Journal of Physical Chemistry B. 2003, 107(15), 3591-3597.

27. Cantale, Vera. Towards label-free biosensors based on localized surface plasmon resonance. Università degli Studi di Ferrara. (2011), 15-17.

28. Xie T, Jing C, Long YT. Single plasmonic nanoparticles as ultrasensitive sensors. Analyst. 2017;142(3): 409–420.

29. Gardiner, D.J. (1989). Practical Raman spectroscopy. Springer-Verlag. ISBN 978-0-387-50254-0.

30. [Web-resource]: <https://www.edinst.com>, (Viewed on: 25.03.2020).

31. Hammes, Gordon G. (2005). Spectroscopy for the biological sciences. Wiley. ISBN 9780471733546. OCLC 850776164.

32. [Web-resource]: <https://en.wikipedia.org/wi>, (Viewed on: 1.04.2020).

33. Richard P. Olenick, Tom M. Apostol, David L. Goodstein Beyond the mechanical universe: from electricity to modern physics, Cambridge University Press (1986) ISBN 0-521-30430-X, p. 160.

34. Dinish, U. S. et al.: Development of highly reproducible nanogap SERS substrates: Comparative performance analysis and its application for glucose sensing. *Biosensors and Bioelectronics* 26, 1987-1992 (2011).
35. Downes, A., & Elfick, A. (2010). Raman Spectroscopy and Related Techniques in Biomedicine. *Sensors*, 10(3), 1871–1889.
36. Yang, W.; Xiao, X.; Tan, J.; Cai, Q. In situ evaluation of breast cancer cell growth with 3D ATR-FTIR spectroscopy. *Vib. Spectros.* 2009, 49, 64–67.
37. De Gelder, J.; De Gussem, K.; Vandenabeele, P.; Moens, L. Reference database of Raman spectra of biological molecules. *J. Raman Spectrosc.* 2007, 38, 1133–1147.
38. Schlücker, S. (2014). Surface-Enhanced Raman Spectroscopy: Concepts and Chemical Applications. *Angewandte Chemie International Edition*, 53(19), 4756–4795.
39. Fleischmann, M.; Hendra, P. J.; McQuillan, A. J. Raman Spectra of Pyridine Adsorbed at a Silver Electrode. *Chem. Phys. Lett.* 1974, 26, 163–166.
40. Zong, C., Xu, M., Xu, L.-J., Wei, T., Ma, X., Zheng, X.-S., ... Ren, B. (2018). Surface-Enhanced Raman Spectroscopy for Bioanalysis: Reliability and Challenges. *Chemical Reviews*, 118(10), 4946–4980.
41. Ding, S.-Y.; Yi, J.; Li, J.-F.; Ren, B.; Wu, D.-Y.; Panneerselvam, R.; Tian, Z. Q. Nanostructure-Based Plasmon-Enhanced Raman Spectroscopy for Surface Analysis of Materials. *Nat. Rev. Mater.* 2016, 1, 16021.
42. Xu, H.; Bjerneld, E. J.; Aizpurua, J.; Apell, P.; Gunnarsson, L.; Petronis, S.; Kasemo, B.; Larsson, C.; Hook, F.; Kall, M. Interparticle Coupling Effects in Surface-Enhanced Raman Scattering. *Proc. SPIE* 2001, 4258, 35–42.
43. Fang, Y.; Seong, N.-H.; Dlott, D. D. Measurement of the Distribution of Site Enhancements in Surface-Enhanced Raman Scattering. *Science* 2008, 321, 388–392.
44. Zhu, W.; Esteban, R.; Borisov, A. G.; Baumberg, J. J.; Nordlander, P.; Lezec, H. J.; Aizpurua, J.; Crozier, K. B. Quantum Mechanical Effects in Plasmonic Structures with Subnanometre Gaps. *Nat. Commun.* 2016, 7, 11495.

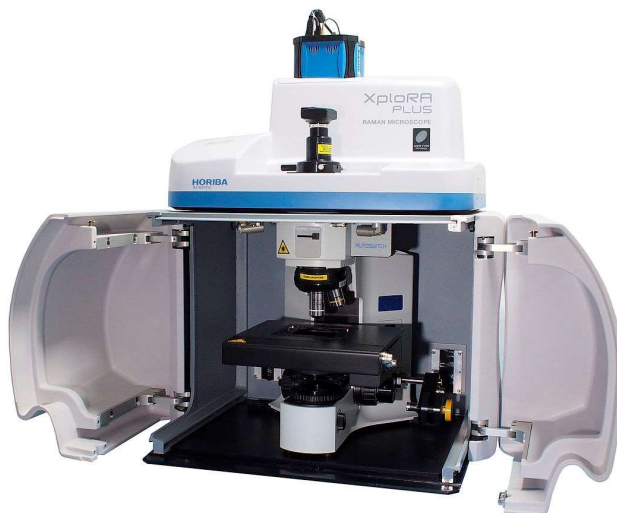
45. Le Ru, E. C.; Etchegoin, P. G. Single-Molecule Surface-Enhanced Raman Spectroscopy. *Annu. Rev. Phys. Chem.* 2012, 63, 65–87.
46. Wang, Y.; Tang, L.-J.; Jiang, J.-H. Surface-Enhanced Raman Spectroscopy-Based, Homogeneous, Multiplexed Immunoassay with Antibody-Fragments-Decorated Gold Nanoparticles. *Anal. Chem.* 2013, 85, 9213–9220.
47. Li, M.; Cushing, S. K.; Zhang, J.; Suri, S.; Evans, R.; Petros, W. P.; Gibson, L. F.; Ma, D.; Liu, Y.; Wu, N. Three-Dimensional Hierarchical Plasmonic Nano-Architecture Enhanced Surface-Enhanced Raman Scattering Immunosensor for Cancer Biomarker Detection in Blood Plasma. *ACS Nano* 2013, 7, 4967–4976.
48. Kim, N. H.; Lee, S. J.; Moskovits, M. Aptamer-Mediated Surface Enhanced Raman Spectroscopy Intensity Amplification. *Nano Lett.* 2010, 10, 4181–4185.
49. Li, M.; Zhang, J.; Suri, S.; Sooter, L. J.; Ma, D.; Wu, N. Detection of Adenosine Triphosphate with an Aptamer Biosensor Based on Surface-Enhanced Raman Scattering. *Anal. Chem.* 2012, 84, 2837–2842.
50. He, Y.; Yang, X.; Yuan, R.; Chai, Y. Off’ to “On” Surface Enhanced Raman Spectroscopy Platform with Padlock Probe-Based Exponential Rolling Circle Amplification for Ultrasensitive Detection of MicroRNA 155. *Anal. Chem.* 2017, 89, 2866–2872.
51. Bantz, K. C., Meyer, A. F., Wittenberg, N. J., Im, H., Kurtuluş, Ö., Lee, S. H., ... Haynes, C. L. (2011). Recent progress in SERS biosensing. *Physical Chemistry Chemical Physics*, 13(24), 11551.
52. Maiti, K. K., Dinish, U. S., Samanta, A., Vendrell, M., Soh, K.-S., Park, S.-J., ... Chang, Y.-T. (2012). Multiplex targeted in vivo cancer detection using sensitive near-infrared SERS nanotags. *Nano Today*, 7(2), 85–93.
53. Zhang, Y., Mi, X., Tan, X., & Xiang, R. (2019). Recent Progress on Liquid Biopsy Analysis using Surface-Enhanced Raman Spectroscopy. *Theranostics*, 9(2), 491–525.
54. [Web-resource]: <https://www.horiba.com>, (Viewed on: 14.04.2020).

55. Pozzi, E. A., Goubert, G., Chiang, N., Jiang, N., Chapman, C. T., McAnally, M. O., ... Duyne, R. P. V. (2016). Ultrahigh-Vacuum Tip-Enhanced Raman Spectroscopy. *Chemical Reviews*, 117(7), 4961–4982.
56. Kumar, N., Mignuzzi, S., Su, W. & Roy, D. Tip-enhanced Raman spectroscopy: principles and applications. *EPJ Tech. Instrum.* 2, 9 (2015).
57. Verma, P. Tip-enhanced Raman spectroscopy: technique and recent advances. *Chem. Rev.* 117, 6447–6466 (2017).
58. Deckert-Gaudig, T., Taguchi, A., Kawata, S. & Deckert, V. Tip-enhanced Raman spectroscopy—from early developments to recent advances. *Chem. Soc. Rev.* 46, 4077–4110 (2017).
59. Wang, X. et al. Tip-enhanced Raman spectroscopy for surfaces and interfaces. *Chem. Soc. Rev.* 46, 4020–4041 (2017).
60. Hartschuh, A. Tip-enhanced near-field optical microscopy. *Angew. Chem. Int. Ed. Engl.* 47, 8178–8191 (2008).
61. Kumar, N., Weckhuysen, B.M., Wain, A.J. et al. Nanoscale chemical imaging using tip-enhanced Raman spectroscopy. *Nat Protoc* 14, 1169–1193 (2019).
62. Coronado, Juan M.; Fresno, Fernando; Hernández-Alonso, María D.; Portela, Racquel (2013). *Design of Advanced Photocatalytic Materials for Energy and Environmental Applications*. London: Springer. pp. 1–5.
63. A. Kudo, K. Sayama, A. Tanaka, K. Asakura, K. Domen, K. Maruya, T. Onishi, *J. Catal.* 1989, 120, 337.
64. Zhu, S., & Wang, D. (2017). Photocatalysis: Basic Principles, Diverse Forms of Implementations and Emerging Scientific Opportunities. *Advanced Energy Materials*, 7(23), 1700841.
65. a) P. Zhang, J. Zhang, J. Gong, *Chem. Soc. Rev.* 2014, 43, 4395; b) T. Simon, M. T. Carlson, J. K. Stolarczyk, J. Feldmann, *ACS Energy Lett.* 2016, 1, 1137.
66. T. Gershon, B. Shin, N. Bojarczuk, M. Hopstaken, D. B. Mitzi, S. Guha, *Adv. Energy Mater.* 2015, 5, 1400849.

67. Melis, A. (2012). Photosynthesis-to-fuels: from sunlight to hydrogen, isoprene, and botryococcene production. *Energy Environ. Sci.*, 5(2), 5531–5539.
68. H. Robatjazi, H. Zhao, D. F. Swearer, N. J. Hogan, L. Zhou, A. Alabastri, M. J. McClain, P. Nordlander and N. J. Halas, *Nat. Commun.*, 2017, 8, 1.
69. Zhou, J., Zhang, J., Yang, H., Wang, Z., Shi, J., Zhou, W., ... He, S. (2019). Plasmon-Induced Hot Electron Transfer in Au-ZnO Heterogeneous Nanorods for Enhanced SERS. *Nanoscale*.
70. Shan, H., Yu, Y., Wang, X., Luo, Y., Zu, S., Du, B., ... Fang, Z. (2019). Direct observation of ultrafast plasmonic hot electron transfer in the strong coupling regime. *Light: Science & Applications*, 8(1).
71. Skrabalak, S. E.; Au, L.; Li, X.; Xia, Y. Facile Synthesis of Ag Nanocubes and Au Nanocages. *Nat. Protoc.* 2007, 2, 2182–2190.
72. Khlebtsov, B.; Panfilova, E.; Khanadeev, V.; Bibikova, O.; Terentyuk, G.; Ivanov, A.; Rumyantseva, V.; Shilov, I.; Ryabova, A.; Loshchenov, V. Nanocomposites Containing Silica-Coated Gold–Silver Nanocages and Yb–2, 4-Dimethoxyhematoporphyrin: Multifunctional Capability of Ir-Luminescence Detection, Photosensitization, and Photothermolysis. *ACS Nano* 2011, 5, 7077–7089.
73. Ye, X.; Zheng, C.; Chen, J.; Gao, Y.; Murray, C. B. Using Binary Surfactant Mixtures to Simultaneously Improve the Dimensional Tunability and Monodispersity in the Seeded Growth of Gold Nanorods. *Nano Lett.* 2013, 13, 765–771.
74. Khlebtsov, B. N.; Khanadeev, V. A.; Ye, J.; Sukhorukov, G. B.; Khlebtsov, N. G. Overgrowth of Gold Nanorods by Using a Binary Surfactant Mixture. *Langmuir* 2014, 30, 1696–1703.
75. Fedosova V. D., Brenchugina M. V. Calculation of artificial lighting. Guidelines for independent work on the discipline "Life Safety" for students of all specialties. - Seversk: SGTA, 2006. 28 p.

Appendix A

Xplora Raman spectrometer specifications



- Research grade optical microscope: Olympus BX, complete microscope with 2 position motorized white light illuminator Koehler illumination by reflection (LED eqv 100 W)/ transmission (Halogen 30 W), Abbe condenser and 2 objectives

1. 20X (NA=0.4 WD=1.3mm), 100(NA=0.9 WD=0.21mm);

2. 50X LWD visible objective (NA=0.50 WD=10.6mm);

- Raman spectrometer: Integrated imaging spectrometer with 4 gratings mounted on motorized turret with gratings: 600gr, 1200gr, 1800gr and 2400gr;

HORIBA Scientific CCD detector, TE air cooled (-60°C), 1024×256 -pixel, 16 bits;
Range: 200-1050 nm, QE: $\sim 60\%$ @ 700nm@ RT;

- Laser:

1. Air-cooled solid-state laser, 532 nm/ 25mW. Edge and Band pass filters set at 532 nm for measurements from 60 cm^{-1} ;

2. Air-cooled solid-state laser, 638 nm/30 mW. Edge and Band pass filters set at 638 nm for measurements from 50 cm^{-1} ;
 3. Air-cooled solid-state laser, 785 nm/100 mW. Edge and Band pass filters set at 785 nm for measurements from 50 cm^{-1} ;
- Spectral resolution: With 532 nm wavelength $\leq 1.4 \text{ cm}^{-1}/\text{pixel}$ with 2400 grooves/mm;
 - Confocal resolution: $\leq 500 \text{ nm}$ lateral XY (with 532 nm);
 - Motorized PC controlled 6 position ND filter wheel for laser power adjustment (0.1%, 1%, 10%, 25%, 50%, 100%);
 - Motorized PC controlled confocal pinhole;
 - Motorized PC controlled entrance slit for resolution selection Confocal coupling optics and motorized filter selection;
 - XY motorized stage, X=75 mm-Y=50mm.PC controlled by LabSpec software includes Z profiling;
 - XY specifications: minimum step size=10nm; repeatability=1 μm ; resolution: 100 nm;
 - LabSpec6 spectral software suite for the easy acquisition and analysis and analysis of Raman data. Includes control of the hardware and acquisition parameters, AUTO calibration, customizable methods, FLAT fluorescence subtraction, peak label and fit, image capture, smoothing, spectral subtraction etc.;
 - SWIFT fast confocal Raman mapping.

Appendix B

LabRAM HR Evolution specifications.



Spectrograph: focal length is 800 mm; there are 3 diffraction gratings at 600 l/mm, 1800 l/mm;

Spectral range: 4000-100 cm^{-1} ;

Spectral resolution: up to 1.5 cm^{-1} ;

Accuracy of wavenumber: 1 cm^{-1} ;

Spatial resolution: up to 1 micron;

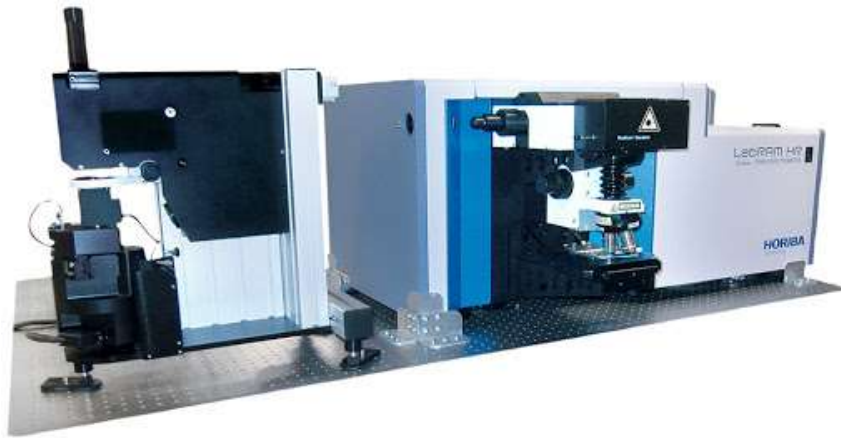
Lasers: tunable Ar⁺ laser with power up to 50mW and with notch filters at 488nm and 514 nm; He-Ne at 632nm and power up to 10 mW;

Microscope: Olympus BX41 with objectives 10X (NA 0.25), 50X (NA 0.75), 50X (NA 0.5), 100X (NA 0.9);

Detector: Peltier-cooled CCD 1024X256 px.

Appendix C

OmegaScope-R specifications



AFM head:

Laser wavelength: 1300 nm;

Noise recording system: <0.1 nm;

Optical Access:

Top lens: 100x, NA = 0.7 max.;

Bottom lens: 100x, NA = 1.4 (immersion) max.;

Side lens: 50x, NA = 0.5 max.;

Controller - number of synchronous detectors: 2;

Digital generator:

- quantity: 6 pcs.;

- bit: 32 bits;

- range: up to 5 MHz;

DSP Frequency: 300 MHz;

Interface: USB 2.0; ADC;

- frequency: 500 kHz;

- capacity: 18 bits;

- number of channels: 20;

High voltage amplifiers:

- voltage: -5 ... + 120 V;
- noise: not more than 0.4 ppm;

Offset voltage (AC, DC): -10 ... + 10 V;

Bias voltage in the mode of electric nanolithography: -50 ... + 50 V;

Frequency range of voltage, 0 ÷ 2 MHz;

Sample Scanner:

Scan Range: 100 x 100 x 15 ($\pm 10\%$) μm ;

XY axis non-linearity: not more than 0.04%;

Z axis non-linearity: not more than 0.04%;

Noise (RMS), nm:

- XY in the 200 Hz band with sensors on: 0.1;
- XY in the 100 Hz band with sensors off: 0.02;
- Z sensor noise in the 1000 Hz band: <0.04;

Digital feedback along the axes X, Y and Z:

XY resonant frequency, no load, 7 kHz;

Resonant frequency in Z, no load, 15 kHz;

Motorized Sample Positioning:

- range, 5 mm;
- resolution, 1 micron;

Lens Scanner:

Scanning range, microns;

30 x 30 x 15 ($\pm 5\%$);

Digital feedback along the axes X, Y and Z;

Spatial Resolution:

In a semi-contact AFM, <1 nm;

In nano spectroscopy, <10 nm.

Appendix D

Agilent 5420 AFM specifications



Noise: 0.5\AA

Scan Range: $90\mu\text{m} \times 90\mu\text{m} \times 8\mu\text{m}$;

Scanners:

Large Multi-Purpose Scanner:

Scanning Range - $90\mu\text{m} \times 90\mu\text{m}$;

Z Range - $8\mu\text{m}$;

Vertical Noise - 0.5\AA RMS;

Small Scanner:

Scanning Range - $9\mu\text{m} \times 9\mu\text{m}$;

Z Range - $2\mu\text{m}$;

Vertical Noise - $< 0.2\text{\AA}$ RMS;

Sample Plate Sizes:

Kinematic Mount Translatable Sample Plate - 2mm x 2mm;

Translation Stage - 20mm x 20mm;

Controller:

Input - Ten 16-bit channels

Drive - 5 channels $\pm 215\text{V}$, 24-bit

Output - Four 24-bit channels, $\pm 10\text{V}$

Interface - USB

Power - 100 - 120V AC or 220 - 240V AC 1A; 50 - 60Hz

Facilities Specifications:

Acoustic Noise - $< 75\text{dBc}$

Temperature Variation - Does not exceed $\pm 2^\circ\text{F}$

Humidity Variation - Does not exceed $\pm 20\% \text{ RH}$